Cellulose Nanofibril Films as Bioinspired Membranes

Capitalizing on Water Interactions

Minna Hakalahti

A? Aalto University

Cellulose Nanofibril Films as Bioinspired Membranes

Capitalizing on Water Interactions

Minna Hakalahti

A doctoral dissertation completed for the degree of Doctor of Science (Technology) to be defended, with the permission of the Aalto University School of Chemical Engineering, at a public examination held at the Auditorium of Haukilahti Upper Secondary School on 23rd of February 2018 at 12.

Aalto University
School of Chemical Engineering
Department of Bioproducts and Biosystems
Materials Chemistry of Cellulose

Supervising professor
Prof. Eero Kontturi, Aalto University, Finland

Thesis advisor
Dr. Tekla Tammelin, VTT Technical Research Centre of Finland Ltd, Finland

Preliminary examiners
Prof. Takuya Kitaoka, Kyushu University, Japan
Prof. Torbjörn Pettersson, KTH Royal Institute of Technology, Sweden

Opponent
Prof. Derek Gray, McGill University, Canada

NORDIC ECOLABEL

441   697
Printed matter

Abstract

This work represents an effort to exploit the inherent features of nanoscaled cellulose as practical advantages in membrane materials. The approach was to systematically explore the behavior of 2,2,6,6-tetramethylpiperidine-1-oxyl radical oxidized cellulose nanofibrils (TEMPO CNF) with respect to water vapor sorption mechanisms and transport of water, to tune the inherent properties using facile strategies and to expose the materials to performance testing. Surface-sensitive methods were used for revealing molecular scale phenomena directly at interfaces, whereas bulk methods were used to demonstrate their significance in macroscopic scale. Films made from TEMPO CNF were in the main role, complemented by synthetic polymers to introduce new performance features with significance for membrane materials.

Water vapor sorption of TEMPO CNF thin films was studied by precise surface-sensitive analytical methods, i.e. quartz crystal microbalance with dissipation monitoring and spectroscopic ellipsometry, and combined with classical physicochemical models. It was established that water vapor sorption into TEMPO CNF thin films occurs through distinct underlying mechanisms: specific sorption below 10% RH, association of Flory-Huggins population of molecules with the films at 10-75% RH and clustering of water molecules above 75% RH. Kinetic parameters defining the transport of water molecules in the TEMPO CNF film structure were determined. The results showed that diffusion of water vapor could be used as a probing tool for elucidating structural details of moisture-responsive materials in the presence of water.

Bulk and interfacial chemical modification approaches were applied. Enhancement of wet strength of TEMPO CNF films was achieved by crosslinking, whereby inherent characteristics, such as hydrophilicity, were not compromised. The water stable structure was suitable for further functionalization with a thermoresponsive polymer, poly(NIPAM). Covering mere 8% of the surface with poly(NIPAM) caused drastic changes in the performance of the TEMPO CNF film, as the increment in slope of relative water permeance around the lower critical solution temperature of poly(NIPAM) increased from 18% to 100%, showcasing the efficiency of the interfacial modification approach. CNF films were also subjected to performance testing in tetrahydrofuran and n-hexane, whereby their suitability for organic solvent nanofiltration was demonstrated.

This thesis furthers the fundamental understanding of water interactions of cellulosic nanomaterials and other complex moisture-sensitive structures in the biomaterial genre. It also proposes concrete means to tune selected material properties toward desired environments and effects. In the view of this thesis, inherent structure-derived properties are the key for achieving performance features that will carry future biomaterials development beyond conventional applications.

Tekijä
Minna Hakalahti

Väitöskirjan nimi
Nanoselluloosafilmit membraanimateriaalina - Vesivuorovaikutusten hyödyntäminen

Julkaisija Kemian tekniikan korkeakoulu

Yksikkö Biotuotteiden ja biotekniikan laitos

Sarja Aalto University publication series DOCTORAL DISSERTATIONS 31/2018

Tutkimusala Biotuotetekniikka

Käsikirjoituksen pvm 15.11.2017   **Väitöspäivä** 23.02.2018

Julkaisuluvan myöntämispäivä 25.01.2018   **Kieli** Englanti

☐ **Monografia**   ☒ **Artikkeliväitöskirja**   ☐ **Esseeväitöskirja**

Tiivistelmä

Tässä työssä tutkittiin nanoselluloosan luontaisten ominaisuuksien hyödyntämistä membraanimateriaaleissa. Aihetta lähestyttiin tarkastelemalla 2,2,6,6-tetrametyylipiperidiini-1-oksyyli-radikaali-hapetettujen nanoselluloosafibrillien (TEMPO CNF) vesihöyryn sorptiomekanismeja ja vesimolekyylien kuljetusominaisuuksia. Lisäksi työssä muokattiin kemiallisesti nanoselluloosakalvojen ominaisuuksia ja tutkittiin kalvojen suorituskykyä membraanimateriaalina. Materiaaliominaisuuksia ja ilmiöitä karakterisoitiin sekä pintarakennetta että koko materiaalirakennetta analysoivilla menetelmillä. Työssä keskeisessä roolissa olivat sekä ohut- että makrokokoiset nanoselluloosapohjaiset kalvot, joiden ominaisuuksia muokattiin synteettisillä polymeereillä membraanimateriaaleilta vaadittujen suorituskykyominaisuuksien aikaansaamiseksi.

TEMPO CNF-ohutkalvojen vesihöyrysorptiota tutkittiin tarkkojen pintamenetelmien, kuten kvartsikidemikrovaa'an ja spektroskooppisen ellipsometrian avulla. Tuloksia tulkittiin klassisten fysikokemiallisten mallien avulla. Vesihöyrysorptio TEMPO CNF-ohutkalvoihin tapahtui erillisten vallitsevien mekanismien kautta: spesifisenä sorptiona alle 10% suhteellisessa kosteudessa, Flory-Huggins-mekanismin kautta 10-75% suhteellisessa kosteudessa, ja vesimolekyylien klusterointina yli 75% suhteellisessa kosteudessa. Yhdistämällä pintaherkkä lähestymistapa Fickin diffuusiomalleihin pystyttiin selvittämään kineettiset lainalaisuudet, jotka määrittävät vesimolekyylien kulkeutumisen TEMPO CNF -ohutkalvoissa. Saatujen tulosten perusteella vesihöyryn diffuusiota voidaan hyödyntää kosteusherkkien materiaalien rakenteellisten yksityiskohtien tutkimuksessa.

Ilmiöiden perustutkimukselliseen ymmärrykseen pohjautuen vesivuorovaikutuksia tutkittiin myös sovelluslähtöisesti räätälöimällä CNF-kalvoja membraanimateriaaliksi soveltuvaksi. Kalvojen vesilujuutta parannettiin merkittävästi polyvinyylialkoholi-ristisilloituksen avulla. Ristisilloitus ei kuitenkaan vaikuttanut kalvon toivottuihin luontaisiin ominaisuuksiin, kuten hydrofiilisyyteen. Vedessä stabiilit ristisilloitetut CNF-kalvot soveltuivat jatkomuokkaukseen lämpövasteisella polymeerillä (poly(*N*-isopropyyliakryyliamidi)). Merkittäviä suorituskykymuutoksia veden läpäisevyyden suhteen saavutettiin jo 8%:n peittoasteella. Lisäksi työssä havaittiin, että CNF-kalvot soveltuvat orgaanisten liuottimien, esim. tetrahydrofuraanin ja *n*-heksaanin nanosuodatukseen.

Tämä väitöskirjatyö lisää perustavanlaatuista tietoa nanomittakaavaisten selluloosamateriaalien vesivuorovaikutuksista ja niiden monimuotoisista kosteusherkistä rakenteista. Työssä esitetään konkreettisia tapoja, joiden avulla ominaisuuksia voidaan muokata haluttuihin ympäristöihin sopiviksi. Tämän väitöskirjatyön tulokset osoittavat, että luontaiset, materiaalirakenteesta johtuvat ominaisuudet ovat avainasemassa, kun pyritään saavuttamaan suorituskykyisiä tulevaisuuden biomateriaaliratkaisuja.

Avainsanat selluloosananofibrillit, vesivuorovaikutukset, membraanit, pintaherkät analyysit

Preface

My warmest gratitude is split two-ways between my advisor Dr. Tekla Tammelin and supervising professor Eero Kontturi. I thank them for the countless hours of discussions, for the mountains of lessons learnt and for frequently giving me feedback in a direct, yet discreet way. Eero, I admire your breadth and depth of knowledge and greatly appreciate your willingness to share it with others. Tekla, your continued support, expertise and relentless attitude have repeatedly inspired me to try my best.

I would also like to thank my co-authors, Prof. Alexander Bismarck, Prof. Kang Li, Prof. Jukka Seppälä, Dr. Andreas Mautner, Dr. Tuomas Hänninen, Dr. Marco Faustini, Dr. Cédric Boissière, Dr. Tuomo Hjelt, Dr. Harri Setälä, Dr. Koon-Yang Lee, Dr. Leena-Sisko Johansson, Arto Salminen and Panu Lahtinen for the pleasant and fruitful collaboration.
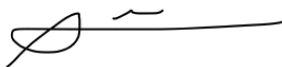
Prof. Takuya Kitaoka of Kyushu University and Prof. Torbjörn Pettersson of KTH are acknowledged for acting as pre-examiners of this dissertation and for providing valuable comments.

I warmly thank my current and former managers, Pia Qvintus, Dr. Jani Lehto, Dr. Annaleena Kokko and Dr. Heli Kangas for providing excellent working facilities and for supporting this research endeavor. I have been lucky to have Dr. Tekla Tammelin, Dr. Katri Kontturi, Marie Gestranius, Tiia Tenhunen, Ville Rissanen and Jonas Hartman to share with me the everyday struggles and successes. Dr. Jaakko Pere, Dr. Soledad Peresin, Dr. Hannes Orelma, Dr. Reeta Salminen, Dr. Elina Niinivaara, Dr. Reina Tanaka, Dr. Ben Wilson, Kari Kammiovirta, Vuokko Liukkonen, Mari Leino, Ulla Salonen and Katja Pettersson are enormously thanked for all the help. In particular, Katja Pettersson deserves my sincerest gratitude for her very valuable help on many occasions, all the way up to the final minutes before submitting this thesis.

Importantly, to all my friends near and far - thank you for the encouragement and simply for the friendship!

Finally, Äiti, Iskä and Tapio, thank you for the support, curiosity and love.

Helsinki, February 1st, 2018

List of Publications

This dissertation is based on the following original publications which are referred to in the text as I–V. The publications are reproduced with kind permission from the publishers.

I   Hakalahti, M.; Faustini, M.; Boissière, C.; Kontturi, E.; Tammelin, T. Interfacial Mechanisms of Water Vapor Sorption as Revealed by Quantitative Models. *Biomacromolecules* **2017**, *18*, 2951-2958.

II   Hakalahti, M.; Hjelt, T.; Faustini, M.; Boissière, C.; Kontturi, E.; Tammelin, T. Cellulose Nanofibril Film Structure Probed by Water Vapor Diffusion. *Submitted to J. Phys. Chem. Lett.*

III   Hakalahti, M.; Salminen, A.; Seppälä, J.; Tammelin, T.; Hänninen, T. Effect of Interfibrillar PVA Bridging on Water Stability and Mechanical Properties of TEMPO/NaClO$_2$ Oxidized Cellulosic Nanofibril Films. *Carbohydr. Polym.* **2015**, *126*, 78-82.

IV   Hakalahti, M.; Mautner, A.; Johansson, L.-S.; Hänninen, T.; Setälä, H.; Kontturi, E.; Bismarck, A.; Tammelin, T. Direct Interfacial Modification of Nanocellulose Films for Thermoresponsive Membrane Templates. *ACS Appl. Mater. Interfaces* **2016**, *8*, 2923-2927.

V   Mautner, A.; Lee, K.-Y.; Lahtinen, P.; Hakalahti, M.; Tammelin, T.; Li, K.; Bismarck, A. Nanopapers for Organic Solvent Nanofiltration. *Chem. Commun.* **2014**, *50*, 5778-5781.

Authors' Contributions

Paper I: MH was responsible for the experimental design together with co-authors, performed the experimental work, analyzed the results and wrote the manuscript under supervision of EK and TT. MF and CB contributed to the spectroscopic ellipsometry measurements, analysis of the results and critically reviewed the conclusions.

Paper II: MH was responsible for the experimental design together with co-authors, performed the experimental work, analyzed the corresponding results and wrote the manuscript. EK and TT contributed to the experimental planning and critically reviewed the results and conclusions. MF and CB contributed to the spectroscopic ellipsometry measurements, analysis of the results and critically reviewed the conclusions. TH took part in diffusion modeling and critically reviewed the conclusions.

Paper III: MH performed the main part of the experimental work, analyzed the results together with the co-authors and wrote the manuscript under the supervision of TT and TH. AS performed the DMA and tensile testing measurements. JS critically reviewed the results and conclusions.

Paper IV: MH prepared the samples, performed the FT-IR measurements and AFM imaging, analyzed the results together with the co-authors and wrote the manuscript under the supervision of EK and TT. AM performed the filtration measurements and LSJ performed the XPS measurements. TH and HS contributed to the chemical modifications.

Paper V: MH performed the AFM experiments, analyzed the corresponding experimental results and wrote the corresponding part in the manuscript. AM and KYL carried out the main part of the experimental work, analyzed the results and wrote the manuscript. PL prepared the raw material. TT, KL and AB contributed to the experimental planning, critically reviewed the results and conclusions and supervised the writing.

Contents

List of Symbols

a	water activity
AFM	atomic force microscopy
B	affinity of water
BC	bacterial cellulose
BET	Brunauer-Emmett-Teller theory
CAM	contact angle measurement
CNF	cellulose nanofibrils
CNC	cellulose nanocrystals
CMF	cellulose microfibrils
CP	cross polarization
D	diffusion coefficient
DH	degree of hydrolysis
DMA	dynamic mechanical analysis
DVS	dynamic vapor sorption
ΔD	change in dissipation of energy
Δf	change in resonance frequency
E`	storage modulus
FT-IR	Fourier-transform infrared spectroscopy
GAB	Guggenheim–Anderson–de Boer-model
K	concentration of specific sorption sites
LCST	lower critical solution temperature
MAS	magic angle spinning

MSE	mean squared error
MWCO	molecular weight cut off
n	number of water molecules in a cluster
^{13}C NMR	carbon-13 nuclear magnetic resonance
P	permeability
(poly)NIPAM	poly(N-isopropylacrylamide)
PAA	poly(acrylic acid)
PVA	poly(vinyl alcohol)
PEI	poly(ethylene imine)
ppm	parts per million
p^o_v	saturation vapor pressure
QCM-D	quartz crystal microbalance with dissipation monitoring
RH	relative humidity
RI	refractive index
RPM	revolutions per minute
S	solubility
SE	spectroscopic ellipsometry
SEM	scanning electron microscope
SPR	surface plasmon resonance
TEMPO	2,2,6,6-tetramethylpiperidine-1-oxyl radical
THF	tetrahydrofuran
UV	ultraviolet radiation
V_c	clustering fraction of water
V_{FH}	Flory-Huggins fraction of water
V_L	Langmuir fraction of water
χ	Flory- Huggins interaction parameter
λ	wavelength
W	Watt
XPS	X-ray photoelectronspectroscopy

1. Introduction

Through nature's evolutionary perfection of structure, property and function, many of the most crucial biological and terrestrial operations, e.g. photosynthesis[1] and water transport in plant plasma membrane by aquaporins[2,3] occur at nanoscale. In such dimensions interfacial interactions determine the behavior of the materials and particles due to the distinctively large surface area. For this reason, the characteristic responses toward external stimuli tend to be magnified, especially in constructions assembled from nanoscaled building blocks – particles with at least one of the external dimensions in the size range of 1 nm - 100 nm[4].

In the realm of nanoscaled materials, wood-based cellulose nanofibrils (CNFs) are intriguing elementary building blocks: aside from hydrophilicity and abundance in nature, assemblies thereof are highly hygroscopic[5-7]. The strong interactions with water distinguish CNFs from many other nanomaterials that may be comparable in terms of high aspect ratios, surface areas and tensile properties[5,6]. The unique combination of large surface area and hygroscopicity is an advantageous premise for applications operating in aqueous environments, e.g. membrane materials designed to entrap small particles and molecules.

The objective of this dissertation is to exploit the inherent features of CNF in an entirely new way with focus on hydrophilicity and hygroscopicity in the context of membrane materials. These features are indispensable for many membrane systems and rarely available in current membrane materials. Strong interactions with water have often been considered a challenge and a detrimental feature for cellulosic materials since people are well aware that their properties are largely downgraded after immersion in water, and often also when exposed to high humidity. In contrast, in the concepts developed here, moisture sensitivity and specific water interactions are perceived as key enablers for development of new materials

solutions for water purification applications. Thereby an entirely new type of tight and hydrophilic material is introduced into the field of membranes, with the potential to arrest particles and molecules beyond the capability of current filter and membrane systems.
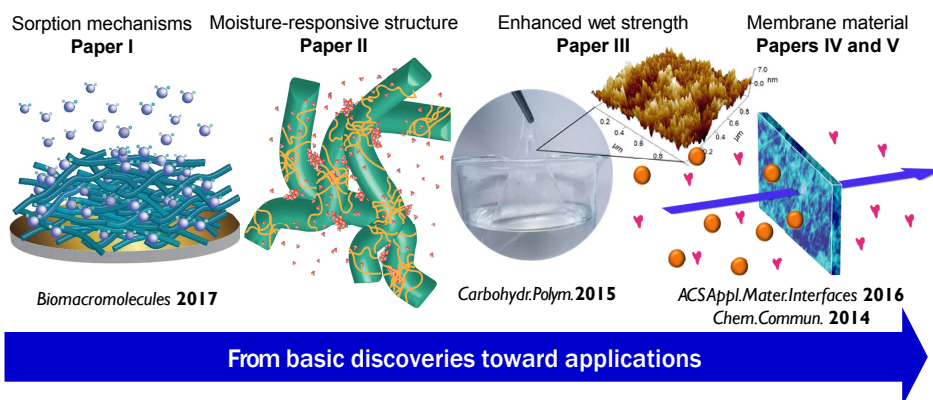
Figure 1. Research strategy and main results *en route* to finding fresh perspectives for exploiting inherent features of CNF in membrane materials.

The approach taken in this dissertation is fundamental with an applied angle: in-depth fundamental insight centered on the moisture sensitive structure and the underlying mechanisms are exploited to develop facile strategies for refining CNF films toward membrane materials, as depicted in Figure 1. Complementary methods are used to enable operations at all relevant scales for taking basic discoveries toward applications: the surface-sensitive approach is used for revealing molecular-scale phenomena directly at interfaces, whereas the bulk methods demonstrate their significance at macroscopic scale. **Paper I** is a fundamental study revealing the underlying mechanisms of sorption of water molecules into CNF thin film assemblies. As a direct continuation, **Paper II** presents an entirely new approach for elucidating structural details of moisture responsive materials by using diffusion of water vapor as a probing tool. With this approach, also the kinetic parameters defining the transport of water molecules in the CNF film structure were determined. In **Papers III and IV** highly moisture sensitive CNF films are adapted toward use as membrane materials by enhancing

the wet strength of the films and by tailoring the film surface with a stimuli-responsive poly-mer for temperature-controllable performance in aqueous environments. Moreover, **Paper V** demonstrates the use of membranes made entirely from CNF in organic solvent media.

The dissertation builds on established understanding of isolation of CNF, especially by a means of 2,2,6,6-tetramethylpiperidine-1-oxyl radical (TEMPO) catalyzed oxidation by NaClO[8]. Films made from TEMPO CNF are in the main role, complemented by synthetic polymers to introduce new performance features with significance for membrane materials. In essence, the research depicted in this dissertation utilizes the inherent features of CNF and turns their fundamental behavior into practical advantages that may deliver a new material solution for the membrane domain.

2. Cellulose at Nanoscale

The hierarchical nature of cellulose in its native surroundings, i.e. the plant cell wall, warrants review at multiple levels for a comprehensive view on its structure and interactions. Here, the molecular level is surveyed, followed by a zoom out therefrom to higher structural levels and film assemblies, with focus on the implications for nanoscaled cellulose; its isolation from the complex plant cell wall, the resultant properties and modification opportunities.

2.1 Hierarchically Structured Cellulose in the Plant Cell Wall

At molecular level, cellulose is a linear syndiotactic homopolymer of D-anhydroglucopyranose units (Figure 2a) in alternating positions along the polymer chain. In crystalline cellulose the D-anhydroglucopyranose rings are linked together by β-(1→4)-glycosidic bonds with each ring rotated 180° with respect to the adjacent ring. Two D-anhydroglucopyranose units linked together in this manner make up the dimer cellobiose[6,9].
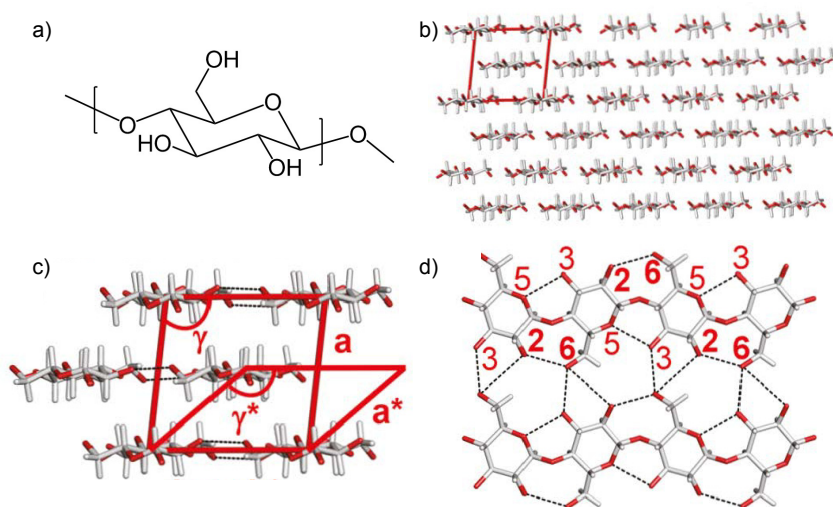

Figure 2. a) Molecular structure of glucose, the repeating unit of cellulose. b) Cross-sectional, c) equatorial and d) top views of glucan chain organization and hydrogen bonds of cellulose $I_β$. Adapted from Chundawat et al. 2011[10].

Cohesive interactions of cellulose at the molecular level have immense implications for the utilization and transformation of cellulose. The literature emphasizes the role of hydrogen bonding as the most important form of interaction occurring inter- and intramolecularly[6,11]. Considering the intrachain stability of cellulose, the glycosidic linkages between D-anhydroglucopyranose rings are stabilized by hydrogen bonds between O3 H O5 of the neighboring molecules in the chain, resulting in a rather stiff polymer chain structure[12,13]. Interchain hydrogen bonds between adjacent chains running parallel to each other promote the arrangement of the chains into planar sheets, which are connected by interplanar London dispersion interactions[14]. Interestingly, recent literature[14] suggests that the role of hydrogen bonding in the structure of cellulose is often over-emphasized due to its demonstrative experimental nature: hydroxyl groups usually find their counterparts from the parallel running cellulose chains, which appear as stretching bands that are shifted to a lower wavenumber in comparison to isolated hydroxyl groups when investigated by spectroscopic methods. Based on molecular modelling and macroscopic evaluation of the Hamaker constants[15], the additive contribution of short-range London dispersive attraction to the overall stabilization is approximated to be 50% to 70% of the total cohesive interactions in cellulose and to correspond to a compressive force of approximately 3 GPa.[14]

Due to the cohesive forces, cellulose chains characteristically form highly organised aggregate structures in the plant cell wall. These bundles of cellulose chains are generally regarded as the elementary supramolecular units of native cellulose and are called elementary fibrils[11,16]. The exact shape and size of the elementary fibrils is under debate with several competing models. Currently the most popular model describes the elementary fibril as a 36 (6 × 6) chain aggregate[17], although 24 chain[18] and 18 chain models[19] have also been proposed. The width of the elementary fibril has been shown to depend on its origin, with highly developed plants, such as trees, with thinner elementary fibrils in the range from ca. 2-5 nm[20,21]. In a recent op-ed piece, Jarvis[22] completely ruled out the 36 chain model in the light of current evidence as it would be too large to fit the dimensions of microfibrils in electron micrographs. The debate is still ongoing.

Regardless of the source of the elementary fibrils, regions of high order and low(er) order are present, and they are commonly referred to as crystalline and amorphous regions, respectively[6,9]. Thus the elementary fibrils are often described by the classical fringed-fibrillar model, which depicts the elementary fibril system as highly ordered crystalline segments disrupted at irregular intervals by amorphous sections[23,24,25]. However, contemporary analytical tools have provided experimental evidence suggesting that the amorphous regions or, rather, transitions, are comprised of only 4-5 units of D-anhydroglucose, amounting to ca. 2 nm in length. This is in contrast to crystalline regions which are tens or hundreds of nanometers in length[13]. Within the ordered regions, crystallites can coexist in three different polymorphs, cellulose I, II and III. Cellulose I – the only polymorphic form relevant for native cellulose – is actually a common term for two distinct polymorphs, I_α and I_β coexisting in varying proportions depending on the source of cellulose[26]. Wood cellulose is typically dominated by the I_β form[12,27]. Elementary fibrils with hemicellulose are further packed together by hydrogen bonding into bundles classically known as microfibrils and further with hemicellulose and lignin into fibers[5].

In nature, cellulose exists in the plant cell wall (Figure 3), providing strength and load-bearing support functions, especially for woody plants, e.g. trees and shrubs that extend far above ground level. In this respect, herbaceous plants without a persistent woody stem above ground are different, as they do not need similar structural support from cellulose. This is reflected in the structures of the plant cell walls: the woody plant cell wall consists of the middle lamella, and primary and secondary cell walls, whereas the herbaceous plant cell wall does not have a secondary cell wall layer. From the perspective of this cellulose-oriented dissertation, this is significant, as most cellulose is located in the secondary cell wall which makes up the bulk of the woody plant cell wall.[28] For this reason all further references made in this dissertation to the plant cell wall refer specifically to the woody plant cell wall.
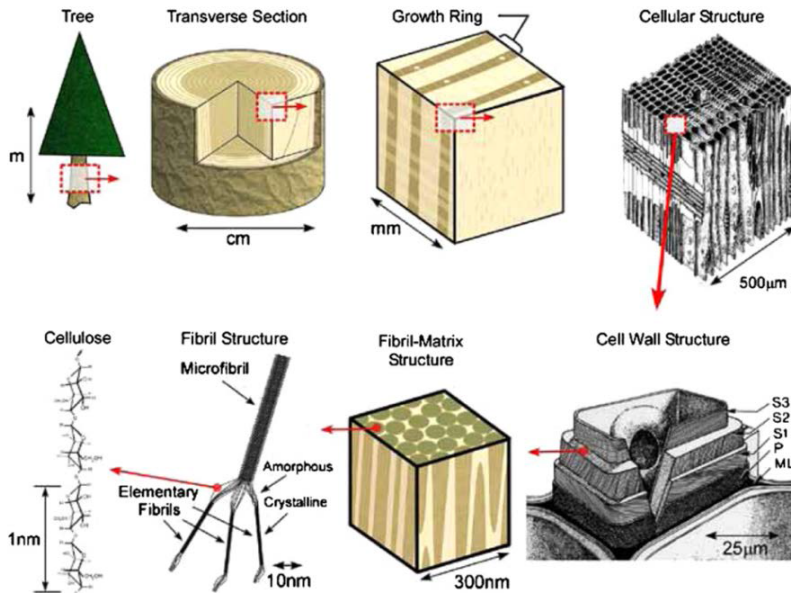
Figure 3. The hierarchical structure of a tree. Adapted from Postek et al. 2011.[29]

Primary and secondary cell wall are natural composites of exceptional design, consisting mainly of cellulose embedded in a network of hemicellulose and lignin. Hemicellulose is a heteropolysaccharide with a structure dependent on the wood species. For softwood, hemicellulose consists of mostly galactoglucomannans and arabinoglucuronoxylans, whereas hemicellulose in hardwood consists of glucomannan and glucoronoxylan. Lignin is a polyphenolic polymer comprised of coniferyl, sinapyl and coumaryl alcohols in ratios depending on the wood source[28]. The reader is referred to reviews by Scheller et al.[30] and Ralph et al.[31] for details on structures of hemicellulose and lignin. Playing an integral role in the plant cell wall assembled in a complex composite manner, hemicellulose and lignin make up of ca. 50-60% of the woody plant cell wall[28,32]. The primary cell wall is typically so thin and difficult to distinguish in structural analysis that for most purposes it is considered in conjunction with middle lamella. In contrast, the secondary cell wall can be further divided into three separate

layers (S1, S2 and S3)[28] with specific orientations at different microfibril angles. The exact structure of the secondary cell wall is under debate, as orientation also depends on the technique of analysis[33]. Nonetheless, the microfibrillar angle determines the properties of the plant, e.g. axial stiffness and resistance toward collapse and rupture, as well as has implications for isolation of nanoscaled cellulose from the plant cell wall[34].

2.2 Isolation of Nanoscaled Cellulose

A considerable portion of academic research on nanoscaled cellulose, and cellulose altogether, has focused on developing efficient ways to liberate the nanomaterial from the multicomponent woody plant cell wall. Isolation of nanoscaled cellulose involves the top-down degradation and disintegration of the plant cell wall structure by chemical, mechanical[5,9] and/or enzymatic means[35,36]. Nanoscaled cellulose grades (Figure 4) produced via the top down approach fall into two categories: cellulose nanocrystals (CNC) and cellulose nano- and microfibrils (CNF and CMF)[9]. In turn, an isotropic network of bacterial cellulose (BC) microfibrils can be obtained by the bottom-up process by certain types of bacteria, e.g. *Glucanobacter xylinum*[37], that extrude cellulose fibrils synthesized from sugar, as first observed by Brown in 1886.[38]

The production of CNC is based on acid hydrolysis of cellulose fibers with strong acids, e.g. H_2SO_4[39,40] or HCl vapor[41], whereby glycosidic bonds of the less ordered domains are efficiently cleaved leading to the release of individual nanocrystals. The dimensions of the rod-like nanocrystals are dependent on the cellulose source and hydrolysis conditions. The length of the crystal varies from 100 nm to 1000 nm, whereas the width is only in the range of a few nanometers up to tens of nanometers.[40]

Fibrillated cellulose grades (CNF and CMF) are manufactured using intensive mechanical disintegration methods often combined with chemical and/or enzymatic pre-treatments in order to facilitate the liberation of the fibrils from the plant cell wall and fibers. The outcome of the final nanofibril morphology greatly varies depending on the pretreatment procedures, mechanical fibrillation protocol and energy consumption, with CMF generally coarser com-

pared to CNF. Typically, CNF and CMF grades, which are manufactured by means of mechanical disintegration, possibly assisted only with enzymatic pre-treatments, are polydisperse with broad size distributions and branched structures. The overall dimensions of CMF are micrometer scale, whereas the fine branches are nanometer scale in size. All CNF and CMF grades form strong hydrogels with very low solids content (0.5-3 wt.-%) due to the large surface area, high aspect ratio, nanoscale fine structure and high swelling ability, coupled with strong mutual attraction of the fibrils to one another.[7,9]

Chain or rod-like structures

True nanoscale behaviour

Nanocrystals   Nanofibrils   Nanofibrillated

Acid hydrolysis   Chemical pretreatment   Microfluidization

Colloidal dispersion   Polyelectrolyte-like

Branched structure

Overall dimensions in macroscale, fine structure in nanoscale

High-consistency   Microfibrillated

Enzymatic   Micro-grinding

Plant fiber-like

Figure 4. Grades of nanoscaled cellulose.

A technique has been developed recently to produce CNF in high consistency (20-40% solids content). This is based on combined action of tailored cellulase enzymes and fiber-fiber friction during gentle mixing at low water content. Through a peeling type of action, a paste-like fibril network is formed. Since no chemicals are involved in the treatment, the basic properties of the starting cellulose material, e.g. charge and crystallinity, remain unchanged. Based on scanning electron microscopy (SEM) and atomic force microscopy (AFM) imaging, the lateral width of the fibrils is typically between 15 nm and 200 nm.[36,42]

2.2.1 TEMPO Oxidized Cellulose Nanofibrils

The nanoscaled cellulose that is the main building block used for materials construction in this dissertation, is TEMPO CNF. In TEMPO-mediated oxidation, primary hydroxyl groups of cellulose at C6 positions are selectively converted to sodium C6-carboxylate groups through C6-aldehydes by a sequential reaction of the TEMPO radical and NaClO oxidant with NaBr for regenerating TEMPO at pH 10-11 (Figure 5b). In other terms, the glucose units in cellulose are oxidized to sodium glucoronate units. Consequently, the negative charge on fibril surfaces introduced with the carboxylate groups forces the fibrils apart due to electrostatic repulsion. At a carboxylate content of ca. 1.5 mmol g^{-1} only mild mechanical treatment is needed to convert the oxidized cellulose fiber dispersion into transparent and highly viscous nanocellulose gels with solid content of a few percentages. Moreover, a TEMPO/NaClO/NaClO$_2$-based oxidation at close to neutral pH conditions has been developed, whereby discoloration and depolymerization are avoided and the resulting fibrils are free of aldehydes, which otherwise are present when alkaline reaction conditions are used[8,43].

Individual TEMPO CNFs are 3-4 nm wide and several micrometers long, see AFM topography image in Figure 5b. The dimensions yielding transparent assemblies along with the charge introduced with carboxyl groups set TEMPO oxidized CNFs apart from other nanoscaled cellulosic materials.[8,44,45] TEMPO-mediated oxidation of cellulose is an efficient pre-treatment concept for fibrillation and yields individual and almost monodisperse nanofibrils after rather low-energy mechanical disintegration. The energy consumption of fibrillation in the case of TEMPO oxidized CNF is 2 MWh/tonne[8], which is significantly lower in comparison to CFN production by mechanical disintegration (27 MWh/tonne – 70 MWh/tonne[46] and similar to other pre-treatment methods, such as enzymatic pre-treatment (~1.8 MWh/tonne)[42].
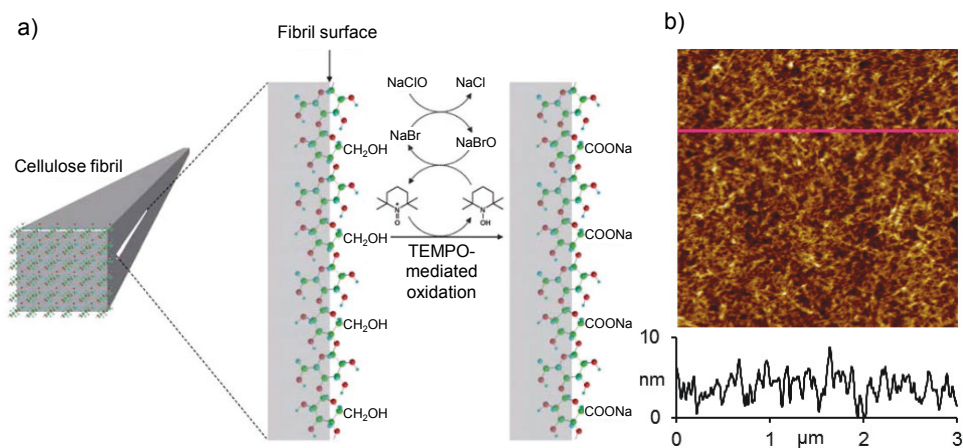
Figure 5. a) Schematic illustration of selective TEMPO mediated oxidation of C6 primary hydroxyls on fibril surfaces by the TEMPO/NaBr/NaClO-system. Schematic illustration adapted from Okita et al.[20] b) A typical 3 × 3 μm topographic AFM image with height scan of TEMPO CNF fibrils. The pink line represents the height scan underneath the topographic image.

2.3 Film Assemblies

One of the defining characteristics of CNFs is their inherent tendency to form strong and transparent/translucent films. Film formation tendency is a result of the strong interaction between the numerous hydroxyl groups on fibril surfaces upon drying.[47,48] Relevant to the present work, the physical thickness of CNF films can be tailored over a wide range to fit the designated purpose. Ultrathin films add a fundamental aspect to the physical chemistry of CNF, enabling precise detection and interpretation of molecular-scale phenomena occurring at interfaces. On the other hand, macroscopic films are needed when true applications such as packaging materials, displays and membranes are considered. Such films are also utilized when solving the application specific performance-related challenges.

2.3.1 Ultrathin Films

Supported ultrathin films are very thin (generally less than 100 nm thick)[49,50] films with de-fined chemical compositions and morphologies and smooth surfaces[49]. Today, the method-ology of preparation and analysis of such model surfaces is well-established in the fields of polymer chemistry and organic chemistry. A versatile range of ultrathin film samples can be prepared by several deposition techniques, such as Langmuir-Blodgett deposition[51], layer-by-layer assembly[52], spincoating[53], and combinations thereof. Several of these methods have been adapted for preparation of ultrathin films of nanoscaled cellulose[54,55].

The reasoning behind supported ultrathin films especially in the context of CNF is multi-fold. Ultrathin films provide a means to study behaviors at interfaces – where phenomena related to nanoscaled particles mostly occur. On the other hand, in terms of chemical com-position and size CNF is a heterogeneous moisture-sensitive biomaterial and, as such, a dif-ficult subject for precise research. Hence, ultrathin films with defined chemical character and morphology, as well as confined space for dimensional changes provided by the substrate, simplify detection and interpretation of complex phenomena, e.g. swelling and sorption. Moreover, certain contemporary surface-sensitive techniques, such as quartz crystal micro-balance with dissipation monitoring (QCM-D)[56-59] and surface plasmon resonance (SPR)[60] are suited for supported ultrathin films. Compared to macroscale materials, ultrathin films coupled with surface-sensitive analytical methods have unquestionable advantages with re-gard to sensitivity and providing explicit information about material interfaces.

2.3.2 Macroscale Films

Differing from supported ultrathin films, macroscale CNF films are self-standing assemblies with thickness at least in the micrometer range. Macroscale cellulose nanofibril films are pro-duced by a multitude of methods, with solvent casting[61-63] and filtration-based methods[64-66] most prominent, although freeze-drying has been suggested[67]. The main process step in the production of macroscale CNF films is dewatering which can be assisted by over-pressure filtration[64] or heat treatment.

In air, CNF films display typical mechanical characteristics of a brittle plastic-like material with high tensile strength (100-200 MPa), high elastic modulus (5-10 GPa) and low strain at break (<10%)[68]. For TEMPO CNF, tensile strength of over 300 MPa has been reported[43]. Overall, mechanical property values vary notably in literature, which probably derives from complex chemical composition of the raw material, the wide range in pre-treatment techniques, fibril size and size distribution, the method applied for film-forming, as well as humidity. The mechanical strength properties of pure CNF films are lost in aqueous environments, as water molecules penetrate between the fibrils, causing significant swelling and disintegration of the film.

Similarly to various natural polymer films with high hydroxyl group densities, CNF films are grease resistant and show low oxygen permeability[7], as non-polar grease and oxygen exhibit only weak interaction with the polar hydroxyl groups. This makes CNF an interesting material for, e.g., packaging applications, where good barrier properties are required. However, at high humidity levels the barrier properties are deteriorated as water is able to penetrate the film and change the fine structure. Hence, numerous strategies toward hydrophobizing CNF film surface have been proposed[68,69] to overcome moisture-related challenges.

2.4 Modification of CNF Film Assemblies

Many high performance applications cannot rely solely on the inherent material properties of nanoscaled cellulose and further tuning of e.g. the hydrophilic character is often desired. Reactivity of nanoscaled cellulose arises from the high specific surface area and availability of numerous hydroxyl groups suitable for chemical reactions. The feasible reaction pathways are those of alcohols, including esterifications[70], etherifications[71], and oxidations[8] whereby functional groups or polymers are covalently attached to the hydroxyl groups of CNF or CNC. In addition, non-covalent-modifications[72] for nanoscaled cellulose have been developed. In the case of TEMPO CNF, carboxyl groups on the fibril surfaces further diversify the possible

chemical modification routes. Hence, TEMPO oxidation has been recognized as an ideal approach to increase the reactivity of nanoscaled cellulose.[45] For a summary of proposed modification routes for nanoscaled cellulose the reader is referred to reviews by Habibi[73] and Eyley & Thielemans[74].

2.4.1 Wet-Strength Enhancement

Macroscale assemblies made purely from nanoscaled cellulose, including macroscale CNF films, suffer from poor water stability limiting their use in aqueous environments. In water, CNF films swell and eventually disintegrate. A phenomenological treatise of the water interactions of nanoscaled cellulose and the underlying reasons related to instability of the films in water is given in Chapter 3.

Most approaches developed to overcome poor water tolerance involve chemical crosslinking of the fibrils. For instance, Mertaniemi et al.[75] suggested the crosslinking of CNFs by glutaraldehyde, reaching wet tensile strengths of 111 ± 20 MPa. Recently, a photo-cross-linking approach based on aminated benzophenone grafted onto TEMPO CNF was applied to enhance the wet strength of films[76] and filaments[77], reaching wet tensile strengths of 103 MPa. Additionally, CNF crosslinking with poly(acrylic acid)[78] has been shown to render water stable CNF based membranes. The strategies suggested for wet strength enhancement in the literature are versatile and generally applicable to 1D, 2D and 3D assemblies.

2.4.2 Interfacial Surface Modification

In principle, most chemical modifications for nanoscaled cellulose can be performed in dispersion form (i.e. surfaces of individual nanoscaled particles are subject to modification). Water, the natural medium of CNFs, can hinder reactivity and tedious solvent exchange procedures to non-polar solvents are required to enable the introduction of new organic functionalities. Even with cellulose compatible solvents, in which the high specific surface area of CNF can be retained, the removal of reagents and side-products can be challenging, requiring, e.g. prolonged dialysis, as nanoscaled materials thwart filtration and other conventional

purification procedures. Therefore, a more efficient route to circumvent the challenges of nanoscaled cellulose modification is to proceed by preparing a water/solvent stable macroscopic structure and subsequently perform interfacial chemical reactions directly on the surface of the structure. This approach results in surface-only modification and streamlines the purification of the product to simple rinsing.

Surface-modifications on cellulosic film surfaces have been successfully performed in gas-phase reactions[79] and in cellulose compatible solvents[68]. Filpponen et al. demonstrated a generic "double-click" surface modification of cellulose, whereby carboxymethyl cellulose functionalized with azide or alkyne functionality was adsorbed on a cellulosic surface, followed by reaction with a complementary click unit[80]. Moreover, in a recent study by Kontturi et al.[81] cellulosic films were hydrophobized by non-covalent adsorption of hydrophobic poly(styrene) or poly(trifluoroethylene) from aprotic solvents.

The reaction efficiency in interfacial surface modification can be improved by activating the CNF surface by using a commonly applied cleaning method based on UV radiation in the presence of ozone (UV/O_3)[82]. UV/O_3 treatment removes organic contaminants from the surface by decomposing them into volatile organics by cleaving bonds like C-C, C-H and O-H. Thereby CNF surfaces are activated and become more hydrophilic. Demonstrated by a simple silylation reaction on the CNF surface, the degree of surface substitution calculated based on the relative amount of silicon on the CNF film surface showed a fourfold increase from 0.07 to 0.26 in reaction efficiency due to the UV/O_3 treatment.[82]

3. Water Interactions of Nanoscaled Cellulose

All living plants are comprised of substantial amounts of water, although virtually none of the plant components, including cellulose, dissolve in water. Here, the peculiar relationship is scrutinized from the perspective of nanoscaled cellulose, with focus on its amphiphilic character, swelling, water vapor uptake, and water transport of assemblies made thereof.

3.1 Hydrophilic Nanomaterial with Amphiphilic Character

The large surface area of CNFs[5,6,9] carries an enormous amount of hydroxyl groups with high affinities toward water. In the case of TEMPO CNF, hydrophilicity and hygroscopicity are further promoted by the presence of carboxyl groups – at high humidities dissociated carboxylic acid groups show an even higher affinity toward water compared to hydroxyl groups.[83] Piringer et al.[83] report molar water content of 0.5 and 0.75 at 50% RH and 70% RH, respectively, for hydroxyl groups. For dissociated carboxyls, the respective molar water content values are 2.1 and 4.2. For CNF films, water contact angle values of 30-50° are typical[62], although values as low as 10° have been reported[82].

It is somewhat counterintuitive, that rather than exhibiting pure hydrophilicity, cellulosic materials essentially display amphiphilic character arising from inherent structural anisotropy[84,85]. Hydroxyl groups are located at equatorial positions of D-anhydroglucopyranose rings, whereas hydrogen atoms are located at axial positions. Consequently, the equatorial plane exhibits hydrophilicity, whereas the axial plane displays hydrophobic properties[84-86]. Nanoscaled cellulosic materials (CNC, CNF, TEMPO CNF) have also been shown to adsorb and self-assemble to the oil/water interface, stabilizing oil-in-water emulsions[87-89]. Similar tendencies have also been shown in foam systems for air/water interfaces[90]. Although the dominating characteristic in cellulose is hydrophilicity, the underlying amphiphilic features highlight the multidimensional nature of cellulose as a complex and versatile biomaterial. Amphiphilicity also at least partly explains the insolubility of cellulose in water, whilst bearing in mind the role of hydrogen bonding and the rigidity of the cellulose chain[91,92].

3.2 Swelling in Aqueous Environments

Swelling derived from hydrophilicity of (nano)cellulosic materials has significant implications for all cellulosic materials and applications. In the context of nanoscaled cellulose assemblies it should be noted that the fibrils/crystals do not swell, but water penetrates in between fibrils causing the enlargement of interfibrillar space. In contrast, amorphous entities, such as hemicellulose between the fibrils and on fibril surfaces swell readily[93,94].

Common methods to evaluate swelling and water uptake include the water retention value[95] and thermogravimetric analysis[96,97]. Recently, research has largely been expedited by the development of contemporary surface analytics, e.g. QCM-D[56-59], SPR[60], and SE[98], that can provide unprecedentedly precise information about swelling under controlled environments. Thereby knowledge of the peculiar swelling behavior of cellulose and dependence on external factors is constantly expanded and focused into a comprehensive view on cellulose-water interactions and the underlying molecular mechanisms.

The effect of crystalline ordering and mesostructure of the films on liquid water uptake was clarified by Aulin et al.[55]: amorphous films prepared of cellulose dissolved in LiCl/DMAc (crystallinity index 14.7%) exhibited the highest water uptake (48%), exceeding cellulose nanocrystals (crystallinity index 87%) and Langmuir-Schäfer deposited films (crystallinity index 63%) with water uptake of 24% and 7%, respectively. The results suggested that the water uptake behavior of cellulosic films is determined by the molecular structure of the cellulose and the mesostructure of the films.[55] Moreover, using surface-sensitive methods, Ahola et al.[50] have demonstrated that swelling and water uptake depend on the charge of the cellulosic material, with higher charge generally corresponding to a higher degree of swelling as also demonstrated for cellulosic materials in bulk[99]. Olszewska et al.[100] demonstrated that the swelling of cationic 2,3-epoxypropyl trimethylammonium chloride functionalized CNF showed pH dependency in aqueous media. At pH 4.5 partial protonation of the carboxyl groups caused the cationic CNF to exhibit a swelling of 303 wt.-%, which was considerably higher compared to swelling of 137 wt.-% at pH 8.0. At pH 4.5 the film behaved as a polyelectrolyte gel, expelling water upon increase of the electrolyte concentration in the range from 1 mM to 100 mM of NaCl.

Reid et al.[101,102] proposed that water uptake of CNC thin films occurs through two distinct steps: capillary-action-driven rapid penetration of the solvent (water) through the porous structure, followed by swelling induced by the solvent forcing the CNCs apart and widening the intercrystalline spaces. The maximum spacing between CNCs in the swollen state has been reported to be 1.2-1.6 nm, which corresponds to 4-6 molecular layers of water. In a former study, Reid et al.[102] reported that the films of CNC contain 35 wt.-% of water in the swollen state – a significantly lower value compared to 74 wt.-% for CNC and 70-85 wt.-% for CNF as reported by Kittle et al.[103] and Kontturi et al.[104], respectively. Currently there is no solid explanation for the discrepancies in the literature highlighting the complex nature of the biomaterial. However, CNF films are able to swell more due to the flexibility of the fibrils, whereas in rigid films made from stiff CNCs, water uptake is limited to intercrystalline spaces. In the future, new approaches such as computational quantitative models[105,106] could complement surface-sensitive methods to provide even more detailed information on water uptake and swelling behavior of nanoscaled cellulosic assemblies beyond state-of-the-art.

3.3 Water Vapor Sorption into Films

Similarly to swelling, water vapor sorption on cellulosic materials has been extensively studied within the past century[107-111] due to its significance for, e.g. papermaking and food preservation. The vast majority of the published studies related to water vapor sorption of nanoscaled cellulosic assemblies have been conducted using bulk methods, mainly the Dynamic Vapor Sorption (DVS)[110,111] as well as the manometric approach[112,113]. It is well known that, similarly to most hydrophilic biomaterials, nanoscaled cellulose including CNC[108,109] and CNF[111] exhibit sigmoidally shaped moisture sorption isotherms.

Several studies have investigated the maximum sorption capacity of cellulosic thin films (CNC, CNF, amorphous cellulose) at hydrated state (97% RH) and typically values of ~0.3 g g^{-1} are reported[94,109,115]. Moreover, using surface-sensitive analytics, Tenhunen et al.[94] demonstrated that CNF thin films with high xylan (glucuronoxylan) content demonstrate a stronger response upon exposure to humid air in comparison to CNF with low xylan content

– a difference that was not apparent in DVS measurements. The results indicate that on macroscale the significance of xylan diminishes and the water vapor uptake is dominated by the fibrillar network.

Recently, polarized light microscopy digital image correlation[108, 114] was used for studying dimensional changes induced by in-plane hygroscopic swelling in CNC films. A clear difference between self-organized and shear-oriented films was detected: whereas self-organized films showed isotropic swelling and a coefficient of hygroscopic swelling of 0.04 %strain/%C, shear-oriented films exhibited anisotropic swelling with 0.02 parallel and 0.3%strain/%C perpendicular to CNC alignment.

3.4   Sorption Models

Research on water vapor and gas adsorption at various interfaces has long and sturdy roots in the areas of, e.g. heterogeneous catalysis[116,117] and chromatographic analysis[118]. Sorption isotherms are often fitted with sorption models, to better understand the physicochemical mechanisms and underlying phenomena and to predict the behavior of the materials. The quantification of gas adsorption in these fields of study is typically achieved by the classical Brunauer-Emmett-Teller (BET) theory[119] or its modern variants[120,121]. Sorption of solvents to polymeric materials, has been interpreted using dual sorption models[122], e.g. combinations of the classical Langmuir theory[123], Henry's Law[124] and the Flory-Huggins mixing theory[125]. Water vapor sorption into cellulose has been quantitatively interpreted using models, such as the Park's model[111], the Guggenheim-Anderson-de Boer (GAB) model[111] and the Hailwood-Horrobin model[126].

Hernandez et al.[127] proposed combining of the classical Langmuir and Flory-Huggins models with the clustering term into an additive model to describe the behavior of amorphous polyamide. The Langmuir – Flory-Huggins – clustering model is interesting also from the nanoscaled cellulose perspective, because in addition to its simplicity, its additive nature enables the fitting of the terms within the limits of the most relevant RH% zones of the isotherm.

Langmuir adsorption describing specific binding of gas molecules to solid surfaces is defined by equation 1:

$$V_L = \frac{Ka}{1+Ba}$$ (1)

where V_L is the fraction of water in the film due to Langmuir type adsorption, K represents the concentration of the specific sorption sites, B is the affinity of water for these sites and a is the water activity.[123,127] Values of a are the ratio of partial pressure of water vapor divided by the saturation vapor pressure and were considered to be equal to % RH divided by 100.

The Flory-Huggins equation, originally developed for dissolution of high molecular weight polymers in terms of fractions of solvent and solvent activity (a) can be expressed as follows[125,127]:

$$\ln a_1 = \ln V_{FH} + (1 - V_{FH}) + \chi (1 - V_{FH})^2$$ (2)

where a is the water activity, χ is the Flory-Huggins interaction parameter and V_{FH} is the Flory-Huggins population or fraction of water associating with the film.

Moreover, the clustering term in the Langmuir – Flory-Huggins – clustering model can be expressed by equation 3:

$$V_C = a^n$$ (3)

where V_c represents the fraction of water associated with the film due to clustering, a is water activity and n describes the number of water molecules associated with each cluster[111,128]. The total fraction of water (V) absorbed in the solid can be predicted by the additive Langmuir – Flory-Huggins – clustering function:

$$V = V_L + V_{FH} + V_C = \frac{Ka}{1+Ba} + f(a,\chi) + Ca^n$$ (4)

The fitting of the Langmuir-Flory-Huggins-clustering model can be performed in three parts to obtain physicochemically most relevant estimates for the parameters.[127] Hernandez

et al.[127] used nonlinear regression to solve the Flory-Huggins interaction parameter (χ) in the 30-70% RH range, where it plays the most important role in water sorption. Following this, the Langmuir coefficients were solved using non-linear regression, yielding multiple mathematical solutions due to the underdefined nature of equation 1. Furthermore, the clustering coefficient was also solved by a nonlinear regression method. As shown by Hernandez et al.[127], the additive nature of the model enables accurate fitting of the data to the sorption isotherm where the terms are physicochemically most relevant.

3.5 Transport of Water

To predict and to control water interactions of assemblies built from nanoscaled cellulose building blocks, an understanding of kinetic and thermodynamic factors is required. Kinetics is related to how fast water moves within the structure upon sorption and it is described by the diffusion coefficient (D). From Fick's Second Law it can be derived, that when a porous solid film is placed in contact with a gaseous phase containing a sorbate, the sorbate is taken up by the solid film[129-131] as described in equation 5:

$$\frac{\delta c}{\delta t} = \frac{\delta}{\delta x}\left(D\frac{\delta c}{\delta x}\right) \tag{5}$$

The mathematical model for transient uptake under the assumption of Fickian diffusion in the case of a film, assuming the diffusion coefficient, D, to be constant, can be expressed by equation 6[132]:

$$\frac{m_t}{m_\infty} = 1 - \sum_{n=0}^{\infty}\frac{8}{(2n+1)^2\pi^2}e^{\left(\frac{-D(2n+1)^2\pi^2 t}{l^2}\right)} \tag{6}$$

where t embodies time, m_∞, m_t, and m_0 are the mass values of the TEMPO CNF thin film at equilibrium (at each %RH level) and at t=t and t=0, respectively, and l signifies the thickness of the thin film. The diffusion model (equation 6) assumes that the rate of water vapor uptake is controlled by diffusion into the interior of the solid film[131]. Simplifying equation 6

using the first term of the series of the right hand side results in equation 7, that can be solved numerically for the diffusion coefficient (D)[130,132]:

$$-\frac{1}{\pi^2} ln\left[\frac{(m_\infty - m_t)\pi^2}{8(m_\infty - m_0)}\right] \times l^2 = Dt \tag{7}$$

where t marks the time, m_∞, m_t, and m_o are the mass values at equilibrium and at t=t and t=0, respectively, and l represents the thickness of the film.

Whereas the diffusion model (equation 7) assumes transfer of water molecules solely into pores, the effective diffusion model (equation 8), based on Newman's solution to Fick's Second Law[131] postulates diffusion into the pores of the solid film and the accumulation of a (liquid) water molecule layer on top of the film[131,133]:

$$\frac{m(t)}{m(\infty)} = 1 - \sum_1^\infty \frac{2\alpha^2}{\beta^2(\alpha(\alpha+1)+\beta^2)} e^{\left(-\beta\frac{Dt}{L^2}\right)} \tag{8}$$

where β are the roots of the equation $\alpha = \beta sin\beta$, L is thickness divided by 2 and α is the ratio of diffusion into the pores to accumulation of (liquid) water on top of the film. The diffusion model and the effective diffusion model can be used to fit sorption isotherms to gain insight into the movement and accumulation of water within the film. Together with solubility, diffusion is a necessary parameter for calculation of permeability (P) commonly used to describe membrane performance.

Similarly to diffusion, solubility coefficients (S) at given RH% levels can be solved from mass uptake data using equation 9:

$$S = \frac{m_\infty}{m_p \times p_v^0 \times a} \tag{9}$$

where m_p represents the mass of the dry thin film, p^o_v is the saturation vapor pressure at 23 °C and a is water activity. By combining the diffusion and solubility coefficients as depicted in Equation 9, permeability of water vapor can be calculated[130,132] (equation 10):

$$P = D \times S \tag{10}$$

3.6 CNF as Membrane Material

In the light of its renewability, hydrophilicity and water transport capability, CNF and CNF films possess many of the desired properties for a membrane material. Membranes are selective, semi-permeable barriers used for recovery, purification and separation as an established part of processes across disciplines and industries.[134] Membranes play an integral role in the manufacture of dairy products, recovery of electro-painting-baths in the automotive industry as well as in kidney disease treatment by hemodialysis. Furthermore, millions of people worldwide depend on membranes for production of clean water. A variety of materials with different and tailorable character is required to rise to the wide range of practical challenges across different membrane application areas and to function in, e.g., aqueous, organic or gaseous operating environments. Membranes can be classified according to their performance characteristics, such as molecular weight cut-off (MWCO), morphology or material. Existing commercial membranes are typically prepared from solution by solvent evaporation or by extrusion of melted polymer, possibly combined with additional processing steps, such as stretching, leaching or sintering from a synthetic polymer, for example polyethylene terepthtalate, polyamide, polysulfone and biobased cellulose acetate.[134]

Films from nanoscaled cellulose as membrane materials offer a new material concept for membrane production and processes. Aside from their biobased origin, films prepared thereof are produced using an organic solvent-free manufacturing process. Importantly, pollutants including nitrates[135], viruses[136] and metal ions[137,138] can be captured by films based on nanoscaled cellulose. The recent entries on the use of CNFs and other nanoscaled cellulosic particles as membrane building blocks and as the main active components represent the new front of biobased and nanoenhanced materials for water and air purification.

4. Experimental

Papers I and II made use of TEMPO CNF in the form of ultrathin films for fundamental studies as approached through surface-sensitive techniques, principally QCM-D and SE. In Papers III-V surface sensitive and bulk methods were used together in a complementary way to characterize tailored macroscale TEMPO CNF films and to demonstrate their performance as membrane materials. Here, the materials, main experimental procedures, and techniques used to carry out the studies are described, with a more detailed description available in Papers I-V.

4.1 Materials

4.1.1 TEMPO Oxidized CNF

For production of TEMPO CNF, never-dried, bleached softwood pulp was obtained from a pulp mill in Finland. TEMPO, sodium bromide (solid) and 10% sodium hypochlorite (aqueous) were obtained from Sigma-Aldrich. Sodium hydroxide solution (0.1 M) was received from Fluka Analytical. All reagents were of analytical grade and used as received unless stated otherwise. Softwood pulp was TEMPO oxidized according to the well-established procedure of alkaline oxidation with hypochlorite, catalyzed by TEMPO according to a previously published protocol[45]. As an exception, in Paper III TEMPO oxidization was performed according to TEMPO/NaClO/NaClO$_2$-system[43] to rule out aldehyde-based reactions in further modifications.

TEMPO oxidized pulp was fibrillated using a high pressure fluidizer, Microfluidics M-110EH-30 (Microfluidics Int., USA), equipped with two Z-type chambers. The chambers had diameters of 400 μm and 100 μm and the pulp was passed through the fluidizer two times at 1850 bar operating pressure to obtain TEMPO CNF with a final consistency of approximately 1 wt.-%. Charge of the oxidized pulps was 0.836-1.13 mmol g^{-1} as determined with a standard

conductometric titration method[139]. Neutral sugar composition as analyzed using high performance liquid chromatography after acid hydrolysis[140] showed that the neutral sugar content of hemicellulose in the TEMPO CNF used throughout this dissertation was 8% (Table 1).

Table 1. Neutral sugar composition of TEMPO CNF (**Papers I and II**).

Glucose (%)	Galactose (%)	Mannose (%)	Arabinose (%)	Xylose (%)	Rhamnose (%)	Fructose (%)	Total (%)	Others[a] (%)
64.0	0	2.1	0	6.2	0	0	72.3	27.7

[a] Others predominantly consists of glucuronic acids originating from TEMPO oxidized cellulose nanofibrils.

4.1.2 Polymers

Poly(vinyl alcohol) (PVA) was used for wet-strength enhancement of CNF films by crosslinking in Papers III and IV. Two different grades of PVA were used: partly hydrolyzed PVA (degree of hydrolysis 88%) (Mowiol 40-88, M_w 205 000 g mol^{-1}, DP 4200) and fully hydrolyzed PVA (degree of hydrolysis 98%) (Mowiol 56-98, M_w 195 000 g mol^{-1}, DP 4300) purchased from Sigma-Aldrich. Before use, both grades were dissolved in water (5 wt.-% concentration) at 95 °C during at least 3 hours under constant stirring.

To introduce a thermoresponsive polymer to CNF films in Paper IV, amine-terminated poly(N-isopropylacrylamide) (M_n 5500 g mol^{-1}) purchased from Sigma-Aldrich was used. Branched cationic poly(ethylene imine) (PEI, 30 wt.-% in water, M_w 70 000 g mol^{-1}) used as an anchoring polymer in Papers I and II was purchased from Poly Sciences Inc., Warminster, PA, USA).

4.1.3 Thin Film Supports

QCM-D sensor surfaces were used as thin film supports in Papers I and II. AT-cut gold sensors with a fundamental resonance frequency, f_o, of 5 MHz and a sensitivity constant, C, of 0.177 mg m^{-2} Hz^{-1} as reported by the supplier, were purchased from Q-Sense AB, Gothenburg, Sweden.

4.2 Methods

4.2.1 Film Preparation and Modification

Supported TEMPO CNF Thin Films

For fundamental studies in Papers I and II, supported thin films of TEMPO CNF needed for surface-sensitive analytics were prepared according to the slightly modified procedure described by Eronen et al.[140] In brief, TEMPO CNF suspension was diluted to a concentration of 0.15 wt.-% using milli-Q water and sonicated using a Branson Digital Sonifier (400 W; 20 kHz) at 40% amplitude for 2 minutes. Gold coated QCM-D sensor surfaces were rinsed with water, dried with nitrogen gas, and cleaned using UV/O$_3$ (Bioforce Nanosciences, CA) for 10 minutes. The supports were coated with 1 mg ml^{-1} PEI (anchoring polymer) by drop casting lasting 30 minutes and heat treating at 80 ˚C for 10 minutes to ensure attachment. Furthermore, 200 μl of TEMPO CNF was dispensed onto the PEI-coated sensors and spincoated (WS-400BZ-6NPP/Lite, Laurell, North Wales, PA, USA) at 3000 rpm for 3 minutes followed by annealing for 10 minutes at 80 ˚C to ensure fibril attachment.

Macroscopic TEMPO CNF Films with Enhanced Wet Strength

Papers III and IV were based on macroscopic TEMPO CNF films. The wet strength of the CNF films was enhanced by crosslinking with PVA. To prepare the self-standing films, TEMPO CNF suspension was diluted to 0.3 wt.-% and sonicated using Branson Digital Sonifier (400 W; 20 kHz) at 40% amplitude for 5 minutes to form a homogeneous dispersion. PVA at 0.3 wt.-% concentration was added to TEMPO CNF in 10:90 and 25:75 weight ratios. In Paper III the crosslinking reaction was assisted by adjusting the pH of the mixture to 4 to facilitate crosslinking by esterification. The mixtures were poured into poly(styrene) Petri dishes and dried (at 23°C/50% RH) for several days before use.

Interfacial Surface Modification of TEMPO CNF Films for Thermoresponsive-ness

In Paper IV, macroscale PVA crosslinked TEMPO CNF films with enhanced wet strength were further modified with poly(NIPAM) to introduce thermoresponsiveness to the material. After UV/O$_3$ treatment[82], the films were subjected to esterification followed by poly(NIPAM) attachment.

For the esterification step, the films were submerged in ethanol with a catalytic amount of concentrated H$_2$SO$_4$ (0.145 ml 98 % H$_2$SO$_4$/100 ml ethanol) and the reaction was continued at room temperature under mild stirring for 24 hours. Films were washed in three steps with ethanol and finally they were dried in air and activated again using the UV/O$_3$ cleaning protocol.

To graft the thermoresponsive polymer onto the film surface, 1 g of amine-terminated poly(NIPAM) was dissolved in 100 ml of ethanol or ethanol-water mixture with 3:1 volume ratio at room temperature. Esterified films were submerged in the solution and the reactions were carried out for 24 hours at room temperature or at 50 °C. Films were washed in three steps using ethanol to remove unreacted poly(NIPAM).

4.2.2 Water Vapor Sorption Analysis

Quartz Crystal Microbalance with Dissipation Monitoring (QCM-D)

Water vapor uptake of TEMPO CNF thin films with respect to mass (Papers I and II) was probed using the E4 QCM-D instrument equipped with a QHM 401 humidity module (Q-Sense AB, Gothenburg, Sweden). The surface-sensitive QCM-D instrument is designed for in-situ studies of mass changes taking place at solid-liquid or solid-gas interfaces by monitoring the changes in resonance frequency of the oscillating sensor crystal.

A piezoelectric quartz sensor between two electrodes oscillates at a specific fundamental resonance frequency, f_o, and its overtones as pulsed electric field (AC voltage) is applied. The resonance frequency changes as the total mass of the film on the surface of the sensor increases or decreases. When the film is evenly distributed, rigidly adhered, fully elastic and has a small mass in comparison to the mass of the sensor crystal, the change in frequency is

directly proportional to the change in areal mass and can be calculated according to the Sauerbrey equation (equation 11)[142]:

$$\Delta m = -C \frac{\Delta f}{n} \qquad (11)$$

where $\Delta f = f - f_o$ is the change in resonance frequency, C is the sensitivity constant of the sensor and n represents the measurement overtone number (n = 1, 3, 5, 7, 9, 11).

When voltage is cut off, the oscillation gradually decreases. The resonance amplitude attenuates due to the frictional losses (dissipation of energy) with a decay rate, which is dependent on the viscoelastic properties of the layer adhered on the sensor surface. The attenuation of the amplitude, i.e. dissipation of energy, D, is a measure of viscoelastic properties of the layer as described in equation 12:

$$D = \frac{E_{dissipation}}{2\pi E_{storage}} \qquad (12)$$

where $E_{dissipation}$ is the dissipated energy and $E_{storage}$ is the total energy stored during one oscillation cycle in the oscillator. A fully elastic and rigid film displays $\Delta D \leq 1 \times 10^{-6}$, and ΔD and Δf overtones that do not spread significantly. For more details on the interpretation of QCM-D data, the reader is referred to literature[56-59].

Areal Mass of TEMPO CNF Thin Film in Dry Air as Measured by QCM-D

Prior to water vapor uptake measurements presented in Papers I and II, the initial areal mass of the spincoated TEMPO CNF thin film was determined. Firstly, the frequency change of the pristine QCM-D sensor was measured in air using a QHM 401 humidity module (23 °C, air flow rate 0.1 ml min^{-1}) at 6% RH. Similarly, the frequency change in air was measured after spincoating TEMPO CNF on the sensor surface. Prior to collecting the TEMPO CNF frequency change values, the sensor was allowed to stabilize at 6% RH inside the humidity cell for at least 13 hours in order to attain stable and repeatable conditions with respect to the

thin film's initial moisture content[94]. Finally, the frequency data was stitched together using the QTools Software and the third overtone (15 MHz, f_0 = 5 MHz, n = 3) was used for quantitative areal mass calculations according to the Sauerbrey equation (equation 11).

Humidity Measurements by QCM-D and Determination of Mass Fractions

Typically the QCM-D measurements involving soft matter (e.g. adsorption, desorption and swelling studies) are performed in liquid phase. Here, a specifically designed humidity module for vapor sorption was utilized for studying water vapor sorption directly at gas-solid interface. Figure 6a shows typical changes in frequency (Δf) and dissipation (ΔD) over incrementally increasing RH% as a function of time as detected for TEMPO CNF thin films. Changes in % RH were achieved by passing saturated salt solutions and milli-Q water through the humidity module at 0.1 ml min^{-1} rate for 30 minutes at 23 °C. The 100% humidity step is omitted in the calculations, as passing Milli-Q water (100% RH) through the humidity module could cause condensation effects inside the measurement chamber. Similarly to mass determination in dry air, the QTools Software was used for quantitative calculations based the Sauerbrey equation (equation 11).

Mass fractions of water were calculated by dividing the mass increase due to water vapor during the humidity measurement by the total mass of the TEMPO CNF thin film system. Moreover, the viscoelastic behavior of thin films of TEMPO CNF was evaluated from ΔD. Each measurement was repeated three times and average values were used in calculations.
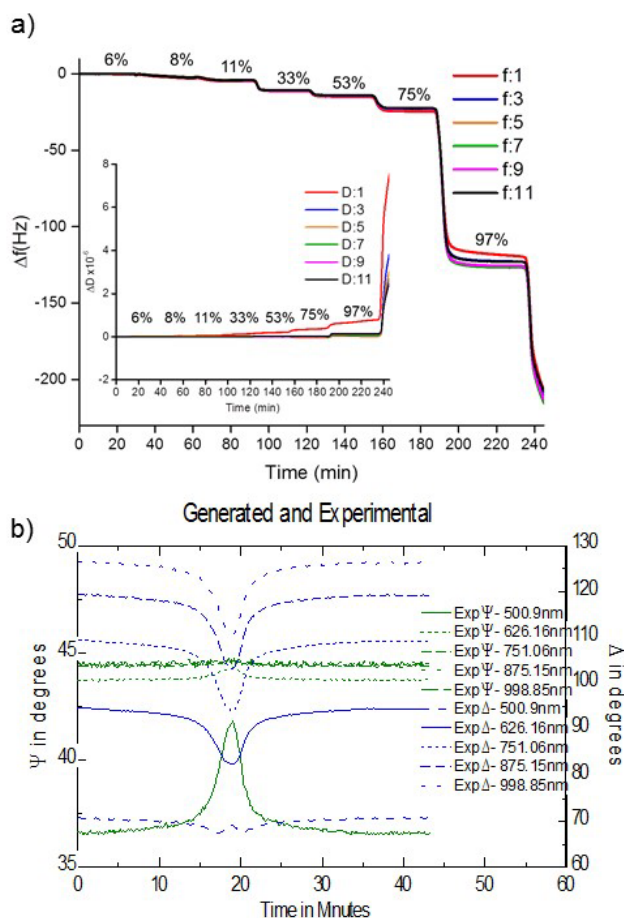
Figure 6. Typical responses detected for TEMPO CNF thin film by a) QCM-D and b) SE, upon exposure to changing relative humidity (% RH) in water vapor sorption measurements in **Papers I and II**.

Spectroscopic Ellipsometry (SE)

Spectroscopic Ellipsometry (SE) is an optical surface measurement technique based on the polarization of light. It is used for determining optical constants and film thickness with sub-nanometer precision. In the context of the fundamental studies performed in this dissertation, SE is used to monitor changes in refractive index and thickness evolution as a function of relative humidity of the entire multicomponent thin film system, including TEMPO CNF, water vapor and air. SE detects the change in the state of polarization of light (phase and amplitude) upon reflection from

a surface. The quantity being tracked is the complex reflectance ratio (ρ), denoted as the ratio of p (r_p) and s (r_s) components of the reflected light as shown in equation 13:

$$\rho = \frac{r_p}{r_s} = \tan(\Psi)\, e^{i\Delta} \hspace{4cm} (13)$$

where Ψ is the amplitude ratio upon reflection and Δ is the phase shift upon reflection. Based on Ψ and Δ, physically meaningful values, such as the thickness of the film, can be inferred according to Fresnel equations using ideal layer models, e.g. the classical Cauchy model for transparent (nano)materials.[143,144]

Water vapor sorption measurements by SE in Papers I and II were performed on a UV-Vis (λ = 500 - 998.85 nm) variable angle spectroscopic ellipsometer (Vase-2000U, Woollam Inc., Lincoln, NE, USA) equipped with a humidity chamber and stepless humidity control adjustment. Supported thin films of TEMPO CNF were placed on a sample plate inside the humidity chamber and a beam of polarized light from the SE was focused on the sample and aligned with the light detector. The initial theoretical thickness and refractive index were determined by conducting an initial spectroscopic scan and applying the classic Cauchy model, which was validated by fitting measured refractive indices to model data (mean square error-value < 4).

Humidity Measurements by SE and Determination of Thickness Fractions

To carry out the dynamic sorption measurements, a 3 l min^{-1} flux of air containing a fixed partial pressure of water was continuously injected into the humidity chamber, while continuously monitoring the real *in-situ* % RH inside the humidity chamber. Incremental 2% RH humidity steps lasting 20 s were used throughout the dynamic measurements. Data analysis based on using the Cauchy model were performed using Wvase32 software. A typical dynamic scan raw data is shown in Figure 6b. The raw data obtained using SE does not indicate strong hysteresis.

The refractive index (RI) and thickness of the film as a function of relative humidity was recorded with the SE system. Here it should be noted, that SE detects the refractive index and thickness evolution of the entire multicomponent thin film system, including TEMPO CNF, water vapor and air. Optical thickness, which is defined as the natural logarithm of

incident to transmitted radiant power through a material (IUPAC), was calculated by multiplying thickness with refractive index values.

Thickness fractions of water were calculated by the following procedure: thickness increase due to water vapor sorption at a given point along the % RH spectrum was divided by the total thickness of the TEMPO CNF thin film at the same % RH point. This was done under the assumption that all changes in thickness or optical thickness took place due to water vapor uptake. Therefore, the thickness fraction of water describes the added thickness due to sorption of water. However, it does not differentiate between actual physical thickness of the water molecules and thickness changes in the film due to moisture-induced structural changes, e.g. swelling or reconfiguration of individual fibrils or hemicellulose.

4.2.3   Chemical Analysis

X-Ray Photoelectron Spectroscopy (XPS)

Elemental composition of the interfacially modified TEMPO CNF films by thermoresponsive poly(NIPAM) in Paper IV was determined using surface-sensitive X-Ray photoelectron spectroscopy (XPS) with analysis depth less than 10 nm. Measurements were carried out with a Kratos Analytical AXIS Ultra electron spectrometer with monochromatic A1 Kα irradiation at 100 W and effective charge neutralization with slow thermal electrons. Details of the experimental set-up including acquisition parameters is reported elsewhere[145]. Surface coverage values were calculated using nitrogen as the elemental marker representing poly(NIPAM). Based on the molecular formula of the repeating unit of poly(NIPAM), the ratio of nitrogen to the total number of atoms visible in XPS (carbon, nitrogen, oxygen) was assumed to be 1:8.

Fourier Transform Infrared Spectroscopy (FT-IR)

Through papers III and IV a Nicolet iS50 FT-IR spectrometer (ThermoScientific, USA) equipped with a built-in diamond iS50 ATR was used to characterize the chemical structure

of modified TEMPO CNF films in bulk. Spectra were scanned within the range of 350 to 4000 cm^{-1} with a total of 32 scans with resolution 4 cm^{-1}.

In Paper IV, the attachment of poly(NIPAM) to TEMPO CNF film was further scrutinized by FT-IR. Following a procedure described by De Cuadro et al.[146] in a modified form, esterified films were subjected to counterion exchange at (pH 10) and to saponification (pH 13) in order to distinguish ester bands from carboxylic acid contributions.

Solid State Nuclear Magnetic Resonance (^{13}C NMR)

To further verify the chemical modifications performed in Paper IV in bulk, the ^{13}C cross polarization (CP) magic angle spinning (MAS) NMR measurements were performed using an Agilent 600 NMR spectrometer with magnetic flux density of 14.1 T, equipped with a 3.2 mm triple-resonance MAS NMR probe operating at double resonance mode and MAS rate set to 10 kHz. 30,000 transients were accumulated with a 3.0 s delay between successive scans, cross polarization contact time was 1.0 ms, and a 70 kHz proton decoupling (spinal-64) was used. The chemical shifts were externally referenced via adamantane by setting the low field signal to 38.48 ppm. Rf-field strengths for cross polarization and decoupling were calibrated using α-glycine. Processing of the spectra was carried out with Bruker TopSpin 3.5 software.

4.2.4 Membrane Performance Testing

Tensile Testing

Wet strength properties of PVA-modified TEMPO CNF films (Paper III) were determined using a 33R4204 universal testing machine (Instron, UK) equipped with a 100 N static load cell. The specimens were immersed in deionized water for 24 hours prior to wet strength measurements performed in a controlled atmosphere (23°C/50% RH) using crosshead speed of 0.5 mm/min.

Dead-end filtration

To demonstrate the performance of TEMPO CNF films as a membrane material in Paper IV and V, permeance was measured in a Sterlitech HP4750 dead-end stirred cell (Sterlitech, Kent, USA). Feed, i.e. water or organic solvent (tetrahydrofuran and *n*-hexane) was forced through the films using nitrogen at a head pressure of 0.2 MPa. The water permeance is reported as L m^{-2} h^{-1} MPa^{-1}.

Temperature dependence of water permeance in Paper IV in the range from 20–60 °C involved placing the dead-end cell set-up in a water bath and controlling the temperature of the water bath with a temperature controller (RCT classic IKAMAG® safety control with VT-5 contact thermometer, VWR, UK). Permeance at each temperature was collected until it did not change more than one % per hour.

4.2.5 Supplementary Techniques

Atomic Force Microscopy (AFM)

Throughout the dissertation (Papers I-V) AFM was used for characterization of surface morphologies of both thin films and macroscale films. For most AFM images taken in the context of this dissertation, the instrument in use was afm+ from Anasys Instruments Inc. (Santa Barbara, CA, USA) and it was used in tapping mode with EX-T125 probes from ST Instruments B. V. (Groot-Ammers, The Netherlands). Typical cantilever resonance frequency was 200-400 kHz, spring constant 13-77 N m^{-1} and radius of the curvature of the cantilever was 10 nm as reported by the manufacturer. Flattening was the only image processing tool used. AFM images were analyzed using the Analysis Studio software (version 3.11).

Contact Angle Measurements

In Paper IV, the sessile drop method was employed for determination of water contact angles using CAM 200 from KSV Instruments Ltd., Finland. Milli-Q water was used in the measure-ments performed within 15 minutes of UV/O$_3$ treatment.[82]

Dynamic Vapor Sorption (DVS)

DVS was performed in Paper III to study the water vapor sorption into PVA modified TEMPO CNF films, i.e. wet-strength enhanced assemblies, using DVS-1 instrument (Surface Measurement Systems, UK). The mass of the sample at RH 0%, 50% and 90% was registered with a resolution of 1 µg at a constant temperature of 30 °C. Each humidity level was maintained for 300 minutes.

Karl-Fischer Titration

To complement the DVS measurements performed on PVA modified TEMPO CNF films (Paper III), residual moisture content of dry films was determined by Karl-Fischer titrations performed with Mettler Toledo DL31 apparatus. Hydranal Titrant 2 was used as the Karl-Fischer reagent. 100 mg of sample was weighed into vials and water was extracted in anhydrous methanol for 16 hours. The titrant was calibrated with water using sodium tartrate dihydrate as a calibration control.

Dynamic Mechanical Analysis (DMA)

In Paper III DMA was carried out on TEMPO films modified with PVA using tensile mode and film geometry at 0%, 50%, 90% RH at 30 °C temperature, each humidity level lasting 300 minutes. Q800 Dynamic Mechanical Analyzer (TA Instruments, USA) equipped with DMA-RH accessory was used for measurements. Preload force, amplitude and frequency of 0.05 N, 5.0 µm and 1 Hz, respectively, were used during the analysis.

5. Results and Discussion

This chapter summarizes the most important fundamental discoveries and more applied findings attained in the context of this dissertation. Section 5.1 focuses on fundamental aspects of the moisture-sensitive structure of TEMPO CNF thin films.

Surface-sensitive methods coupled with quantitative sorption models reveal the TEMPO CNF behavior with respect to vapor sorption mechanisms and water transport properties (**Papers I and II**). In Section 5.2 facile strategies to modify the properties of macroscopic TEMPO CNF films are presented: wet strength is enhanced using a PVA crosslinking in bulk (**Paper III**), and thermoresponsive character is introduced using interfacial surface modification (**Paper IV**). As a continuation, the (modified) properties are exposed to performance testing in aqueous and organic solvent environments (**Paper V**) in Section 5.3., to showcase their potential as membrane materials.

5.1 Moisture-Sensitive Structure of Nanoscaled Cellulose Films

5.1.1 Water Vapor Sorption

Water vapor sorption into TEMPO CNF thin films was investigated by using a complementary combination of precise surface-sensitive analytics, i.e. QCM-D and SE, designed to detect changes in not just mass and thickness, but also solid state rheology and optical properties. TEMPO CNF films were subjected to increasingly humid air over a wide RH% range (0-97% RH) while tracking their moisture-responses *in-situ*.

The changes in frequency recorded by QCM-D (Figure 6a) suggest that water uptake into the TEMPO CNF takes place upon exposure to higher RH% levels. This is also manifested in the mass isotherm (Figure 7a) calculated from the frequency changes using the Sauerbrey equation (equation 11). The isotherm reveals that, whereas sorption of water vapor is steady in the 6 – 75% RH range, it is significantly magnified in humid air (RH > 75%). At high relative humidity (97% RH), the water vapor uptake capacity of TEMPO CNF as measured by QCM-D is 0.94 ± 0.11 g g^{-1} (**Paper II**) which exceeds other nanoscaled cellulosic materials,

such as cellulose nanocrystals (0.28 g g^{-1})[109] native CNF (0.35 g g^{-1})[94] or even completely iso-tropic amorphous cellulose (0.45 g g^{-1})[115] and is at an equal level with certain metal organic frameworks (0.97 g g^{-1})[147], which are considered state-of-the art sorption materials of today.

Simultaneously, minor changes in dissipation recorded by QCM-D (Figure 6a) indicate changes in the solid-state rheology of the film. At low and moderate humidity levels (RH < 75%) no change in dissipation is detected ($\Delta D = 0$), suggesting that all deformations upon exposure to oscillating stress are fully reversible in spite of water vapor uptake. This indicates that the TEMPO CNF thin film behaves as a fully elastic material below 75% RH. Upon reaching humidity levels above 75% RH, a minor increase in the dissipation change is detected ($\Delta D > 0$), signifying that a portion of the energy is dissipated during the oscillation cycle, essentially meaning that the film undergoes irreversible structural deformations. To understand the changes in solid-state rheological properties of the film, the heterogeneous and multi-component composition of TEMPO CNF must be considered: along with highly crystalline nanofibrils, ca. 10% of TEMPO CNF consists of amorphous hemicellulose polysaccharides deposited along the nanofibril surfaces. While the crystalline regions are impregnable to water molecules, the amorphous parts show strong swelling ability in water. This suggests that water vapor adsorption occurs only at the surface of the nanofibrils, and that changes in, e.g., solid state rheology, are mostly induced by water molecules penetrating between the nano-fibrils.
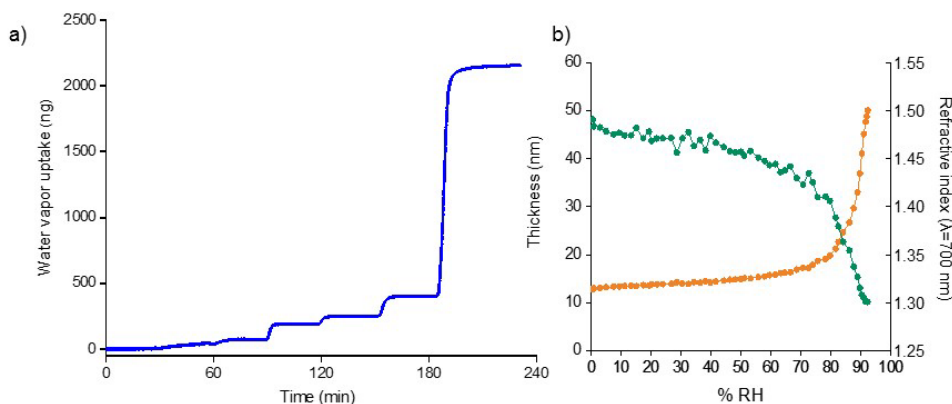
Figure 7. a) Water vapor uptake by TEMPO CNF thin film upon exposure to air with incrementally increasing relative humidity over time as monitored by QCM-D and calculated from Δf using the Sauerbrey equation (equation 11) (**Paper II**). b) Refractive index (at λ = 700 nm) (green) and thickness (orange) of TEMPO CNF thin film upon exposure to increasing RH% as measured by SE (**Paper I**).

Closer inspection of the data collected by SE (Figure 7b) reveals that the refractive index (RI) of the thin films decreases slowly in the RH range from 0 to 75%, but undergoes a steep decrease upon reaching approximately 75% RH. Interestingly, in dry air the RI of the TEMPO CNF film is close to RI values reported in literature for crystalline cellulose (1.554 as reported by Cranston et al.[148]) and a dense macroscale TEMPO CNF film (1.545 as reported by Isogai et al.[8]). In very humid air (~90% RH) the RI of the TEMPO CNF film (1.30) is similar to the RI of water (1.33). This suggests that a continuous film of water molecules has formed and that water exists in liquid form within the TEMPO CNF thin film in the high % RH region. However, it does not point to capillary condensation, because although close, the measured RI (1.30) differs from the RI of pure water. Also the development of refractive index upon moisture exposure is distinct in capillary condensation, with abrupt alterations in the index profile when the condensation occurs.

Similar tendencies in water vapor uptake by the TEMPO CNF films are observed when the mass and thickness results are converted into mass and thickness fractions (Figure 8). The differences in isotherms collected by QCM-D and SE probably originate from the nature of the surface-sensitive techniques: QCM-D detects changes in mass due to uptake of water

molecules, whereas the SE senses changes in the entire multicomponent thin film system including water, TEMPO CNF and air.
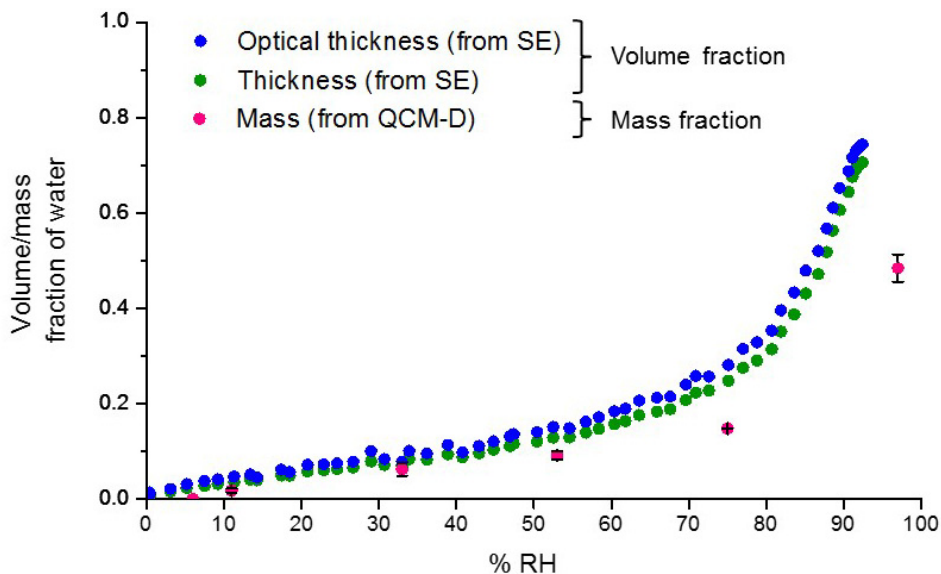

Figure 8. Mass (pink), optical thickness (blue) and thickness (green) fractions of water in TEMPO CNF thin films due to water water vapor uptake as a function of relative humidity. Thickness and optical thickness fractions of water are deduced from data collected by SE. (**Paper I**)

5.1.2 Mechanisms of Water Vapor Sorption

Interpretation of gas and vapor sorption is classically approached via fitting with sorption models. As shortly discussed in Section 3.4, the additive Langmuir-Flory-Huggins-clustering model originally used in the context of amorphous polyamide[127] is also an intriguing sorption model from the TEMPO CNF perspective: the additive nature of the model allowing for fitting of the three terms separately, at RH% zones where they are most relevant compensates for

the complex sorption behavior of TEMPO CNF. In this dissertation, the TEMPO CNF sorption isotherm was fitted by the Langmuir-Flory-Huggins-clustering model (Figure 9a) and a complementary BET model (Figure 9b) to reveal the mechanisms of water vapor sorption into TEMPO CNF thin films.

The optical thickness isotherm was selected for fitting instead of the mass isotherm collected by QCM-D due to higher frequency of data points and the inclusion of the entire thin film system (including air) in the optical response detected by SE. Differing from the geometric thickness, the optical thickness is the product of the geometric thickness and the refractive index. In some cases, e.g. in rigid mesoporous films, water condenses into the pores causing the physical thickness to decrease and refractive index to increase as shown by Boissière et al.[149] Therefore, solely analyzing the geometric thickness would lead to completely missing the information on water uptake. In the case of TEMPO CNF film, either the geometric thickness or the optical thickness could have equally been used in calculations, as the optical thickness curve matches the physical thickness curve (Figure 8), indicating that water vapor uptake only provokes swelling of the TEMPO CNF thin film.
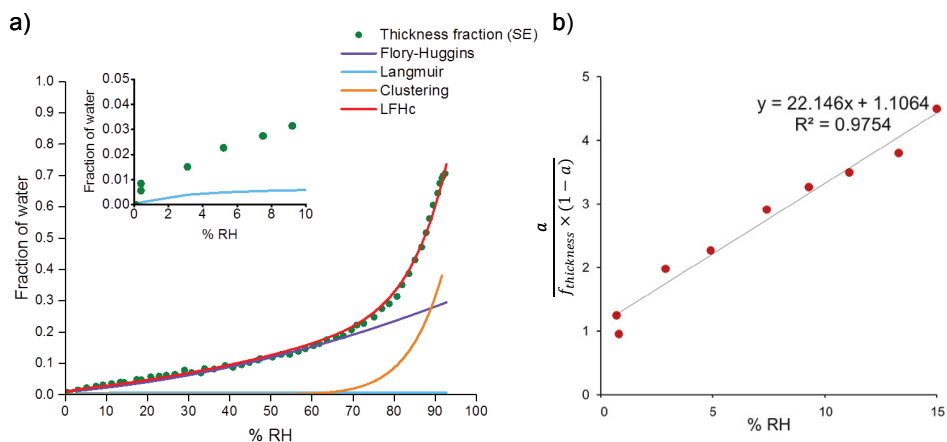

Figure 9. a) Optical thickness isotherm of TEMPO CNF film fitted by the Langmuir – Flory-Huggins – clustering model. The inset shows the Langmuir adsorption isotherm in dry air. b) Optical thickness isotherm fitted by the BET model in the range from 0-15% RH. (**Paper I**)

Each term in the Langmuir–Flory-Huggins–clustering model was solved at a limited RH% range, where the term was assumed to be most relevant from the physicochemical point of view. In agreement with earlier studies, the resulting Langmuir parameters corresponding to the concentration of the specific sorption sites (K) and the affinity of water for these sites (B)[111,150] were 1.408 and 223 respectively. The fit showed that the contribution of Langmuir-type sorption was most prominent below 5% RH and remained constant at higher humidity levels. This indicates that at said humidity level the specific sorption sites reached their saturation point. Nonetheless, the total sorption cannot be solely attributed to Langmuir adsorption, as it underpredicts the sorption of water vapor even in dry air (RH < 10%). The difference likely stems from the heterogeneous nature of TEMPO CNFs: ca. 90% is comprised of highly crystalline fibrils, whereas ca. 10% of the material consists of amorphous hemicellulose. Water molecules cannot impregnate cellulose nanofibrils, suggesting that sorption only occurs at the surface of the fibrils. In contrast, amorphous hemicellulose located on fibril surfaces swells readily in water. Hemicellulose is likely to exhibit significantly different behavior compared to materials that the Langmuir isotherm was originally designed for, i.e. morphologically homogeneous monocomponent surfaces[123], leading to underestimation of sorption.

According to the model, Flory-Huggins type sorption or random mixing dominates the water-vapor uptake in the range of 5% to 75% RH, where the Flory-Huggins interaction parameter, χ, for the curve is 0.67. The regression coefficient (R^2=0.977) between the model and the experimental data in the range from 30-70 % RH confirms that the model strongly correlates with the experimental data. Above ~70% RH the experimental data deviates from the Flory-Huggins-type sorption, indicating contribution from clustering to the total water sorption. According to the clustering function fitted to the experimental sorption curve, the size of the formed clusters is on average 10 water molecules, indicating that at high humidity levels water probably functions as a structural element of the TEMPO CNF thin film.

To further elucidate sorption of water especially in dry air, the optical thickness isotherm was also fitted by the BET model (Figure 9b) in the range of 0% to 15% RH. According to the BET model the apparent water molecule monolayer thickness adsorbed on the TEMPO CNF

thin film was 4.3% of the total thickness of the TEMPO CNF thin film. Curiously, the monolayer thickness and the specifically adsorbed water revealed by the Langmuir isotherm are significantly different. When applied to smooth materials, e.g. mica, the monolayer volume solved by BET classically corresponds to the Langmuir adsorption. Here, the underlying reason for the discrepancy is probably the heterogeneous chemical and morphological nature of TEMPO CNF thin film system. Nonetheless, the combination of isotherms collected by precise surface-sensitive methods and physicochemically meaningful quantitative models provides insight into the complex moisture-sensitive structure of nanoscaled cellulose films (Figure 10).
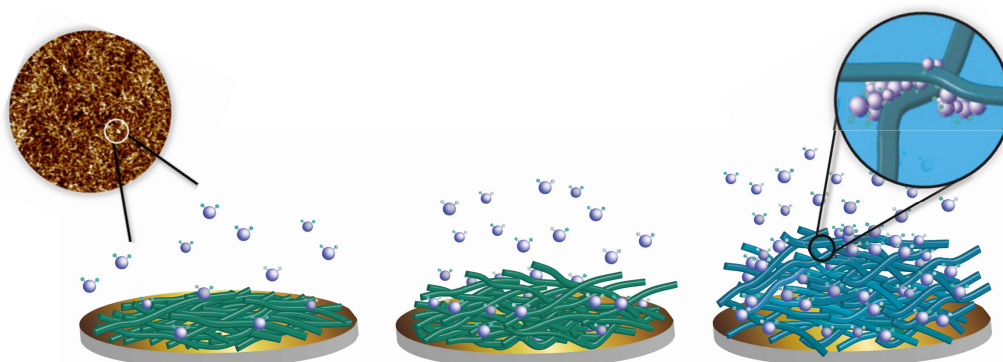

Figure 10. Highly schematic illustration of water vapor uptake of TEMPO CNF thin film in dry air (RH < 10%), in humid air (10-75% RH) and at high humidity levels (RH > 75%) with clustering shown in the right inset. In the left inset, a portion of a 3 μm × 3 μm AFM image of the fibril surface is displayed. (**Paper I**)

5.1.3 Water Vapor Transport Properties for Probing Moisture-Sensitive Structures

Diffusion models based on Fick's second law can be used to reveal molecular transport properties, as elucidated in Section 3.5. Here, to further elucidate the peculiar interdependency between water vapor sorption and the moisture-sensitive structure of TEMPO CNF thin films, sorption isoterms were treated with the diffusion model[130] and the effective diffusion

model[131]. The diffusion model assumes that diffusion of molecules occurs only into the pores of the films, whereas the effective diffusion model describes diffusion of molecules into the pores and accumulation of a (liquid) layer on the surface of the film.

The diffusion model (equation 7) describes the sorption of water vapor into TEMPO CNF thin films accurately only at low relative humidity levels, between 11-33% RH (Figure 11a). At higher RH levels the deviation from linearity progressively increases, indicating that mass uptake due to water vapor sorption is not entirely explicable by diffusion into the pores of the TEMPO CNF thin film above 33% RH. In contrast, the effective diffusion model (equation 8) describes the experimentally measured sorption behavior with sufficient accuracy ($R^2 = 0.93$) (Figure 11b) for allowing the calculation of effective diffusion coefficients over the humidity range from 11 to 97% RH. The better applicability of the effective sorption model suggests that in the case of TEMPO CNF thin films, sorption of water vapor is a combined effect of diffusion into the pores of the thin film and accumulation of a (liquid) layer of water on top of the thin film.

The effective diffusion coefficients increase as a function of RH%, indicating faster movement of water molecules within the TEMPO CNF thin film upon exposure to humid air (Table 1). Progression of the effective diffusion coefficients could stem from high water content of the film in humid air. Packing of water molecules, i.e., clustering, could induce local vapor-to-liquid transitions and increase affinity of TEMPO CNF film toward water. Such regions are most likely to occur at fibril intersections (Figure 11c), where density of hydrophilic moieties is high.
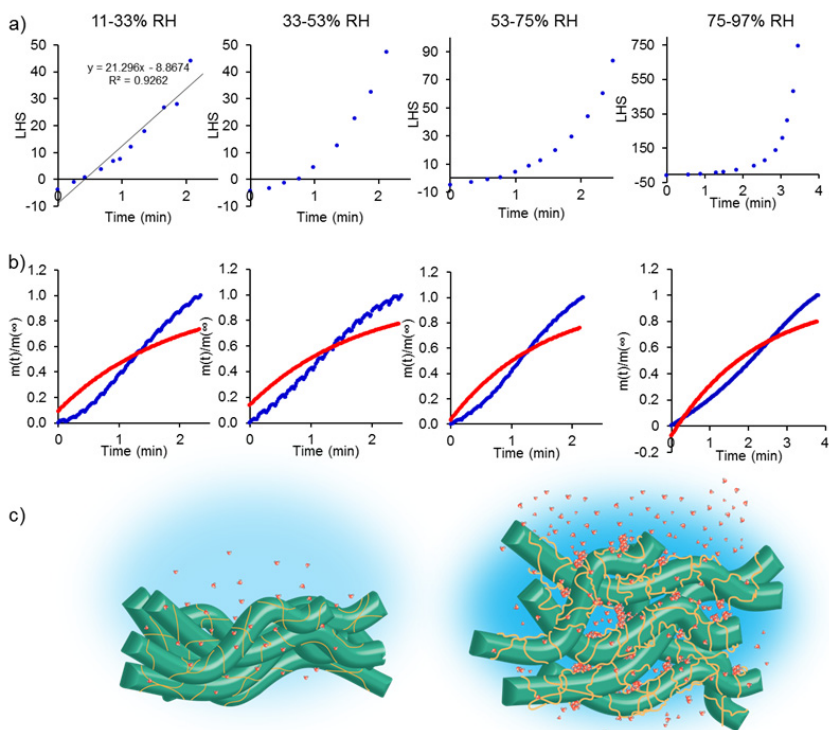
Figure 11. a) Diffusion coefficients based on the diffusion model (LHS $=-\frac{1}{\pi^2} ln \left[\frac{(m_\infty - m_t)\pi^2}{8(m_\infty - m_0)} \right] \times l^2$).
b) Uptake of water vapor (blue) fitted by the effective diffusion model (red) (equation 8). c) Highly schematic illustration of the proposed structural changes within TEMPO CNF with ca. 10% hemicellulose (orange) thin film upon sorption of water vapor in dry air (left) and humid air (right). (**Paper II**)

It should be noted that there is systematic deviation between the shapes of the experimental data curves and the effective diffusion model curves, as depicted in Figure 11b. The differences probably arise from the moisture-sensitive nature of TEMPO CNF thin film system. In dry air, abundant hydroxyl and carboxyl groups located on fibril surfaces are sites for specific adsorption. As the humidity increases, water molecules penetrate into the interfibrillar spaces. Simultaneously, the amorphous hemicellulose chains (ca. 10%) on fibril surfaces swell[93,151], become more mobile and thereby expose new adsorption sites on TEMPO CNF fibril surfaces. This sequence of events results in a sigmoidally shaped sorption curve. The diffusion of water molecules into materials exhibiting sigmoidally shaped isotherms is generally non-Fickian and cannot be accurately described in terms of models derived from Fick's second law. The simple Fickian diffusion models do not account for complex and anomalous

phenomena, such as swelling and relaxation of polymer chains, increasing interfibrillar spacing and clustering of water molecules[128]. However, Fickian models provide a simple means to monitor vapor-induced physical changes in moisture-sensitive materials and to elucidate the structure of complex, multicomponent systems based on discrepancies between models and measured data. The method presents a significant conceptual advance for *in situ* structural analysis of complex moisture-sensitive, biological structures, such as nanoscaled cellulose. The approach is totally different from the existing in situ geometric analysis with, e.g., high speed AFM[152] or in situ TEM[153] whose use has been limited to fairly simple systems so far.

Table 2. Diffusion coefficients, effective diffusion coefficients, solubility and permeability of water vapor in TEMPO CNF thin films. (**Paper II**)

% RH	Diffusion $\frac{nm^2}{min}$		Solubility* $\frac{cm^3(STP)}{cm^3(kPa)}$	Effective Permeability $10^{-11} \times \frac{cm^3(STP) \times cm}{cm^2 \times s \times kPa}$
	D^*	D_{eff}^*		
11			67.97 ± 17.25	
33	24.92 ± 3.32	23.10 ± 3.39	84.57 ± 19.91	1.95
53	30.37 ± 3.94	28.16 ± 7.93	79.55 ± 7.46	2.24
75	-	49.60 ± 7.20	187.47 ± 0.23	9.30
97	-	64.15 ± 20.53	408.18 ± 45.70	26.20

*The reported values for D, D_{eff} and S are average values of at least three measurements.

5.2   Tailoring Film Properties toward Membrane Material

5.2.1   Wet-Strength Enhancement

Highly moisture-sensitive self-standing TEMPO CNF films are not stable in water, unless their wet strength is enhanced by specific strategies developed to overcome disintegration. Here, a crosslinking involving PVA was used to enhance the wet strength of TEMPO CNF films to enable their use in aqueous environments, e.g. as membranes. Carboxyl groups introduced to CNF through TEMPO/NaClO/NaClO$_2$ oxidation were exploited by reacting them with the hydroxyl groups of PVA (Figure 12) in a similar manner to literature[154-157]. Unlike films made entirely of TEMPO CNF that disintegrated almost immediately upon exposure to

water, films crosslinked with PVA remained intact for prolonged periods of time (up to several months) immersed in water, suggesting that covalent ester bonds were formed upon drying. The crosslinking method with PVA is also applicable to aldehyde-containing TEMPO CNF, oxidized using the TEMPO/NaClO/NaBr-system at pH 10-11. In the presence of aldehyde groups, hydroxyl moieties of PVA could undergo hemiacetal formation, further contributing to the crosslinking of the film.
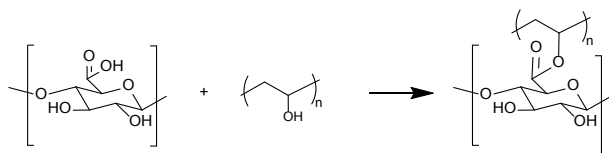

Figure 12. Schematic illustration of the acid-initiated esterification reaction between carboxyl groups of TEMPO CNF and hydroxyls groups of PVA on fibril surfaces. (**Paper III**)

Mechanical properties of crosslinked films in wet state could be tuned by changing the ratio and type of PVA (Figure 13). Highest stress at break (~30 MPa) was achieved with 10 wt.-% PVA content. The degree of hydrolysis, i.e. the degree of unhydrolyzed acetate groups, did not affect the stress resistance significantly, but it did have an impact on the strain: films with partly (88%) hydrolyzed PVA showed larger strain at break-values in comparison to films containing equal amounts of fully (98%) hydrolyzed PVA. On the other hand, in the tested range, the amount of PVA did not appear to have an effect on the toughness of the films, i.e. overall work to fracture, which was at the level of ~2 MJ m^{-3} for all PVA-containing films tested and corresponds to the toughness of keratin (1.8 MJ m^{-3})[158].
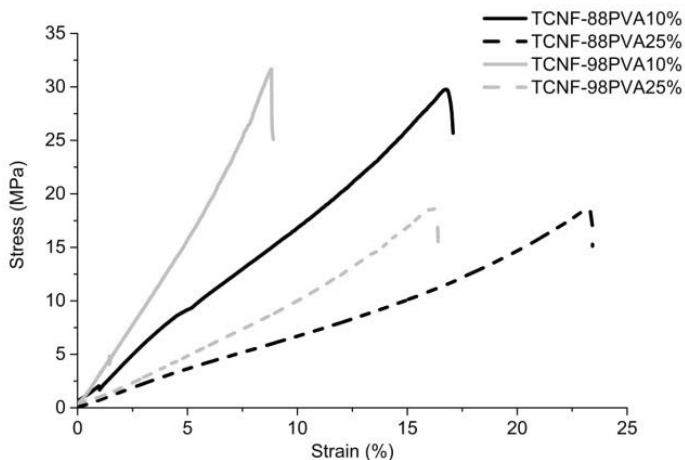
Figure 13. Stress-strain curves of TCNF-PVA films containing 10 wt.-% or 25 wt.-% fully (98%) or partly (88%) hydrolyzed PVA following immersion in water for 24 hours. (**Paper III**)

5.2.2 Direct Interfacial Modification for Thermoresponsiveness

Many applications envisioned for nanoscaled cellulose cannot rely only on the inherent material properties and further functionalization is often required. In principle, all chemical reactions of nanoscaled cellulose can be performed in dispersion form, but as described in Section 2.4.2, the direct interfacial modification is often a more facile approach to tailoring. In this work, TEMPO CNF films with PVA-enhanced wet-strength were subjected to modification with poly(NIPAM) to demonstrate the surface-tailoring approach and its advantages, such as effortless cleansing. Poly(NIPAM), a popular thermoresponsive polymer, undergoes a temperature-induced transition from hydrophilic to a more hydrophobic state at around 32 °C in water[159] and has been linked to membranes with controllable gating mechanisms[160,161] and switchable wettability[162].

The advantage of TEMPO CNF over other nanoscaled cellulosic materials lies not just in their affinity toward water, but also in the availability of carboxyl group precursors for further functionalization. Amine groups react more readily with esters compared to carboxylates to form amides[163], which is why an intermediate esterification step was implemented to facilitate the attachment of amine terminated poly(NIPAM) on the film surface (Figure 14).
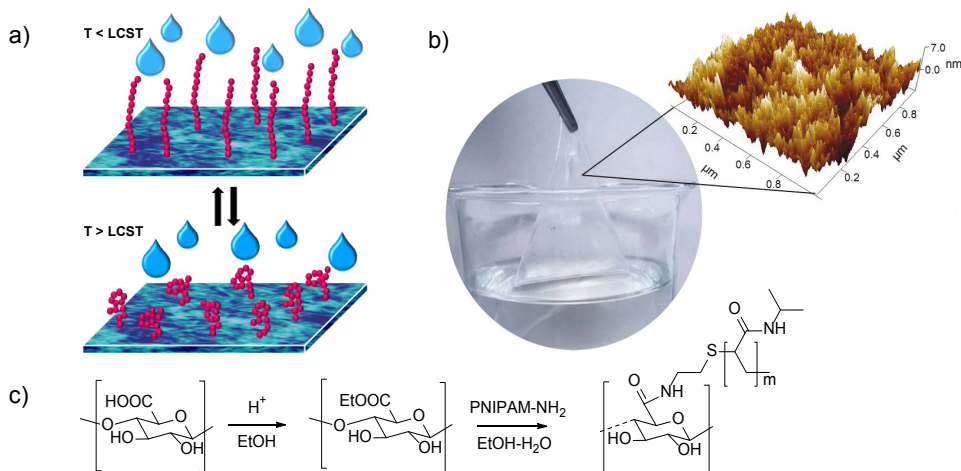
Figure 14. a) Illustration of CNF film surface grafted with poly(NIPAM) exhibiting thermoresponsive behavior around its LCST (32 °C). b) Macroscopic film of TEMPO CNF with wet-strength enhanced by PVA (Paper III). AFM topography image (1 μm × 1μm) of the dry film surface is shown in the inset. c) Proposed chemical pathway for attaching poly(NIPAM) onto the TEMPO CNF film surface by an esterification step followed by poly(NIPAM) grafting step. (**Paper IV**)

The efficiency of poly(NIPAM) attachment in different reaction conditions, i.e. temperature and reaction media, was studied by surface chemical analysis (XPS) and bulk chemical analysis methods (FT-IR and ^{13}C NMR). XPS revealed that films modified in water-ethanol medium carried significantly larger amounts of nitrogen and sulfur (Table 1) compared to films surface modified in pure ethanol, indicating a more successful attachment of poly(NIPAM). This was also attested by the calculated surface coverages based on elemental concentrations. At increased temperature (50 °C) the reaction efficiency was lowered, probably due to poly(NIPAM) taking a coiled conformation in temperatures above the 32 °C, which is its lower critical solution temperature (LCST).

Table 3. Elemental concentrations of oxygen (O 1s), carbon (C 1s), sulfur (S 2p) and nitrogen (N 1s) and surface coverage (%) values in film samples as analyzed by XPS.[a] (**Paper IV**).

Sample	Elemental concentration (at-%)				Surface coverage (%)
	O 1s	C 1s	S 2p	N 1s	
TEMPO-CNF-PVA	37	62	0.0	0.0	
Esterified TEMPO-CNF-PVA	38	63	0.0	0.2	
Poly(NIPAM) modified film (RT, ethanol)	36	64	0.2	0.3	1.8
Poly(NIPAM) modified film (RT, ethanol + water)	36	62	0.5	1.2	8.5
Poly(NIPAM) modified film (50 °C, ethanol)	37	62	0.0	0.3	2.0
Poly(NIPAM) modified film (50 °C, ethanol + water)	38	61	0.2	0.6	4.0

[a] Surface coverage percentages are calculated from elemental concentrations.

FT-IR (Figure 15a) further confirmed the attachment of poly(NIPAM) on the film surface. A carbonyl (C=O) stretch at 1605 cm^{-1} due to sodium carboxylate groups (Fujisawa et al. 2011) disappears upon esterification, and a new band marking esterified celluronic carbonyls appears at 1723 cm^{-1} originating from ethyl esters. This is confirmed by performing counterion exchange at pH 10 to sodium, whereby the band at 1723 cm^{-1} is not shifted from a possibly overlapping protonated carboxyl (> 1700 cm^{-1}) to sodium carboxylate (at 1605 cm^{-1}). On the other hand, saponification at pH 13 cleaves the esters and the combined ester-carboxyl band is shifted to sodium carboxylate at 1605 cm^{-1}.[146]

Moreover, after reaction with poly(NIPAM) solid state ^{13}C NMR (Figure 15b) revealed peaks at 23 and 42 ppm, which could be assigned to the −CH and −CH$_3$ groups of the thermoresponsive polymer. Bands at 175 ppm[45] and at 179 ppm were assigned to sodium carboxyl moiety and the C=O of ester group. The peak assigned to carboxyl moieties remains visible in the spectra at each step of the reaction pathway, whereas the signal assigned to ester groups disappears upon reaction with poly(NIPAM).
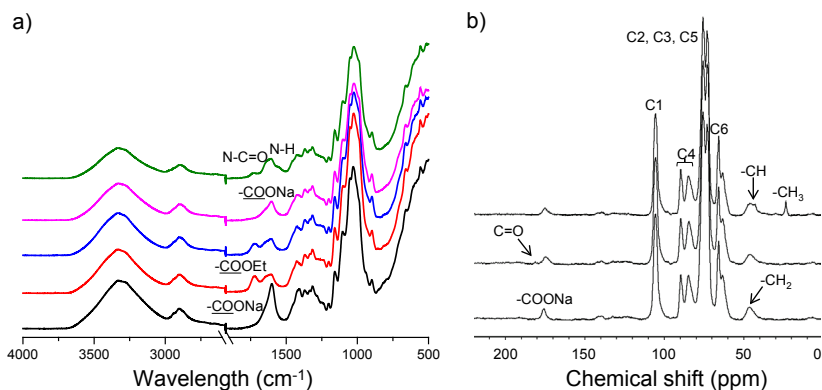
Figure 15. a) FT-IR spectra of TEMPO-CNF-PVA film (black), esterified film (red), esterified film with counterion exchange (pH 10) (blue), esterified film with saponification (pH 13) (pink) and poly(NIPAM) modified film (green) and b) ¹³C NMR spectra of TEMPO-CNF-PVA film (bottom), esterified film (middle) and poly(NIPAM) modified film (top) with peak assignment. (**Paper IV**)

5.3 Performance of CNF Films as Membrane Materials

5.3.1 Thermoresponsive Behavior in Aqueous Environments

The performance of TEMPO CNF films as membrane material was studied by water permeance testing in a dead-end filtration set-up over temperature from 20 °C to 60 °C. At 2 bar operating pressure wet-strength enhanced TEMPO CNF films (with 10% PVA) exhibited permeance of 60 - 180 $Lm^{-2}h^{-1}MPa^{-1}$. The absolute permeance values were significantly decreased as a result of esterification and poly(NIPAM) attachment according to the reaction path described in Section 5.2.2: permeances of 10-30 $Lm^{-2}h^{-1}MPa^{-1}$ and 15-50 $Lm^{-2}h^{-1}MPa^{-1}$ were detected for esterified and poly(NIPAM) modified films, respectively (Paper IV).

Figure 16 shows the absolute permeance values normalized to the permeance at 20 °C as a function of temperature. Due to a decrease in solvent (water) viscosity[164,165], the permeances,

as expected, increased with temperature. However, while the relative permeance of unmodified and esterified films increased at an almost constant rate, two regions of linear growth with different slope between 20-40 ˚C and between 40-60 ˚C were detected for the poly(NIPAM) modified film. The inflection point occurs around the LCST (32˚C) of poly(NIPAM). Between the two temperature regions, the slope of relative permeance for unmodified and esterified films grew by 18 % and 28%, respectively. The corresponding increase for poly(NIPAM) modified films was 100%, indicating that above the LCST of poly(NIPAM) the physical barrier for water is at least partly removed, as poly(NIPAM) chains take their collapsed form (Figure 16). In conclusion, the results showed that wet-strength enhanced TEMPO CNF films modified with poly(NIPAM) (8% surface coverage) can be used as thermoresponsive membrane templates.
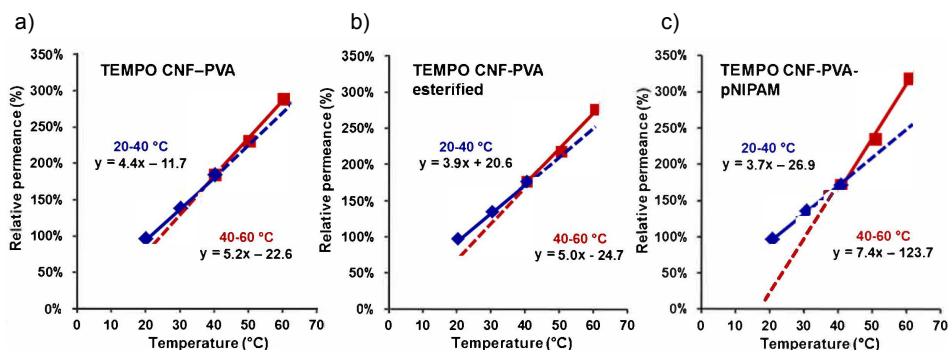

Figure 16. Relative permeance of water (normalized to permeance at 20 °C) plotted as a function of temperature for an unmodified TEMPO-CNF-PVA film, an esterified film and a poly(NIPAM) modified film. Linear regression based on real data points (R^2 values > 0.992) was performed for temperature ranges 20-40 °C (blue) and for 40-60 °C (red). Dashed lines are linear extrapolations of the linear regression lines. (**Paper IV**)

5.3.2 Performance in Organic Solvent Media

Utilization of organic solvents in filtration processes poses a notable challenge for membranes in terms of solvent-stability, which many conventional synthetic polymer-membranes lack. Production of membranes that tolerate solvents, i.e. ceramics and organic-inorganic hybrid materials, has drawbacks with respect to high energy consumption and use of solvents. Thus, solvent-stable membranes produced using simple water-based production processes are desired.

Here, the performance of TEMPO CNF films was studied in a filtration set-up. The permeance and MWCO of TEMPO CNF films in organic solvents was determined. The films were produced using a method based on vacuum-filtration and flocculation of the fibrils upon addition of multivalent ions from an aqueous suspension, combined with hot-pressing to consolidate the films.

Permeance of tetrahydrofuran (THF), n-hexane and water through the films as a function of film grammage are summarized in Figure 17a. The results showed that the permeance increases with increasing hydrophobicity, with water showing the lowest permeance and n-hexane the highest permeance at 2 bar operating pressure at 20 ˚C. This suggests that in the absence of suitable binding sites, hydrophobic molecules diffuse more readily through the film in comparison to water molecules that have high affinity for the vast amount of hydrophilic functional groups within the film. Moreover, permeance was strongly influenced by grammage of the film, with higher permeances linked to lower grammage. Similar tendencies were detected for membranes prepared from mechanically disintegrated CNF. It should be noted, that solvent viscosity differences were not taken into account in permeance calculations.
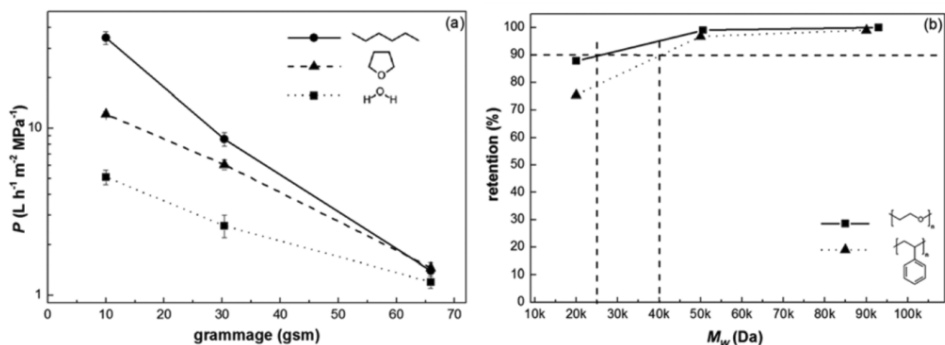
Figure 17. a) Permeance of THF, *n*-hexane and water for TEMPO CNF membrane material of different grammages. b) Retention of poly(styrene) and poly(ethylene glycol) as a function of molecular weight (M_w). The MWCO of is defined as the molecular weight of the polymer of which 90% is rejected.

The MWCO of the TEMPO CNF film, was found to be 3.2 kDa and 6 kDA, respectively as determined from poly(styrene) and poly(ethylene glycol) dissolved in THF with varying molecular weights (Figure 17b). These values correspond to hydrodynamic radii of 1.6 nm[166] and 2.4 nm[167] which are indicative of the pore size. Films made from mechanically disintegrated CNF showed much larger MWCO in the range of 20 kDa – 100 kDa corresponding to pore dimensions of ~50 nm, suggesting that the pore dimensions can be controlled by selecting nanofibrils with different dimensions. This indicates that nanoscaled cellulose has the potential to separate mixtures down to a molecular level in a customized manner. This has relevance to lab-scale operations such as organic syntheses, but also to a wide variety of industrial processes, e.g. edible oil production and recovery of catalysts.[168]

6. Conclusive Outlook

This dissertation explored the materials development of tight and hydrophilic membrane material exploiting the peculiar water-interactions of CNF. The findings presented here provide fundamental information about the behavior of CNF films in presence of water or water vapor, and also suggest facile tailoring approaches to achieve the performance features needed in membrane applications.

The structure-oriented studies reveal a distinct two-way interdependency between structure and moisture uptake of CNF films. Based on studies using the surface-sensitive approach and classical physicochemical theories, it was discovered that at high humidities water packs within the film as clusters, rather than through capillary condensation. This approach also enabled the calculation of diffusion and permeance of water molecules. These parameters are highly relevant from the fundamental perspective in terms of understanding property-function relationships, but also from an applied point of view for evaluating material performance. Moreover, water molecules and transport properties thereof could be used as a tool for revealing moisture-induced structural changes in the complex, multicomponent CNF film system.

Targeted tailoring strategies were developed, with the aim to tune the CNF material properties toward those of membranes. This was realized by applying selected synthetic polymers and chemistries to introduce new properties. The bulk structure of CNF films was cross-linked, which resulted in water stability of the films without compromising inherent characteristics, e.g. hydrophilicity or nanoscale morphology. Furthermore, mere 8% surface coverage by a thermoresponsive polymer resulted in a significant change in water permeance behavior, demonstrating the efficiency of the interfacial modification strategy for achieving nanoenhanced effects. CNF membrane materials were verified suitable for not just water, but also for organic solvent media.

In the view of this dissertation, inherent structure-derived properties are the key for achieving performance features that will carry future biomaterials development beyond conventional applications. As the fundamental behaviors of biomaterials unravel and are transferred to applications in full value, they are anticipated to solve many of the most pressing issues of our contemporary society, related to e.g. resource sufficiency and quality of life.

References

1. Alberts, B.; Lewis, J.; Raff, M., Roberts, K., Watson, J. D. Molecular Biology of the Cell, 2nd ed.; Garland: New York, 1989.

2. Kaldenhoff, R.; Grote, K.; Zhu, J.-J.; Zimmermann, U. Significance of Plasmalemma Aquaporins for Watertransport in Arabidopsis Thaliana. *Plant J.* **1998**, *14*, 121-128.

3. Preston, G. M.; Agre, P. Isolation of the cDNA for Erythrocyte Integral Membrane Protein of 28 Kilodaltons: Member of an Ancient Channel Family. Proc. Natl. Acad. Sci. U. S. A. *88*, **1991**, 11110-11114.

4. IUPAC. Glossary of Terms Used in Toxicology. US Department of Health & Human Services. 2007.

5. Eichhorn, S. J.; Dufresne A.; Aranguren, M.; Marcovich, N. E.; Capadona, J. R.; Rowan, S. J.; Weder, C.; Thielemans, W.; Roman, M.; Renneckar, S.; Gindl, W.; Veigel, S.; Keckes, J.; Yano, H.; Abe, K.; Nogi, M.; Nakagaito, A. N.; Mangalam, A.; Simonsen, J.; Benight, A. S.; Bismarck, A.; Berglund, L. A.; Peijs, T. Review: Current International Research into Cellulose Nanofibres and Nanocomposites. *J. Mater Sci.* **2010**, *45*, 1-33.

6. Moon, R. J.; Martini, A.; Nairn, J.; Simonsen, J.; Youngblood, J. Cellulose Nanomaterials: Structure, Properties and Nanocomposites. *Chem. Soc. Rev.* **2011**, *40*, 3941-3994.

7. Lavoine, N.; Desloges, I.; Dufresne, A.; Bras, J. Microfibrillated Cellulose – Its Barrier Properties and Applications on Cellulosic Materials: A Review. *Carbohydr Polym.* **2012**, *90*, 735-764.

8. Isogai, A.; Saito, T.; Fukuzumi, H. TEMPO-Oxidized Cellulose Nanofibers. *Nanoscale* **2011**, *3*, 71–85.

9. Klemm, D.; Kramer, F.; Moritz, S.; Lindström, T.; Ankerfors, M.; Gray, D.; Dorris, A. Nanocelluloses: A New Family of Nature-Based Materials. *Angew. Chem. Int. Ed.* **2011**, *50*, 5438-5466.

10. Chundawat, S. P. S; Bellesia, G.; Uppugundla, N.; Da Costa Sousa, L.; Gao, D.; Cheh, A. M.; Agarwal, U. P.; Bianchetti, C. M.; Phillips Jr., G. N.; Langan, P.; Balan, V.; Gnanakaran, S.; Dale, B. E. Restructuring the Crystalline Cellulose Hydrogen Bond Network Enhances Its Depolymerization Rate. *J. Am. Chem. Soc.* **2011**, *133*, 11163-11174.

11. Klemm, D.; Philipp, B.; Heinze, T.; Heinze, U.; Wagenknecht, W. General Considerations on Structure and Reactivity of Cellulose: Section 2.3–2.3. 7. Comprehensive Cellulose Chemistry: Fundamentals and Analytical Methods; Wiley-VCH: Chichester, 1998; Vol. 1, 83-129.

12. Nishiyama, Y.; Sugiyama, J.; Chanzy, H.; Langan, P. Crystal Structure and Hydrogen Bonding System in Cellulose I$_\alpha$ from Synchrotron X-ray and Neutron Fiber Diffraction. *J. Am. Chem. Soc.* **2003**, *125,* 14300-14306.

13. Nishiyama, Y.; Langan, P.; Chanzy, H. Crystal Structure and Hydrogen-Bonding System in Cellulose Iβ from Synchrotron X-ray and Neutron Fiber Diffraction. *J. Am. Chem. Soc.* **2002**, *124*, 9074-9082.

14. Nishiyama, Y. Molecular Interactions in Nanocellulose Assembly. *Phil. Trans. R. Soc. A.* **2018**, *376*, 20170047.

15. Hamaker, H. C. The London – van der Waals Attraction between Spherical Particles. *Physica* **1937**, *4*, 1058- 1072.

16. Heyn, A. N. J. The Microcrystalline Structure of Cellulose in Cell Walls of Cotton, Ramie, and Jute Fibers as Revealed by Negative Staining of Sections. *J. Cell. Biol.* **1966**, *29,* 181-197.

17. Endler, A.; Persson, S. Cellulose Synthases and Synthesis in Arabidopsis. *Mol. Plant.* **2011**, *4,* 199-211.

18. Fernandes, A. N.; Thomas, L. H.: Altaner, C. M.; Callow, P.; Forsyth, V. T.; Apperley, D. C.; Kennedy, C. J.; Jarvis, M. C. Nanostructure of Cellulose Microfibrils in Spruce Wood. *Proc. Natl. Acad. Sci. U.S.A.* **2011**, *108*, 1195-1203.

19. Oehme, D. P.; Downton, M. T.; Doblin, M. S.; Wagner, J.; Gidley, M. J.; Bacic, A. Unique Aspects of the Structure and Dynamics of Elementary Iβ Cellulose Microfibrils Revealed by Computational Simulations. *Plant Physiol.* **2015**, *168,* 3-17.

20. Okita, Y.; Saito, T.; Isogai, A. Entire Surface Oxidation of Various Cellulose Microfibrils by TEMPO-mediated Oxidation. *Biomacromolecules* **2010**, *11*, 1696-1700.

21. Garvey, C. J.; Parker, I. H.; Simon, G. P. On the Interpretation of X-ray Diffraction Powder Patterns in Terms of the Nanostructure of Cellulose I Fibres. *Macromol. Chem. Phys.* **2005**, *206*, 1568-1575.

22. Jarvis, M. C. Cellulose Biosynthesis: Counting the Chains. *Plant Physio.* **2013**, *163,* 1485-1486.

23. Mark, H. Intermicellar Hole and Tube System in Fiber Structure. *J. Phys. Chem.* **1940**, *44,* 764-788.

24. Hearle, J. W. S. The Fine Structure of Fibers and Crystalline Polymers. I. Fringed Fibril Structure. *J. Appl. Polym. Sci.* **1963**, *7,* 1175-1192.

25. Scallan, A.M. A Quantitative Picture of the Fringed Micellar Model of Cellulose. *Text. Res. J.* **1971**, *41*, 647-653.

26. O'Sullivan, A. C. Cellulose: the Structure Slowly Unravels. *Cellulose* **1997**, *4,* 173-207.

27. Atalla, R. H.; Vanderhart, D. L. Native Cellulose: A Composite of Two Distinct Crystalline Forms. *Science* **1984**, *223,* 283-285.

28. Sjöström, E. *Wood chemistry: fundamentals and applications*, 1st ed.; Academic Press: New York, 1981.

29. Postek, M. T.; Vladar, A.; Dagata, J.; Farkas, N.; Ming, B.; Wagner, R.; Raman, A.; Moon, R. J.; Sabo, R.; Wegner, T. H.; Beecher, J.; Development of the Metrology and Imaging of Cellulose Nanocrystals. *Meas. Sci. Technol.* **2011,** *22,* 024005.

30. Scheller, H. V.; Ulvskov, P. Hemicelluloses. *Annu. Rev. Plant Biol.* **2010**, *61,* 263-289.

31. Ralph, J.; Brunow, G.; Wout, B. Lignins. *eLS.* 2007.

32. Fengel, D.; Wegener, G. *Wood: Chemistry, Ultrastructure, Reactions*; Walter de Gruyter: Berlin, 1989.

33. Reza, M.; Ruokolainen, J.; Vuorinen, T. Out-of-Plane Orientation of Cellulose Elementary Fibrils on Spruce Tracheid Wall Based on Imaging with High-Resolution Transmission Electron Microscopy. *Planta* **2014**, *240*, 565-573.

34. Donaldson, L. A. Microfibril Angle: Measurement, Variation and Relationships – A Review. *IAWA J.* **2008**, *29*, 345-386.

35. Pääkkö, M.; Ankerfors, M.; Kosonen, H.; Nykänen, A.; Ahola, S.; Österberg, M.; Ruokolainen, J.; Laine, J.; Larsson, P. T.; Ikkala, O.; Lindström, T. Enzymatic Hydrolysis Combined with Mechanical Shearing and High-Pressure Homogenization for Nanoscale Cellulose Fibrils and Strong Gels. *Biomacromolecules* **2007**, *8*, 1934-1941.

36. Hiltunen, J., Kemppainen, K., Pere, J. Process for Producing Fibrillated Cellulose Material. WO2015/092146 A1. Finnish Patent FI126698.

37. Ferguson, A.; Khan, U.; Walsh, M.; Lee, K-Y.; Bismarck, A.; Shaffer, M. S. P.; Coleman, J. N.; Bergin, S. D. Understanding the Dispersion and Assembly of Bacterial Cellulose in Organic Solvents. *Biomacromolecules* **2016**, *17*, 1845-1853.

38. Brown, A. J. XLIII. – On an Acetic Ferment which Forms Cellulose. *J. Chem. Soc., Trans.* **1886**, *49*, 432-439.

39. Rånby, B. The Colloidal Properties of Cellulose Micelles. *Discuss. Faraday Soc.* **1951**, *11*, 158-164.

40. Dong, X. M.; Revol, J.-F.; Gray, D. G. Effect of Microcrystallite Preparation Conditions on the Formation of Colloid Crystals of Cellulose. *Cellulose* **1998**, *5*, 19-32.

41. Kontturi, E.; Meriluoto, A.; Penttilä, P.; Baccile, N.; Malho, J.-M.; Potthast, A.; Rosenau, T.; Ruokolainen, J.; Serimaa, R.; Laine, J.; Sixta, H. Degradation and Crystallization of Cellulose in Hydrogen Chloride Vapor for High-Yield Isolation of Cellulose Nanocrystals. *Angew. Chem., Int. Ed.* **2016**, *55*, 14455-14458.

42. Lehmonen, J.; Pere, J.; Hytönen, E.; Kangas, H. Effects of Cellulose Microfibril (CMF) Addition on Strength Properties of Middle Ply of Board. *Cellulose* **2017**, *24,* 1041-1055.

43. Saito, T.; Hirota, M.; Tamura, N.; Kimura, S.; Fukuzumi, H.; Heux, L.; Isogai, A. Individualization of Nano-Sized Plant Cellulose Fibrils by Direct Surface Carboxylation Using TEMPO Catalyst under Neutral Conditions. *Biomacromolecules* **2009**, *10*, 1992−1996.

44. Saito, T.; Kimura, S.; Nishiyama, Y.; Isogai, A. Cellulose Nanofibers Prepared by TEMPO-Mediated Oxidation of Native Cellulose. *Biomacromolecules* **2007**, *8*, 2485-2491.

45. Saito, T.; Nishiyama, Y.; Putaux J.-L.; Vignon, M.; Isogai, A. Homogeneous Suspensions of Individualized Microfibrils from TEMPO-Catalyzed Oxidation of Native Cellulose. *Biomacromolecules* **2006**, *7*, 1687-1691.

46. Ankerfors, M. Microfibrillated cellulose. Energy-Efficient Preparation Techniques and Key Properties. 2012, Licentiate Thesis, KTH.

47. Fukuzumi, H.; Saito, T.; Iwata, T; Kumamoto, Y.; Isogai, A. Transparent and High Gas Barrier Films of Cellulose Nanofibers Prepared by TEMPO-Mediated Oxidation. *Biomacromolecules* **2008**, *10*, 162−165.

48. Tammelin, T.; Vartiainen, J. Nanocellulose Films and Barriers. In: Oksman K, Mathew, A.P.; Bismarck, A.; Rojas, O.; Sain, M.; Qvintus, P. (Eds.). Handbook of Green Materials Vol 3: Self- and Direct-Assembling of Bionanomaterials, Materials and Energy. 2014, 213-229.

49. Kontturi, E., Tammelin, T., Österberg, M. Cellulose−Model Films and the Fundamental Approach. *Chem. Soc. Rev.* **2006**, *35*, 1287-1304.

50. Ahola, S.; Salmi, J.; Johansson, L-S.; Laine, J.; Österberg, M. Model Films from Native Cellulose Nanofibrils. Preparation, Swelling, and Surface Interactions. *Biomacromolecules* **2008**, *9*, 1273-1282.

51. Langmuir, I.; Blodgett, K. B. Über einige neue Methoden zur Untersuchung von monomolekularen Filmen. *Kolloid-Zeitschriet* **1935**, *73,* 257-263.

52. Decher, G. Fuzzy Nanoassemblies: Toward Layered Polymeric Multicomposites. *Science.* **1997**, *277*, 1232- 1237.

53. Meyerhofer, D. Characteristics of Resist Films Produced by Spinning. *J. Appl. Phys.* **1978**, *49*, 3993-3997.

54. Hoeger, I.; Taajamaa, L.; Kontturi, E.; Laine, J.; Rojas, O. Thin Film Deposition Techniques. In: Oksman K, Mathew, A.P.; Bismarck, A.; Rojas, O.; Sain, M.; Qvintus, P. (Eds.). Handbook of Green Materials Vol 3: Self- and Direct-Assembling of Bionanomaterials, Materials and Energy. 2014, 7-18.

55. Aulin, C.; Ahola, S.; Joseffson, P.; Nishino, T.; Hirose, Y.;Österberg, M.; Wågberg, L. Nanoscale Cellulose Films with Different Crystallinities and Mesostructures-Their Surface Properties and Interactions with Water. *Langmuir* **2009,** 25, 7675-7685.

56. Rodahl, M.; Höök, F., Kasemo, B. QCM Operation in Liquids: An Explanation of Measured Variations in Frequency and Q Factor with Liquid Conductivity. *Anal. Chem.* **1996**, *68*, 2219-2227.

57. Höök, F.; Rodahl, M., Brzezinski, P.; Kasemo, B. Energy Dissipation Kinetics for Protein and Antibody – Antigen Adsorption under Shear Oscillation on a Quartz Crystal Microbalance. *Langmuir* **1998**, *14*, 729-734.

58. Rodahl, M.; Höök, F.; Krozer, A.; Brzezinski, P.; Kasemo, B. Quartz Crystal Microbalance Setup for Frequency and Q-Factor Measurements in Gaseous and Liquid Environments. *Rev. Sci. Instrum.* **1995**, *66*, 3924-3930.

59. Reviakine, I.; Johannsmann, D.; Richter, R. P. Hearing What You Cannot See and Visualizing What You Hear: Interpreting Quartz Crystal Microbalance Data from Solvated Interfaces. *Anal. Chem.* **2011** *83*, 8838-8848.

60. Schasfoort, R. B., Tudos, A. J. Handbook of Surface Plasmon Resonance. Royal Society of Chemistry, Cambridge. 2008.

61. Tammelin, T.; Hippi, U.; Salminen, A.; PCT Int. Appl. 2013, WO 2013060934 A2 20130502.

62. Vartiainen, J.; Lahtinen, P.; Kaljunen, T.; Kunnari, V.; Peresin, M.S.; Tammelin, T. O'Papel, **2016**, *73*, 51-54.

63. Mäkelä, T.; Kainlauri, M.; Willberg-Keyriläinen, P.; Tammelin, T.; Forsström, U. Favbrication of Micropillars on Nanocellulose Films Using a Roll-to-Roll Nanoimprinting Method. *Microelectron. Eng.* **2016**, *163*, 1-6.

64. Österberg, M.; Vartiainen, J.; Lucenius, J.; Hippi, U.; Seppälä, J.; Serimaa, R.; Laine, J. A Fast Method to Produce Strong NFC Films as a Platform for Barrier and Functional Materials. *ACS Appl. Mater. Interfaces* **2013**, *5,* 4640-4647.

65. Mautner, A.; Lee, K-Y.; Tammelin, T.; Mathew, A. P.; Nedoma, A. J.; Li, K.; Bismarck, A. Cellulose Nanopapers as Tight Aqueous Ultra-Filtration Membranes. *React. Funct. Polym.* **2015**, *86*, 209-214.

66. Nakagaito, A. N.; Yano, H. The Effect of Morphological Changes from Pulp Fiber towards Nano-Scale Fibrillated Cellulose on the Mechanical Properties of High-Strength Plant Fiber based Composites. *Appl. Phys. A.* **2004**, *78*, 547-552.

67. Yano, H.; Nakahara, S. Bio-Composites Produced from Plant Microfiber Bundles with a Nanometer Unit Web-Like Network. *J. Mater. Sci.* **2004**, *39*, 1635-1638.

68. Peresin, M. S.; Kammiovirta, K.; Heikkinen, H.; Johansson, L-S.; Vartiainen, J.; Setälä, H.; Österberg, M.; Tammelin, T. Understanding the Mechanisms of Oxygen Diffusion through Surface Functionalized Nanocellulose Films. *Carbohydr. Polym.* **2017**, *174,* 309-317.

69. Rodionova, G.; Eriksen, Ø.; Gregersen, Ø. TEMPO-oxidized cellulose nanofiber films: effect of surface morphology on water resistance. *Cellulose* **2012**, *19*, 1115-1123.

70. Syverud, K.; Xhanari, K.; Chinga-Carrasco, G. Films Made of Cellulose Nanofibrils: Surface Modification by Adsorption of a Cationic Surfactant and Characterization by Computer-Assisted Electron Microscopy. *J. Nanopart. Res.* **2011**, *13*, 773-782.

71. Hasani, M.; Cranston, E. D.; Westman, G.; Gray, D. G. Cationic Surface Functionalization of Cellulose Nanocrystals. *Soft Matter* **2008**, *4*, 2238-2244.

72. Heux, L.; Chauve, G.; Bonini, C. Nonflocculating and Chiral-Nematic Self-Ordering of Cellulose Microcrystals Suspensions in Nonpolar Solvents. *Langmuir* **2000**, *16*, 8210-8212.

73. Habibi, Y. Key Advances in the Chemical Modification of Nanocelluloses. *Chem. Soc. Rev.* **2014**, *43*, 1519-1542.

74. Eyley, S.; Thielemans, W. Surface Modification of Cellulose Nanocrystals. *Nanoscale* **2014**, *6*, 7764-7779.

75. Mertaniemi, H.; Escobedo-Lucea, C.; Sanz-Garcia, A.; Gandi`a,C.; Mäkitie,A.;Partanen, J.; Ikkala,O.; Yliperttula, M. Human Stem Cell Decorated Nanocellulose Threads for Biomedical Applications. *Biomaterials* **2016**, *82*, 208-220.

76. Orelma, H.; Vuoriluoto, M.; Johansson, L.-S.; Campbell, J. M.; Filpponen, I.; Biesalki, M.; Rojas, O. J. Preparation of Photoreactive Nanocellulosic Materials via Benzophenone Grafting. *RSC Adv.* **2016**, *6*, 85100-85106.

77. Vuoriluoto, M.; Orelma, H.; Lundahl, M.; Borghei, M.; Rojas,O.J. Filaments with Affinity Binding and Wet Strength Can Be Achieved by Spinning Bifunctional Cellulose Nanofibrils. *Biomacromolecules* **2017**, *18*, 1803-1813

78. Lu, P.; Hsieh, Y.-L. Cellulose Nanocrystal-Filled Poly(Acrylic Acid) Nanocomposite Fibrous Membranes. *Nanotechnology* **2009**, *20,* 1-9.

79. Chinga-Carrasco, G., Kuznetsova, N., Garaeva, M., Leirset, I., Galilullina, G., Kostochko, A., & Syverud, K. Bleached and unbleached MFC nanobarriers: properties and hydrophobisation with hexamethyldisilazane. *J. Nanopart. Res.* **2012** *14,* 1280-1289.

80. Filpponen, I.; Kontturi, E.; Nummelin, S.; Rosilo, H.; Kolehmainen, E.; Ikkala, O.; Laine, J. Generic Method for Modular Surface Modification of Cellulosic Materials in Aqueous Medium by Sequential "Click" Reaction and Adsorption. *Biomacromolecules* **2012**, *13*, 736-742.

81. Kontturi, K. S.; Biegaj, K.; Mautner, A.; Woodward, R. T.; Johansson, L.-S.; Lee, K.-Y.; Heng, J. Y. Y.; Bismarck, A.; Kontturi, E. Noncovalent Surface Modification of Cellulose Nano Absorption of Polymers from Aprotic Solvents. *Langmuir* **2017**, *33*, 5707-5712.

82. Österberg, M.; Peresin, M. S.; Johansson, L.-S.; Tammelin, T. Clean and Reactive Nanostructured Cellulose Surface, *Cellulose* **2013**, *3*, 983-990.

83. Piringer, O. Permeation of Gases, Water Vapour and Volatile Organic Compounds. In O. Piringer, & A. Baner (Eds.), 2007, *Plastic Packaging Materials for Food* (pp. 239-285). Weinheim: Wiley-VCH.

84. Yamane, C.; Aoyagi, T.; Ago, M.; Sato, K.; Okajima, K.; Takahashi, T. Two Different Surface Properties of Regenerated Cellulose due to Structural Anisotropy. *Polym. J.* **2006**, *38*, 819-826.

85. Yamane C. Structure Formation of Regenerated Cellulose from Its Solution and Resultant Features of High Wettability: A Review. *Nord. Pulp. Pap. Res. J.* **2015** *30*, 78-91.

86. Mazeau, K.; Rivet, A. Wetting the (110) and (100) surfaces of Iβ cellulose studied by molecular dynamics. *Biomacromolecules* **2008**, *9*, 1352-1354.

87. Gestranius, M.; Stenius, P.; Kontturi, E.; Sjöblom, J.; Tammelin, T. Phase Behaviour and Droplet Size of Oil-in-Water Pickering Emulsions Stabilised with Plant-Derived Nanocellulosic Materials. *Colloids Surf. A.* **2017**, *519*, 60-70.

88. Kalashnikova, I.; Bizot, H.; Cathala, B.; Capron, I. New Pickering Emulsions Stabilized by Bacterial Cellulose Nanocrystals. *Langmuir* **2011**, *27*, 7471-7479.

89. Kedzior, S. A.; Marway, H. S.; Cranston, E. D. Tailoring Cellulose Nanocrystal and Surfactant Behavior in Miniemulsion Polymerization. *Macromolecules* **2017**, *50*, 2645-2655.

90. Cervin, N.; Andersson, L.; Sing Ng, J.; Olin, P.; Bergström, L. Lightweight and Strong Cellulose Materials Made from Aqueous Foams Stabilized by Nanofibrillated Cellulose. *Biomacromolecules* **2012**, *14*, 503-511.

91. Medronho, B.; Lindman, B. Competing Forces during Cellulose Dissolution: From Solvents to Mechanisms. *Curr. Opin. Colloid Interface Sci.* **2014**, *19*, 32-40.

92. Medhorno, B.; Duarte, H.; Alves, L.; Antunes, F.; Romano, A.; Lindman, B. Probing Cellulose Amphiphilicity. *Nord. Pulp Pap. Res. J.* **2015**, *30*, 58-66.

93. Uetani, K.; Yano, H. Zeta Potential Time Dependence Reveals the Swelling Dynamics of Wood Cellulose Nanofibrils. *Langmuir* **2011**, *28*, 818-827.

94. Tenhunen, T.-M.; Peresin, M. S.; Penttilä, P. A.; Pere, J.; Serimaa, R.; Tammelin, T. Signifigance of Xylan on the Stability and Water Interactions of Cellulosic Nanofibrils. *React. Funct. Polym.* **2014**, *85*, 157-166.

95. Jayme, G., Rothamel, L. Development of a standard centrifugal method for determining the swelling values of pulps. *Papier*, **1948**, *2*, 7-18.

96. Stannett, V.; Haider, M.; Koros, W. J.; Hopfenberg, H. B. Sorption and Transport of Water Vapor in Glassy Poly(Acrylonitrile). *Polym. Eng. Sci.* **1980**, *20*, 300-304.

97. Pönni, R. ; Vuorinen, T.; Kontturi, E. Proposed Nano-scale Coalescence of Cellulose in Chemical Pulp Fibers During Technical Treatments. *Bioresources* **2012**, *7*, 6077-6108.

98. Fujiwara, H. *Spectroscopic Ellipsometry*; John Wiley & Sons, Ltd.; Chichester, UK, 2007.

99. Girgnon, J.; Scallan, A. M. Effect of pH and Neutral Salts Upon the Swelling of Cellulose Gels. *J. Appl. Polym. Sci.* **1980**, *25*, 2829-2943.

100. Olszewska, A.; Eronen, P.; Johansson, L.-S.; Malho, J. M.; Ankerfors, M.; Lindström, T.; Ruokolainen, J.; Laine, J.; Österberg, M. The Behaviour of Cationic Nanofibrillar Cellulose in Aqueous Media. *Cellulose* **2011**, *18*, 1213-1226.

101. Reid, M. S.; Kedzior, S.; Villalobos, M.; Cranston, E. Effect of Ionic Strength and Surface Density on the Kinetics of Cellulose Nanocrystal Thin Film Swelling. *Langmuir* **2017**, *33*, 7403-7411.

102. Reid, M. S.; Villalobos, M.; Cranston, E. D. Cellulose Nanocrystal Interactions Probed by Thin Film Swelling to Predict Dispersibility. *Nanoscale* **2016**, *8*, 12247-12257.

103. Kittle, J. D.; Du, X.; Jiang, F.; Qian, C.; Heinze, T.; Roman, M.; Esker, A. R. Equilibrium Water Contents of Cellulose Films Determined via Solvent Exchange and Quartz Crystal Microbalance with Dissipation Monitoring. *Biomacromolecules* **2011**, *12*, 2881-2887.

104. Kontturi, K. S.; Kontturi, E.; Laine, J. Specific Water Uptake of Thin films from Nanofibrillated Cellulose. *J. Mater. Chem. A* **2013**, *1*, 13655-13663.

105. Gross, A. S; Chu, J.-W. On Molecular Origins of Biomass Recalcitrance: The Interactions Network and Solvation Structures of Cellulose Microfibrils. *J. Phys. Chem. B.* **2010**, *114*, 13333-13341.

106.   Paajanen, A.; Sonavane, Y.; Ignasiak, D.; Ketoja, J. A.; Maloney, T.; Paavilainen, S. Atomistic Molecular Dynamics Simulations on the Interaction of TEMPO-Oxidized Cellulose Nanofibrils in Water, *Cellulose* **2016**, *23*, 3449–3462.

107.   Urquhardt, A.R.; Williams, A.M. The Effect of Temperature on the Adsorption of Water by Soda-Boiled Cotton. *J. Text. Inst., Trans.* **1924**, 75, 559-572.

108.   Shrestha, S.; Diaz, J. A.; Ghanbari, S.; Youngblood, J. P. Hygroscopic Swelling Determination of Cellulose Nanocrystal (CNC) Films by Polarized Light Microscopy Digital Image Correlation, *Biomacromolecules*, **2017**, *18*, 1282-1490.

109.   Niinivaara, E.; Faustini, M.; Tammelin, T.; Kontturi, E. Water Vapor Uptake of Ultrathin Films of Biologically Derived Nanocrystals: Quantitative Assesment with Quartz Crystal Microbalance and Spectroscopic Ellipsometry. *Langmuir* **2015**, *31*, 12170-12176.

110. Driemeier, C.; Mendes, F. M.; Oliviera, M. M. Dynamic Vapor Sorption and Thermoporometry to Probe Water in Celluloses. *Cellulose* **2012**, *19*, 1051-1063.

111. Belbekhouche, S.; Bras, J.; Siquiera, G.; Chappey, C.; Lebrun, L.; Khelifi, B.; Marais, S.; Dufresne, A. Water Sorption Behavior and Gas Barrier Properties of Cellulose Whiskers and Microfibril Films. *Carbohydr. Polym.* **2011**, *83*, 1740-1748.

112. Mericer, C.; Minelli, M.; Baschetti, M.; Lindström, T. Water Sorption in Microfibrillated Cellulose (MFC): The Effect of Temperature and Pretreatment. *Carbohydr. Polym.* **2017**, *174*, 1201-1212.

113. Minelli, M.; Baschetti, M.; Doghieri, F.; Ankerfors, M.; Lindström, T.; Plackett, D. Investigation of Mass Transport Properties of Microfibrillated Cellulose (MFC) Films). *J. Membr. Sci.* **2010**, *358*, 67-75.

114. Diaz, J.; Wu, X.; Martini, A.; Youngblood, J.; Moon, R. Thermal Expansion of Self-Organized and Shear-Oriented Cellulose Nanocrystal Films. *Biomacromolecules* **2013**, *14*, 2900-2908.

115. Niinivaara, E.; Faustini, M.; Tammelin, T.; Kontturi, E. Mimicking the Humidity Response of the Plant Cell Wall by Using Two-Dimensional Systems: The Critical Role of Amorphous and Crystalline Polysaccharides. *Langmuir* **2016**, *32*, 2032-2040.

116. Thomas, J. M.; Thomas, W. J. *Principles and Practices of Heterogeneous Catalysis*; Wiley: New York, 1996.

117. Ertl, G. Reactions at Surfaces: From Atoms to Complexity (Nobel Lecture). *Angew. Chem., Int. Ed.* **2008**, *47*, 3524-3535.

118. Grob, R. L.; Barry, E. F. Physicochemical Measurements by Gas Chromatography. In *Modern Practice of Gas Chromatography;* Wiley: Hoboken, 2004; pp 605-643.

119. Brunauer, S.; Emmett, P. H.; Teller, E. Adsorption of Gases in Multimolecular Layers. *J. Am. Chem. Soc.* **1938**, *60*, 309-319.

120.   Gocho, H.; Tanioka, A.; Nakajima, T. Sorption Isotherm Analysis of Water by Hydrophilic Polymer Composed of Different Adsorption Sites Using Modified BET Equation. *J. Colloid Interface Sci.* **1998**, *200*, 155-160.

121. Timmermann, E. O. A B.E.T.-like Three Sorption Stage Isotherm. *J. Chem. Soc., Faraday Trans.* **1989**, *85*, 1531-1645.

122.   Barrer, R.; Barrie, J.; Slater, J. Sorption and Diffusion in Ethyl Cellulose. Part III. Comparison between Ethyl Cellulose and Rubber, *J. Polym. Sci.* **1958**, *27*, 177-197.

123.   Langmuir, I. The Adsorption of Gases on Plane Surfaces of Glass, Mica and Platinum. *J. Am. Chem. Soc.* **1918**, *40*, 1361-1403.

124.   Henry, W. Experiments on the Quantity of Gases Adsorbed by Water, at Different Temperatures and under Different Pressures. *Philos. Trans. R. Soc. London* **1803**, *93*, 29-42.

125. Flory, P. J. *Principles of Polymer Chemistry*; Cornell University Press: Ithaca, NY, 1953.

126.   Hailwood, A. J.; Horrobin, S. Absorption of Water by Polymers: Analysis in Terms of a Simple Model. *J. Chem. Soc., Faraday Trans.* **1946**, *42*, B084-B092.

127. Hernandez, R.; Giacin, J.; Grulke, E. The Sorption of Water by an Amorphous Polyamide, *J. Membr. Sci.* **1992**, *65*, 187-199.

128.   Orofino, T.; Hopfenberg, H.; Stannett, V. Characterization of Penetrant Clustering in Polymers, *J. Macromol. Sci., Part B: Phys.* **1969**, *3*, 777-788.

129.   Fick, A. On Liquid Diffusion. *J. Membr. Sci .***1995**, *100*, 33-38.

130.   Crank, J. Mathematics of Diffusion, Brunel University Uxbridge, 2nd Edition, 1975.

131. Newman, A. The Drying of Porous Solids: Diffusion and Surface Emission Equations. *Trans. Am. Inst. Chem. Engr.* **1931**, *27*, 203-211.

132.   Lee, M. H.; Lim, B.; Kim, J. W.; An, E., J., Lee, D. Effect of Composition on Water Permeability of Model Stratum Corneum Lipid Membranes, *Soft Matter* **2012**, *8*, 1539-1546.

133.   Bedane, A. H.; Eic, M.; Farmahini-Farahani, M.; Xiao, H. Water Vapor Transport Properties of Regenerated Cellulose and Nanofibrillated Cellulose Films. *J. Membr. Sci.* **2015**, *439*, 46-57.

134.   Membrane Technology in the Chemical Industry, Part I, Nunes, S. P. Peinemann, K. V. Wiley-VCH, 2001. Weinheim, Germany.

135. Mautner, A.; Maples, H.A.; Sehaqui, H.; Zimmermann, T.; de Larraya, U.P.; Mathew, A.P.; Lai, C.Y.; Li, K.; Bismarck, A. Nitrate removal from water using a nanopaper ion-exchanger. *Environ. Sci. Water Res. Technol.* **2016**, *2*, 117–124.

136.   Metreveli, G.; Wågberg, L.; Emmoth, E.; Belák, S.; Strømme, M.; Mihranyan, A. A Size-Exclusion Nanocellulose Filter Paper for Virus Removal. *Adv. Healthc. Mater.* **2014**, *3*, 1546–1550.

137. Karim, Z.; Claudpierre, S.; Grahn, M.; Oksman, K.;Mathew, A. P. Nanocellulose based Functional Membranes for Water Cleaning: Tailoring of Mechanical Properties, Porosity and Metal Ion Capture. *J. Membr. Sci.* **2016**, 20644-20653.

138.   Karim, Z.; Hakalahti, M.; Tammelin, T.; Matthew, A. In situ TEMPO Surface Functionalization of Nanocellulose Membranes for Enhanced Adsorption of Metal Ions from Aqueous Medium. *RCS Adv.* **2017**, *7*, 5232-5241.

139.   Scandinavian Pulp, Paper and Board Testing Committee, SCAN 65:02. Total Acidic Group Content. Conductometric Titration Method. 2002.

140.   Laukkanen, A.; Pere, J.; Mikkelsson, A. Analytical Method for Determining the Concentration of Oxidized Nanofibrillar Cellulose in a Sample. CA2908852, 2014.

141. Eronen, P.; Laine, J.; Ruokolainen, J.; Österberg, M. Comparison of Multilayer Formation between Different Cellulose Nanofibrils and Cationic Polymers. *J. Colloid Interface Sci.* **2011**, *373*, 84-93.

142.   Sauerbrey, G. The Use of Quartz Oscillators for Weighing Thin Layers and for Microweighing. *Z. Phys.* **1959**, *155*, 206–222.

143.   Woollam, J.A. Co., Inc.; Guide to Using WVASE32 Software for Optical Data Analysis.

144.   Losurdo, M., Hingerl, K. Ellipsometry at the Nanoscale. Springer Science & Business Media. 2013.

145. Johansson, L.-S.; Campbell, J. Reproducible XPS on Biopolymers: Cellulose Studies, *Surf. Int. Analyt.*, **2004**, *36*, 1018-1022.

146.   De Cuadro, P.; Belt, T.; Kontturi, K.; Reza, M.; Kontturi, E.; Vuorinen, T.; Hughes, M. Cross-Linking of Cellulose and Poly(ethylene glycol) with Citric Acid, *React. Funct. Polym.* **2015**, *90*, 21-24.

147. Rieth, A. J.; Yang, S.; Wang, E. N.; Dinca, M. Record Atmospheric Fresh Water Capture and Heat Transfer with a Material Operating at the Water Uptake Reversibility Limit. *ACS Cent Sci.* **2017**, *3*, 668-672.

148. Cranston, E. D.; Grey, D. G. Birefringence in Spin-Coated Films Containing Cellulose Nanocrystals. *Colloids Surf., A*, **2008**, *325*, 44-51.

149. Boissière, C.; Grosso, D.; Lepoutre, S.; Nicole, L.; Bruneau, A.; Sanzchez, C. Porosity and Mechanical Properties of Mesoporous Thin Films Assessed by Environmental Ellipsometric Porosimetry. *Langmuir* **2005**, *21*, 12362-12371.

150. Bessadok, A.; Langevin, D.; Gouanvé, F.; Chappey, C.; Roudesli, S.; Marais, S. Study of Water Sorption on Modified Agave Fibres. *Carbohydr. Polym.* **2009**, *76*, 74-85.

151. Tanaka, R.; Saito, T.; Hänninen, T.; Ono, Y.; Hakalahti, M.; Tammelin, T.; Isogai, A. Viscoelastic Properties of Core-Shell-Structured, Hemicellulose-Rich Nanofibrillated Cellulose in Dispersion and Wet-Film States. *Biomacromolecules* **2016**, *17*, 2104-2111.

152. Ando, T.; Uchihashi, T.; Kodera, N. High-Speed AFM and Applications to Biomolecular Systems. *Annu. Rev. Biophys.* **2013**, *42*, 393-414.

153. Luo, B.; Smith, J. W.; Ou, Z.; Chen, Q. Quantifying the Self-Assembly Behavior of Anisotropic Nanoparticles Using Liquid-Phase Transmission Electron Microscopy. *Acc. Chem. Res.* **2017**, *50*, 1125-1133.

154. Baştürk, E., Demir, S., Daniş, Ö., & Kahraman, M. Covalent immobilization of a-amylase onto thermally crosslinked electrospun PVA/PAA nanofibrous hybrid membranes. *J. Appl. Polym. Sci.* **2013**, *127*, 349-355.

155. Clemons, C.; Sedlmair, J.; Illman, B.; Ibach, R.; Hirschmugl, C. Chemically Imaging the Effects of the Addition of Nanofibrillated Cellulose on the Distribution of Poly(Acrylic Acid) in Poly(Vinyl Alcohol). *Polymer* **2013**, *54*, 2058-2061.

156. Paralikar, S.; Simonsen, J.; Lombardi, J. Poly(Vinyl Alcohol)/Cellulose Nanocrystal Barrier Membranes. *J. Membrane Sci.* **2008**, *320*, 248-258.

157. Spoljaric, S., Salminen, A., Luong, N., & Seppälä, J. Crosslinked Nanofibrillated Cellulose: Poly(Acrylic Acid) Nanocomposite Films; Enhanced Mechanical Performance in Aqueous Environments. *Cellulose* **2013**, *20*, 2991-3005.

158. Vogel, S. *Comparative Biomechanics: Life's Physical World,* 2003, Princeton University Press, Princeton, NJ, Oxford.

159. Heskins, M.; Guillet, J. E. Solution Properties of Poly(*N*-isopropylacrylamide). *J. Macromol. Sci., Part A: Pure Appl.Chem.* **1968**, *2*, 1441-1455.

160.   Xie, R.; Li, Y.; Chu, L.-Y. Preparation of Thermo-Responsive Gating Membranes with Controllable Response Temperature. *J. Membr. Sci.* **2007**, *289*, 76-85.

161.   Schepelina, O.; Zharov, I. PNIPAAM-Modified Nanoporous Colloidal Films with Positive and Negative Temperature Gating. *Langmuir* **2007,** *25*, 12704-12709.

162.   Ganesh, A.; Ranganath, A.; Sridhar, R.; Raut, H.; Jayaraman, J.; Sahay, R.; Ramakrishna, S.; Baji, A. Cellulose Acetate−Poly(*N*-isopropylacrylamide)-Based Functional Surfaces with Temperature-Triggered Switchable Wettability. *Macromol. Rapid Commun.* **2015**, *36*, 1368–1373.

163.   Clayden, J.; Greeves, N.; Warren, S.; Wothers, P. *Organic Chemistry*; Oxford University Press: Oxford, UK, 2005; pp. 279-303.

164.   Bhattacharyya, D.; Williams, M. E. In *Membrane Handbook;* Winston, H.; Sirkar, K., Eds.; Van Nostrand Reinhold: New York, 1992; Chapter 21, pp. 265-268.

165.   Machado, D.; Hasson, D.; Semiat, R. Effect of Solvent Properties on Permeate Flow Through Nanofiltration Membranes. Part I: Investigation of Parameters Affecting Sol-vent Flux. *J. Membr. Sci.* **1999**, *163*, 93-102.

166.   Uliyanchenko, E.; Schoenmakers. P. J. van der Wal, S. Fast and efficient size-based separations of polymers using ultra-high-pressure liquid chromatography. *J. Chromatogr. A* **2011**, *1218*, 1509-1518.

167.   Armstrong, J. K.; Wenby, R. B.; Meiselman, H. J. Fisher, T. C. The hydrodynamic radii of macromolecules and their effect on red blood cell aggregation. *Biophys. J.* **2004**, *87*, 4259-4270.

168.   Vandezande, P.; Gavers, L. Vankellecom, I. Solvent Resistant Nanofiltration: Separating on a Molecular Level. *Chem. Soc. Rev.* **2008**, *37*, 365-405.

Paper I

Hakalahti, M.; Faustini, M.; Boissière, C.; Kontturi, E.; Tammelin, T. Inter-facial Mechanisms of Water Vapor Sorption as Revealed by Quantitative Models. *Biomacromolecules* **2017**, *18*, 2951-2958.

Interfacial Mechanisms of Water Vapor Sorption into Cellulose Nanofibril Films as Revealed by Quantitative Models

Minna Hakalahti,[†] Marco Faustini,[‡] Cédric Boissière,[‡] Eero Kontturi,*[§] and Tekla Tammelin*[†]

[†]High Performance Fibre Products, VTT Technical Research Center of Finland, Ltd, FI-02044, Espoo, Finland

[‡]Sorbonne Universités, UPMC Univ Paris 06, CNRS, Collège de France, UMR 7574, Chimie de la Matière Condensée de Paris, F-75005, Paris, France

[§]Department of Bioproducts and Biosystems, School of Chemical Engineering, Aalto University, 02150 Espoo, Finland

Ⓢ *Supporting Information*

ABSTRACT: Humidity is an efficient instrument for facilitating changes in local architectures of two-dimensional surfaces assembled from nanoscaled biomaterials. Here, complementary surface-sensitive methods are used to collect explicit and precise experimental evidence on the water vapor sorption into (2,2,6,6-tetramethylpiperidin-1-yl)oxyl (TEMPO) oxidized cellulose nanofibril (CNF) thin film over the relative humidity (RH) range from 0 to 97%. Changes in thickness and mass of the film due to water vapor uptake are tracked using spectroscopic ellipsometry and quartz crystal microbalance with dissipation monitoring, respectively. Experimental data is evaluated by the quantitative Langmuir/Flory–Huggins/clustering model and the Brunauer–Emmett–Teller model. The isotherms coupled with the quantitative models unveil distinct regions of predominant sorption modes: specific sorption of water molecules below 10% RH, multilayer build-up between 10 to 75% RH, and clustering of water molecules above 75% RH. The study reveals the sorption mechanisms underlying the well-known water uptake behavior of TEMPO oxidized CNF directly at the gas–solid interface.
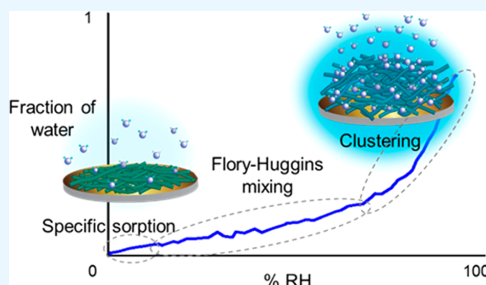
INTRODUCTION

Water vapor sorption into hydrophilic and moisture-sensitive materials is an enticing way to tune local surface geometries at nanoscale. Likewise, many terrestrial phenomena, such as lightning generation[1] or seed dispersion,[2] demonstrate innate functionalities based on vapor interactions. To exploit the native properties in materials construction, one can isolate biological units like cellulose nanofibrils (CNFs) that, due to high density of hydrophilic functional groups,[3–5] exhibit outstanding sensitivity toward humidity[6–8]—a characteristic that distinguishes them from many other nanomaterials that may be comparable in terms of high aspect ratios and tensile strengths.[9,10] Ultrathin layers of CNFs with confined space for expansion and with well-known morphology are potential platforms for humidity-driven and controllable surface architectures.[10,11] However, precise insight on the changes in the physical attributes of the moisture-sensitive films due to water vapor sorption is needed for realizing the use of complex plant-based nanomaterials in vapor-sensitive applications, e.g., nanoenhanced sensors[12,13] and membranes.[14,15]

Research on water vapor and gas adsorption at various interfaces has long and sturdy roots in the areas of e.g. heterogeneous catalysis[16,17] and chromatographic analysis.[18] The quantification of gas adsorption in these applications is typically achieved by the classical Brunauer–Emmett–Teller

(BET) theory[19] or its modern variants.[20–22] On the other hand, sorption of solvents, usually water vapor, onto polymeric materials, has been widely interpreted through additive dual sorption models[23] using combinations of the classical Langmuir theory,[24] Henry's Law,[25] and the Flory–Huggins mixing theory.[26] In the realm of polymeric and fibrous biomaterials, water vapor sorption has a permanent place among the constitutive research topics[23,27–29] due to its high practical value in the context of, for example, papermaking and food preservation. A set of specific models, such as the Park's model,[7,30,31] the Guggenheim–Anderson–de Boer (GAB) model[7,21,33] and the Hailwood–Horrobin model,[33,34] have often been used to quantitatively describe water vapor sorption of cellulosic materials. We selected the additive Langmuir/Flory–Huggins/clustering model, because, in addition to its simplicity, it has been successfully applied to complex, hydrophilic polymer film systems.[35,36]

The vast majority of the accumulated knowledge regarding water vapor sorption is based on experimental evidence collected by gravimetric bulk methods, principally the dynamic vapor sorption.[7,34] The advantage of the surface-sensitive

approach taken in this study over the bulk methods is that it enables investigation of water vapor sorption directly at the surface, where the phenomenon mainly occurs. Moreover, in contrast to gravimetric methods, the changes within the material due to water vapor sorption can be tracked with respect to not just mass, but also thickness, volume and solid state rheology in a noninvasive manner. The use of supported thin films as sample platforms confines dimensional changes merely to one dimension in space,[11] allowing volumetric analysis of the film based on thickness. In this respect, the surface-sensitive approach is transcendent in collecting explicit experimental evidence to accommodate for the complexity of the lignocellulosic CNF and to enable reliable and coherent quantitative model fitting.

Surface-sensitive spectroscopic ellipsometry (SE) and quartz crystal microbalance with dissipation monitoring (QCM-D) are widely used to study surface phenomena of homogeneous thin model surfaces.[37−40] SE is an optical technique based on tracking the change in the state of polarization of light (phase and amplitude) upon reflection for determining thickness with subnanometer preciseness.[37,41] Equally sensitive, QCM-D uses the change in the frequency of acoustic waves generated by oscillating a piezoelectric sensor for monitoring changes in mass with nanogram sensitivity.[38,40] Enabled by characterization of morphology and determination of chemical composition, we use the complementary combination of QCM-D and SE equipped with humidity chambers to precisely monitor changes in mass and thickness of thin films of heterogeneous and complex biomaterial (2,2,6,6-tetramethylpiperidin-1-yl)oxyl oxidized (TEMPO) CNF as a function of relative humidity (RH). Such combination of QCM-D and SE on vapor uptake has been applied before, but chiefly on well-defined, homogeneous model materials and substances.[42−46] Encouraged by the convincing results of Niinivaara et al.[45,46] for acquisition of water vapor sorption data on thin nanocrystalline cellulose (CNC) films, we attempt to achieve a profound understanding of the water sorption mechanisms by fitting the collected *in situ* data using the BET model and the Langmuir/Flory−Huggins/clustering model.[35,36] In addition, the application of the system to illuminate the behavior of a heterogeneous CNF network represents an entirely new perspective for these techniques since the classical physicochemical models were successfully extended to describe the behavior of the complex biomaterials in a gas−solid binary system. Hereby, we expose interesting innate aspects underlying the well-known water vapor uptake behavior directly at the air−cellulose interface and gain revealing information about the potential of the biomaterials for vapor-sensitive applications.

■ EXPERIMENTAL SECTION

Materials. Never dried bleached softwood pulp was obtained from a pulp mill in Finland. TEMPO, sodium bromide (solid) and 10% sodium hypochlorite (aqueous) were obtained from Sigma-Aldrich. Sodium hydroxide solution (0.1 M) was received from Fluka Analytical. Poly(ethylene imine) solution in water (PEI, 30 wt %, M_w = 70 000 g/mol) was purchased from PolySciences Inc., Warminster, PA, USA. LiBr (solid), $ZnBr_2$ (solid), and NaCl (solid) were purchased from Sigma-Aldrich Oy, Helsinki, Finland. LiCl (solid), $MgCl_2 \cdot 6H_2O$ (solid), $Mg(NO_3)_2 \cdot 6H_2O$ (solid), and K_2SO_4 (solid) were purchased from VWR International Oy, Helsinki, Finland. Saturated salt solutions in water were prepared, decanted and used in experiments without any further treatment. Deionized water was purified by a Milli-Q system (Millipore Corporation, Molsheim, France, resistivity 18.2 MΩ) and used in all experiments. TEMPO

CNF thin films were prepared on AT-cut gold sensors with a fundamental resonance frequency, f_0, of 5 MHz and a sensitivity constant, C, of 0.177 mg m^{-2} Hz^{-1} as reported by the supplier, were purchased from Q-Sense AB, Gothenburg, Sweden.

Production of TEMPO CNF. Softwood pulp was TEMPO oxidized according to the previously described procedure of alkaline oxidation with hypochlorite, catalyzed by TEMPO.[47] The charge of the oxidized pulp, as measured by a standard conductometric titration procedure (SCAN-CM 65:02, 2002) was 0.836 mmol g^{-1}. TEMPO oxidized pulp was fibrillated using a high pressure fluidizer, Microfluidics M-110EH-30 (Microfluidics Int., USA), equipped with two Z-type chambers. The chambers had diameters of 400 and 100 μm, and the pulp was passed through the fluidizer two times at 1850 bar operating pressure to obtain TEMPO oxidized cellulose nanofibrils (TEMPO CNF) with final consistency of approximately 1 wt %. Neutral sugar composition analysis showed that the neutral sugar content of hemicellulose in the TEMPO CNF was 8% (Supporting Information).

Preparation of Supported Thin Films of TEMPO CNF. Supported thin films of TEMPO CNF were prepared according to the slightly modified procedure described by Eronen et al.[48] In brief, the TEMPO CNF suspension was diluted to a concentration of 0.15 wt % using milli-Q water and sonicated using a Branson Digital Sonifier (400 W; 20 kHz) at 40% amplitude for 2 min. Prior to deposition of anchoring polymer (PEI) and TEMPO CNF, gold-coated QCM-D sensor surfaces were rinsed with water, dried with nitrogen gas and cleaned using UV/ozone (Bioforce Nanosciences, CA) for 10 min. To deposit the anchoring polymer on the gold sensor surface, cleaned sensors were coated with 1 mg mL^{-1} PEI solution in water by drop casting over 30 min followed by rinsing with milli-Q water, drying with nitrogen gas and heat treatment in an oven at 80 °C for 10 min. 200 μL of TEMPO CNF was dispensed onto the PEI-coated sensor and spin-coated (WS-400BZ-6NPP/Lite, Laurell, North Wales, PA, USA) at 3000 rpm for 3 min followed by annealing for 10 min in 80 °C oven to ensure fibril attachment.[48]

Atomic Force Microscopy (AFM). Characterization of the spin-coated TEMPO CNF sample surface morphology (Figure 1a) was carried out using afm+ from Anasys Instruments, Inc. (Santa Barbara, CA, USA) in tapping mode with EX-T125 probes from ST Instruments B. V. (Groot-Ammers, The Netherlands). Typical cantilever resonance frequency was 200−400 kHz, spring constant 13−77 N m^{-1}, and radius of the curvature of the cantilever 10 nm according to the manufacturer. No other image processing was performed except flattening, and at least five images per sample were taken. AFM images were analyzed using the Analysis Studio software (version 3.11).

Spectroscopic Ellipsometry for Determination of Thickness Fractions. SE measurements were carried out on a UV–vis (λ = 500−998.85 nm) variable angle spectroscopic ellipsometer (Vase-2000U, Woollam Inc., Lincoln, NE, USA) equipped with a humidity chamber. The supported TEMPO CNF thin films coated directly on the gold QCM-D sensor substrate were placed on a sample plate inside the humidity chamber and a beam of polarized light was focused on the sample. The light beam was aligned with the light detector by adjusting the tilt of the sample plate. The initial theoretical thickness and refractive index were determined by conducting an initial spectroscopic scan and applying by the classic Cauchy model. To validate the use of the Cauchy model, the measured refractive indices were fitted to model data (Supporting Information). The RH cycle was then started to conduct a dynamic SE scan.

A 3 l min^{-1} flux of air containing a fixed partial pressure of water was injected continuously to the humidity chamber. The real *in situ* % RH inside the humidity chamber was continuously monitored by a humidity sensor. The humidity cycle consisted of incremental steps of 2% RH each lasting 20 s. Data analyses were performed using the Wvase32 software using the Cauchy model. The evolution of the refractive index (RI) and thickness (shown for a single wavelength (λ = 700 nm) for simplicity) of the film was recorded with the SE system and shown in Figure 1b over the measured relative humidity range. SE detects the refractive index and thickness evolution of the entire
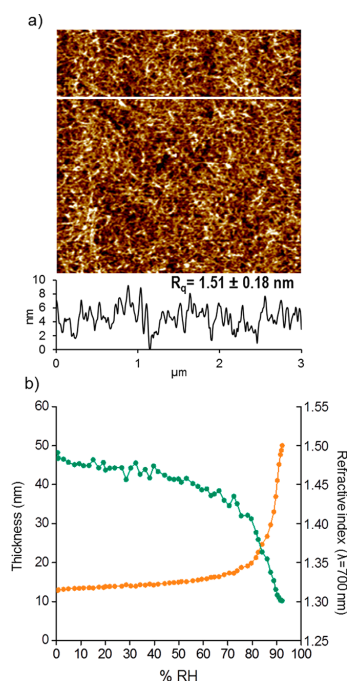
Figure 1. (a) 3 μm × 3 μm AFM height image with topographic profile and root-mean-square roughness-value (R_q) of TEMPO CNF thin film. The topographic profile below the height image is indicated with a white line. (b) Evolution of the refractive index (at $\lambda = 700$ nm) (green) and thickness (orange) of TEMPO CNF thin film as a function of relative humidity as measured by spectroscopic ellipsometry. The refractive index describes the entire multicomponent thin film system, including TEMPO CNF (with hemicellulose), water vapor, and air.

multicomponent thin film system, including TEMPO CNF, water vapor, and air. Optical thickness, which is defined as the natural logarithm of incident to transmitted radiant power through a material,[49] was calculated by multiplying thickness with refractive index at each % RH step.

Thickness fractions of water in the TEMPO CNF thin film were calculated by dividing the thickness increase due to water vapor sorption at a given point along the % RH spectrum by the total thickness of the TEMPO CNF thin film at the same % RH point (see Supporting Information for exemplary calculations). It was assumed that all changes in thickness or optical thickness occurred due to water vapor uptake. Hence, the thickness fraction of water describes the added thickness due to sorption of water, but it does not differentiate between actual thickness of the water molecules and thickness changes in the film due to structural changes, e.g., swelling or reconfiguration of individual fibrils or hemicellulose.

Quartz Crystal Microbalance with Dissipation Monitoring. Water vapor uptake of TEMPO CNF thin films with respect to mass was investigated using the E4 QCM-D instrument equipped with a QHM 401 humidity module (Q-Sense AB, Gothenburg, Sweden).[6,50] The QCM-D instrument is designed for detecting mass changes occurring at solid–liquid or solid–gas interfaces. A piezoelectric quartz sensor between two electrodes oscillates at a specific fundamental resonance frequency, f_0, and its overtones as pulsed electric field (AC voltage) is applied. The resonance frequency changes as the total mass of the film on the surface of the sensor increases or decreases. When the film is evenly distributed, rigidly adhered, fully elastic, and has a

small mass in comparison to the mass of the sensor crystal, the change in frequency is directly proportional to the change in areal mass and can be calculated according to the Sauerbrey equation (eq 1):[51]

$$\Delta m = -C\frac{\Delta f}{n} \tag{1}$$

where $\Delta f = f - f_0$ is the change in resonance frequency, C is the sensitivity constant of the sensor, and n is the measurement overtone number ($n = 1, 3, 5, 7, 9, 11$).

Simultaneously, when voltage is cut off, the oscillation gradually decreases and the resonance amplitude attenuates due to frictional losses in the adsorbed thin film layer. The attenuation of the amplitude, i.e., dissipation of energy, D, can be used as a measure of viscoelastic properties of the sample, and it can be presented as

$$D = \frac{E_{\text{dissipation}}}{2\pi E_{\text{storage}}} \tag{2}$$

where $E_{\text{dissipation}}$ is the energy dissipated and E_{storage} is the total energy stored during one oscillation cycle in the oscillator. A thin film can be considered to be fully elastic and rigid when ΔD is $\leq 1 \times 10^{-6}$, and the overtones of ΔD and Δf do not spread significantly. The interpretation of the QCM-D data is described in detail elsewhere.[36−38]

Initial TEMPO CNF Thin Film Areal Mass Determination by QCM-D. Initial areal mass of the dry TEMPO CNF thin film was determined to set a baseline for water uptake measurements. Prior to thin film preparation, initial mass of pristine QCM-D sensors was measured in a QHM 401 humidity module (23 °C, air flow rate 0.1 mL min^{-1}) of the QCM-D device following a 13 h stabilization at 6% RH. Similarly to Tenhunen et al.,[6] following the TEMPO CNF thin film preparation on the QCM-D sensor surface and overnight stabilization inside the humidity module at 6% RH for 13 h, the initial areal mass of the TEMPO CNF thin films was determined. Data was stitched together using the QTools Software and the third overtone (15 MHz, $f_0 = 5$ MHz, $n = 3$) was used for quantitative calculations in this work for areal mass based on Δf according to the Sauerbrey eq (eq 1).[6,52] (Supporting Information)

Humidity Measurements by QCM-D for Determination of Mass Fractions. Figure 2 shows the measured changes in resonance frequency (Δf) and in dissipation energy (ΔD) that were monitored as a function of time with incrementally increasing % RH. Changes in % RH were achieved by passing saturated salt solutions and milli-Q water through the humidity module to produce eight increasing relative humidity steps (Supporting Information). Each salt solution was
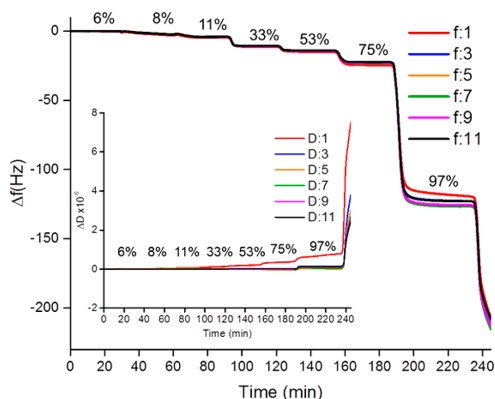

Figure 2. Change in frequency (Δf) and dissipation (ΔD) (shown in the inset) as a function of time in stepwise increasing relative humidity (% RH) as detected by QCM-D water vapor adsorption measurements for TEMPO CNF thin films. Different overtones are indicated with colors.
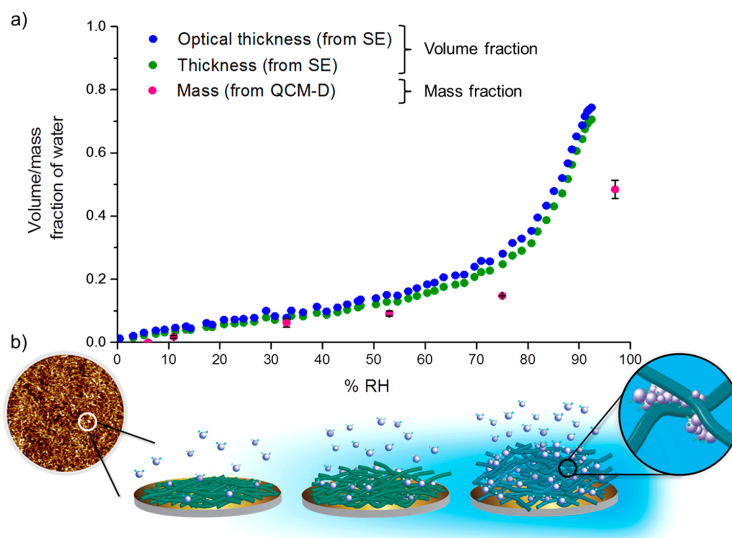
Figure 3. (a) Mass (pink), optical thickness (blue) and thickness (green) fractions of water in TEMPO CNF thin films due to water vapor uptake as a function of relative humidity. Thickness and optical thickness fractions of water are deduced from data collected by SE. Responses of the SE consist of the optical behavior of water, TEMPO CNF and air. Mass fractions of water are based on QCM-D measurements and the use of the Sauerbrey eq (eq 2) (see Supporting Information for calculations). QCM-D senses the changes in mass due to uptake of water molecules by TEMPO CNF. (b) Schematic illustration of the water vapor uptake of TEMPO CNF thin film in dry air (RH < 10%), in humid air (10−75% RH) and at high humidity levels (RH > 75%). In the left inset, a portion of a $3 \times 3 \ \mu m$ AFM image of the fibril surface is displayed.
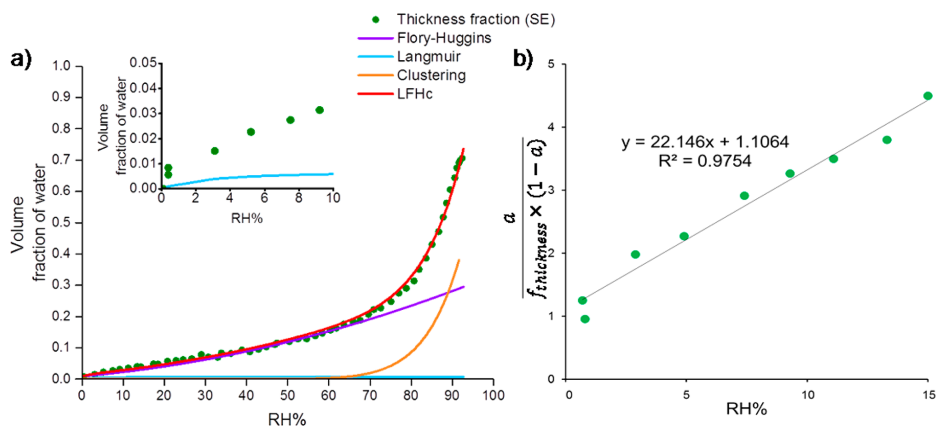
Figure 4. (a) Optical thickness isotherm of TEMPO CNF film fitted by the Langmuir/Flory−Huggins/clustering model. The inset shows the contribution of the Langmuir adsorption to the sorption of water vapor into TEMPO CNF thin films in dry air. (b) Optical thickness isotherm fitted by the BET model in the range from 0 to 15% RH.

passed through the QHM 401 humidity module at 0.1 mL min^{-1} rate for 30 min at 23 °C. Passing Milli-Q water (100% RH) through the humidity module possibly causes condensation effects inside the measurement chamber and the detected frequency and dissipation changes may be unreliable. Therefore, the last step is omitted in the calculations. Data was stitched together using the QTools Software and the third overtone (15 MHz, f_0 = 5 MHz, n = 3) was used for quantitative calculations based on Δf according to eq 1. Moreover, mass fractions of water in the TEMPO CNF film were calculated by dividing the film areal mass at any point over the entire RH% range by the total TEMPO CNF thin film areal mass. In addition to quantitative

calculations, the viscoelastic behavior of the TEMPO CNF thin film was qualitatively evaluated from ΔD values upon exposure to different levels of humidity in air. Each measurement was repeated three times and average values were used in calculations.

■ RESULTS AND DISCUSSION

Mass isotherm, thickness isotherm and optical thickness isotherm (taking into account the refractive index evolution) of the TEMPO CNF thin film over the RH range from 0 to 97% are shown in Figure 3a. The isotherms reveal that the

water fraction within the TEMPO CNF thin film increases as RH % increases. The depicted fractions of water were determined from SE and QCM-D humidity measurements by dividing the thickness or mass exceeding the respective initial (dry) values by the total thickness or mass of the TEMPO CNF thin film at each % RH point (exemplary calculation in Supporting Information). It is important to note that the nanofibrils themselves in the TEMPO CNF network do not notably swell: rather, the thickness increase largely originates from water molecules that penetrate between the nanofibrils, inducing the swelling the entire flexible network (Figure 3b). Three regions are apparent in the sorption isotherms: association of water molecules with the TEMPO CNF thin film in dry air (RH < 10%) through specific sorption; steady buildup of water molecule multilayer in humid air (10−75% RH); and the significant increase of the fraction of water at high humidity levels (RH > 75%) through further accumulation of water molecules and water molecule clusters in the TEMPO CNF thin film. The mass fractions of water appear slightly lower in comparison to the thickness fractions of water, mainly due to a difference in the initial % RH condition used to determine the dry mass (at 6% RH) or thickness (at 0% RH) of the TEMPO CNF thin film. Converting the QCM-D mass fractions to volume fractions by density yields water volume fractions of 0.21 and 0.59 at 75% and at 97% relative humidity, respectively. A significant portion of the difference between the thickness and mass fractions (density-corrected to volume fractions) probably comes from the fact that QCM-D senses the changes in mass due to uptake of water molecules by TEMPO CNF, whereas changes in optical response (SE) consist of the entire optical behavior of water, TEMPO CNF, and air. The water vapor uptake of the TEMPO CNF film is further evaluated by fitting the optical thickness sorption isotherms to the Langmuir/Flory−Huggins/clustering model[45,46] and to the BET model[19] (Figure 4). The models are not mutually exclusive, but they are rarely used in the same context to describe gas sorption.

The Langmuir/Flory−Huggins/clustering model is based on the work of Barrer et al., who suggested that nonlinear sorption isotherms can be decomposed into two distinct parts: the nonlinear Langmuir-type sorption at fixed sites of the sorption medium and linear sorption or the Henry's Law contribution at higher % RH range.[23,53] While the Langmuir−Henry dual sorption model describes sorption of gas above their boiling points into materials such as glassy polymers,[54] it underpredicts the solubility of solutes below their boiling points. Hence, a modification to the dual mode sorption model based on the Langmuir isotherm was proposed to describe specific sorption, and the Flory−Huggins contribution to describe nonspecific sorption.[45,46] In humid air, swelling exposes more binding sites in the sorption medium[45] and loosens the structure, clearing the way for subsequent solvent molecules to enter the structure.[54] This leads to clustering of water molecules, and is considered to be the third effective mechanism of the Langmuir/Flory−Huggins/clustering model.

Langmuir adsorption describing specific binding of gas molecules to solid surfaces is defined by eq 4:

$$V_L = \frac{Ka}{1 + Ba} \tag{4}$$

where K represents the concentration of the specific sorption sites, B is the affinity of water for these sites[24,32,45] and a is the water activity. Values of a are the ratio of partial pressure of

water vapor divided by the saturation vapor pressure and were considered to be equal to % RH divided by 100.

The Flory−Huggins equation for high molecular weight polymers in terms of fractions of water and water activity (a) can be expressed as following:[45]

$$\ln a_1 = \ln V_{FH} + (1 - V_{FH}) + \chi(1 - V_{FH})^2 \tag{5}$$

where a is the water activity, χ is the Flory−Huggins interaction parameter[26] and V_{FH} is the Flory−Huggins population or fraction of water associating with the film. The Flory−Huggins interaction parameter, χ, is fitted from the experimental SE data using eq 6:

$$\chi = \frac{\ln a - \ln V_{SE} - (1 - V_{SE})}{(1 - V_{SE})^2} \tag{6}$$

where V_{SE} is the optical thickness (or volume) fraction of water measured using SE. Customarily, the Flory−Huggins interaction parameter is used as a measure of thermodynamic miscibility of a polymer with a solvent in binary systems. We note that the use of the Flory−Huggins theory in the context of water vapor sorption into isotropic TEMPO CNF thin film differs from its original application in polymer mixing. However, postulating that water molecules can penetrate into the solid matrix, the sorption process mimics the mixing process from a thermodynamic point of view.

The clustering term in the Langmuir/Flory−Huggins/clustering model can be expressed by

$$V_C = a^n \tag{7}$$

where a is water activity and n describes the number of water molecules associated with each cluster.[7,55] Hence, the total fraction of water absorbed in the solid can be calculated by the Langmuir/Flory−Huggins/clustering function:

$$V = V_L + V_{FH} + V_C = \frac{Ka}{1 + Ba} + f(a, \chi) + Ca^n \tag{8}$$

Figure 4a shows the Langmuir/Flory−Huggins/clustering model (eq 8) fitted to the experimental optical thickness sorption isotherm of the TEMPO CNF film. The sorption isotherm collected using SE was selected for quantitative fitting, due to the larger number of data points compared to the isotherm collected by using QCM-D. Following the fitting approach described in detail by Hernandez et al., eq 8 was fitted in three separate parts to obtain the best estimates for the parameters in the physicochemically most relevant RH range. To start with, the Flory−Huggins interaction parameter (χ) was determined in the 30−70% RH range by a nonlinear regression method minimizing the least-squares errors. The Langmuir coefficients were solved using nonlinear regression based on an iterative algorithm with many possible local minima of the sum of the squares and hence multiple solutions to coefficient values. The pair of Langmuir coefficients was selected from the possible solutions by comparing to literature values[7] and evaluating their physicochemical meaningfulness. Moreover, there were systematic deviations from the dual mode model above 70% RH and therefore the clustering term was added to the function. The clustering coefficient was also solved by a nonlinear regression method.

Langmuir parameters representing the concentration of the specific sorption sites (K) and the affinity of water for these sites[24,32,45] were 1.408 and 223, respectively, according to the model. As shown in Figure 4a, the Langmuir contribution

to the total water uptake is most prominent below 5% RH. At higher % RH, the contribution of the water vapor adsorbing through the Langmuir mechanism remains almost constant, which indicates saturation of the specific adsorption sites at 5% RH. The values of K are in agreement with earlier studies reporting Langmuir adsorption onto nanocellulosic materials[7] as expected due to the similarity in abundance of hydrophilic functional groups. Nonetheless, the Langmuir isotherm underpredicts the adsorption of water vapor even in dry air (RH < 10%). Here, the heterogeneous nature of TEMPO CNFs must be considered: ca. 90% consists of cellulose nanofibrils with a high degree of crystallinity, whereas ca. 10% consists of amorphous hemicellulose polysaccharides, deposited along the nanofibril surfaces (Table S1 in the Supporting Information). Cellulose nanofibrils are impregnable to water and water vapor, meaning that vapor adsorption occurs only at the surface of the nanofibrils within the whole network. Amorphous hemicellulose, by contrast, swells significantly in water. Therefore, hemicellulose is likely to have a distinctly higher specific adsorption pattern, resulting in underestimation by the Langmuir model, which was originally designed for morphologically homogeneous monocomponent surfaces.[24]

According to the Langmuir/Flory–Huggins/clustering model in Figure 4a, Flory–Huggins type sorption or random mixing dominates the water vapor uptake in the range from 5% to 75% RH. The Flory–Huggins interaction parameter, χ, for the curve is 0.67, as calculated by a nonlinear regression method and the least-squares sum technique over the range from 30 to 70% RH. Outside this range, the χ-value significantly diverges from this value (Supporting Information), which could indicate deviations from simple Flory–Huggins-type behavior and therefore deviations from random mixing.[54,55] In the range from 30 to 70% RH, however, the regression coefficient (R^2 = 0.977) between the model and the experimental data confirms that the model strongly correlates with the experimental data.

The onset for clustering of water molecules seems to occur at 60% RH and contributes significantly to the total water uptake of the TEMPO CNF film above 75% RH (Figure 4a). According to the clustering function (eq 6) and the clustering coefficient (n), clusters are estimated to consist of on average 10 water molecules.[7] Clustering has commonly been associated with water vapor sorption at high relative humidities onto hydrophilic biomaterials, including nanocellulosic[7] and fibrous materials[32] as well as onto polymers, such as cellulose acetate and ethyl cellulose.[56] Further support for the water molecule clustering effect is apparent in the RI data measured by SE (Figure 1b): the RI decreases slowly in the RH range from 0 to 75%, but undergoes a steep decrease upon reaching approximately 75% RH. This behavior does not point toward capillary condensation, because for example the measured RI (1.30) significantly differs from the RI of pure water (1.33). In dry air, the RI of the TEMPO CNF film concurs with the RI values reported in literature for crystalline cellulose (1.554 as reported by Cranston et al.[57]) and a dense TEMPO CNF film (1.545 as reported by Isogai et al.[47]). In very humid air (~90% RH) the RI of the TEMPO CNF is similar to the RI of water, suggesting that a continuous film of water molecules has formed and that water exists in liquid form within the TEMPO CNF thin film in the high % RH region.[58]

Simultaneously, the minor changes in dissipation recorded by the QCM-D suggest that the thin film solid state rheological changes are taking place at high levels of relative humidity, see the inset in Figure 2. The change in dissipation remains unaltered ($\Delta D = 0$) below the RH level of 75%, indicating that the TEMPO CNF thin film behaves as a fully elastic material, i.e., all the deformations taking place when the thin film is subjected to the oscillating stress are fully reversible. Thus, the thin film structural changes are fully reversible despite of the water uptake attested by the changes in frequency. However, upon reaching 97% RH, an increase in change in dissipation can be observed, indicating that a small part of the energy is dissipated during the oscillating cycle. This dissipated energy is designated to the viscous, i.e., irreversible deformations taking place in the thin film structure as the water vapor is strongly interacting with the TEMPO CNF fibrillar network. Water vapor-induced structural changes can be linked to swelling of the film elucidated by the amplified thickness response to uptake of a (mass) unit of water vapor in high relative humidities (Figure 2a). Considering the heterogeneous and complex composition and structure of the TEMPO CNF thin film, the swelling amounting to the dissipation increase can foremost be attributed to hemicellulose (8%) located on surfaces of the TEMPO CNFs.

The sorption of water vapor into TEMPO CNF thin film was also quantitatively fitted by the BET model to describe the physical adsorption of water vapor in dry air (RH < 15%), as shown in Figure 4b. Due to the confined nature of the thin film with restricted space for expansion only in one dimension, the optical thickness fractions of water could be used as experimental values in the model instead of volume—a more frequently used attribute. According to the BET model calculations (Supporting Information), the apparent water molecule monolayer thickness adsorbed on the TEMPO CNF thin film was 4.3% of the total thickness of the TEMPO CNF thin film. Curiously, the monolayer thickness and the specifically adsorbed water revealed by the Langmuir isotherm do not concur in the case of TEMPO CNF thin film. The noticeable difference could be a result of the aforementioned morphological and chemical heterogeneity due to, e.g., hemicellulose in the TEMPO CNF film, as opposed to smooth surfaces, e.g., mica, where the Langmuir adsorption classically corresponds to the monolayer volume solved by the BET model.

The Langmuir/Flory–Huggins/clustering model appears to describe the sorption behavior of TEMPO CNF thin films over a wide relative humidity range, although in its original purpose of use it predicted the sorption behavior of water vapor into hydrophilic homogeneous polymers, such as semicrystalline Nylon-6[46] and amorphous polyamide.[45] We suggest that the similarity stems from essentially the same sorption mechanisms dominating sorption into synthetic polymers and into TEMPO CNF despite differences in morphology, crystallinity, and availability of hydrophilic functional groups. Nonetheless, with reasonable accuracy it can predict the behavior of the film in a gas–solid binary system with possibilities to extend the classical physicochemical models to describe the behavior of CNF and other complex biomaterials in gas–solid–liquid ternary systems.

■ CONCLUSIONS

The water vapor sorption behavior of the complex and heterogeneous TEMPO CNF thin film system was accurately described by a simple three-component Langmuir/Flory–Huggins/clustering model over the entire relative humidity range. Water vapor sorption isotherms of TEMPO CNF thin films were determined using SE and QCM-D with precision

beyond the capability of bulk methods. Sensitivity and complementarity of the data collection methods coupled with quantitative modeling unveiled distinct zones for specific adsorption of water molecules, association of the Flory–Huggins population of water molecules and clustering of water molecules. The findings contribute to bridging the gap between complex biomaterials and the requirements for advanced humidity-controlled nanoscale architectures for, e.g., sensors, diagnostics, and membranes.

■ ASSOCIATED CONTENT

⑤ Supporting Information

The Supporting Information is available free of charge on the ACS Publications website at DOI: 10.1021/acs.biomac.7b00890.

Neutral sugar composition, figures of raw spectroscopic ellipsometry data and fit between Cauchy model data and experimental data, calculations for thickness fractions of water (SE), table of relative humidities achieved by saturated salt solutions (QCM-D), calculations for areal mass (QCM-D), calculations for mass fractions of water (QCM-D), humidity response of pristine Au QCM-D sensor, Flory–Huggins interaction parameter, and BET calculations (PDF)

■ AUTHOR INFORMATION

Corresponding Authors
*E-mail: tekla.tammelin@vtt.fi.
*E-mail: eero.kontturi@aalto.fi.

ORCID ⓘ
Marco Faustini: 0000-0002-6254-5116
Cédric Boissière: 0000-0003-1212-6850
Eero Kontturi: 0000-0003-1690-5288
Tekla Tammelin: 0000-0002-3248-1801

Notes
The authors declare no competing financial interest.

■ ACKNOWLEDGMENTS

■ REFERENCES

(1) Olivero, J. J.; Stagat, R. W.; Green, A. E. S. Electron Deposition in Water Vapor, with Atmospheric Applications. *J. Geophys. Res.* **1972**, *77*, 4797–4811.

(2) Elbaum, R.; Zaltzman, L.; Burgert, I.; Fratzl, P. The Role of Wheat Awns in the Seed Dispersal Unit. *Science* **2007**, *316*, 884–886.

(3) Yamane, C. Structure Formation of Regenerated Cellulose from Its Solution and Resultant Features of High Wettability: A Review. *Nord. Pulp Pap. Res. J.* **2015**, *30*, 078–091.

(4) Holmberg, M.; Berg, J.; Rasmusson, J.; Stemme, S.; Ödberg, L.; Claesson, P. Surface Force Studies of Langmuir–Blodgett Cellulose Films. *J. Colloid Interface Sci.* **1997**, *186*, 369–381.

(5) Matsunaga, T.; Ikada, Y. Surface Modifications of Cellulose and Polyvinyl Alcohol and Determination of the Surface Density of the Hydroxyl Group. *ACS Symp. Ser.* **1980**, *121*, 391–406.

(6) Tenhunen, T.-M.; Peresin, M. S.; Penttila, P. A.; Pere, J.; Serimaa, R.; Tammelin, T. Significance of Xylan on the Stability and Water Interactions of Cellulosic Nanofibrils. *React. Funct. Polym.* **2014**, *85*, 157–166.

(7) Belbekhouche, S.; Bras, J.; Siqueira, G.; Chappey, C.; Lebrun, L.; Khelifi, B.; Marais, S.; Dufresne, A. Water Sorption Behavior and Gas Barrier Properties of Cellulose Whiskers and Microfibril Films. *Carbohydr. Polym.* **2011**, *83*, 1740–1748.

(8) Lavoine, N.; Desloges, I.; Dufresne, A.; Bras, J. Microfibrillated Cellulose – Its Barrier Properties and Applications in Cellulosic Materials: A Review. *Carbohydr. Polym.* **2012**, *90*, 735–764.

(9) Eichhorn, S. J.; Dufresne, A.; Aranguren, M.; Marcovich, N. E.; Capadona, J. R.; Rowan, S. J.; Weder, C.; Thielemans, W.; Renneckar, S.; Gindl, W.; Veigel, S.; Keckes, J.; Yano, H.; Abe, K.; Nogi, M.; Nakagaito, N.; Mangalam, A.; Simonsen, J.; Benight, A. S.; Bismarck, A.; Berglund, L. A.; Peijs, T. J. Review: Current International Research into Cellulose Nanofibres and Nanocomposites. *J. Mater. Sci.* **2010**, *45*, 1–33.

(10) Moon, R. J.; Martini, A.; Nairn, J.; Simonsen, J.; Youngblood, J. Cellulose Nanomaterials: Structure, Properties and Nanocomposites. *Chem. Soc. Rev.* **2011**, *40*, 3941–3994.

(11) Kontturi, E.; Tammelin, T.; Österberg, M. Cellulose–Model Films and the Fundamental Approach. *Chem. Soc. Rev.* **2006**, *35*, 1287–1304.

(12) Kafy, A.; Akther, A.; Shishir, I. R.; Kim, H. C.; Yun, Y.; Kim, J. Cellulose Nanocrystal/Graphene Oxide Composite Film as Humidity Sensor. *Sens. Actuators, A* **2016**, *247*, 221–226.

(13) Orelma, H.; Filpponen, I.; Johansson, L.-S.; Österberg, M.; Rojas, O.; Laine, J. Surface Functionalized Nanofibrillar Cellulose (NFC) Film as a Platform for Immunoassays and Diagnostics. *Biointerphases* **2012**, *7*, 61–73.

(14) Hakalahti, M.; Mautner, A.; Johansson, L.-S.; Hänninen, T.; Setälä, H.; Kontturi, E.; Bismarck, A.; Tammelin, T. Direct Interfacial Modification of Nanocellulose Films for Thermoresponsive Membrane Templates. *ACS Appl. Mater. Interfaces* **2016**, *8*, 2923–2927.

(15) Mautner, A.; Lee, K.-Y.; Tammelin, T.; Mathew, A. P.; Nedoma, A. J.; Li, K.; Bismarck, A. Cellulose Nanopapers as Tight Aqueous Ultra-Filtration Membranes. *React. Funct. Polym.* **2015**, *86*, 209–214.

(16) Thomas, J. M.; Thomas, W. J. *Principles and Practices of Heterogeneous Catalysis*; Wiley: New York, 1996.

(17) Ertl, G. Reactions at Surfaces: From Atoms to Complexity (Nobel Lecture). *Angew. Chem., Int. Ed.* **2008**, *47*, 3524–3535.

(18) Grob, R. L.; Barry, E. F. Physicochemical Measurements by Gas Chromatography. In *Modern Practice of Gas Chromatography*; Wiley: Hoboken, 2004; pp 605–643.

(19) Brunauer, S.; Emmett, P. H.; Teller, E. Adsorption of Gases in Multimolecular Layers. *J. Am. Chem. Soc.* **1938**, *60*, 309–319.

(20) Gocho, H.; Tanioka, A.; Nakajima, T. Sorption Isotherm Analysis of Water by Hydrophilic Polymer Composed of Different Adsorption Sites Using Modified BET Equation. *J. Colloid Interface Sci.* **1998**, *200*, 155–160.

(21) Dutcher, C.; Ge, X.; Wexler, A.; Clegg, S. Statistical Mechanics of Multilayer Sorption: Extension of the Brunauer-Emmet-Teller (BET) and Guggenheim-Anderson-de Boer (GAB) Adsorption Isotherms. *J. Phys. Chem. C* **2011**, *115*, 16474–16487.

(22) Timmermann, E. O. A B.E.T.-like Three Sorption Stage Isotherm. *J. Chem. Soc., Faraday Trans. 1* **1989**, *85*, 1631–1645.

(23) Barrer, R.; Barrie, J.; Slater, J. Sorption and Diffusion in Ethyl Cellulose. Part III. Comparison between Ethyl Cellulose and Rubber. *J. Polym. Sci.* **1958**, *27*, 177–197.

(24) Langmuir, I. The Adsorption of Gases on Plane Surfaces of Glass, Mica and Platinum. *J. Am. Chem. Soc.* **1918**, *40*, 1361–1403.

(25) Henry, W. Experiments on the Quantity of Gases Absorbed by Water, at Different Temperatures and under Different Pressures. *Philos. Trans. R. Soc. London* **1803**, *93*, 29–42.

(26) Flory, P. J. *Principles of Polymer Chemistry*; Cornell University Press: Ithaca, NY, 1953.

(27) Urquhart, A. R.; Williams, A. M. The Effect of Temperature on the Adsorption of Water by Soda-Boiled Cotton. *J. Text. Inst., Trans.* **1924**, *75*, 559–572.

(28) Assaf, A. G.; Haas, R. H.; Purves, C. B. A New Interpretation of the Cellulose-Water Adsorption Isotherm and Data Concerning the Effect of Swelling and Drying on the Colloidal Surface of Cellulose. *J. Am. Chem. Soc.* **1944**, *66*, 66−73.

(29) Shrestha, S.; Diaz, J. A.; Ghanbari, S.; Youngblood, J. P. Hygroscopic Swelling Determination of Cellulose Nanocrystal (CNC) Films by Polarized Light Microscopy Digital Image Correlation. *Biomacromolecules* **2017**, *18*, 1482−1490.

(30) Stannett, V.; Haider, M.; Koros, W. J.; Hopfenberg, H. B. Sorption and Transport of Water Vapor in Glassy Poly(Acrylonitrile). *Polym. Eng. Sci.* **1980**, *20*, 300−304.

(31) Gouanvé, F.; Marais, S.; Bessadok, A.; Langevin, D.; Morvan, C.; Metayer, M. Study of Water Sorption in Modified Flax Fibers. *J. Appl. Polym. Sci.* **2006**, *101*, 4281−4289.

(32) Bessadok, A.; Langevin, D.; Gouanvé, F.; Chappey, C.; Roudesli, S.; Marais, S. Study of Water Sorption on Modified Agave Fibres. *Carbohydr. Polym.* **2009**, *76*, 74−85.

(33) Hailwood, A. J.; Horrobin, S. Absorption of Water by Polymers: Analysis in Terms of a Simple Model. *Trans. Faraday Soc.* **1946**, *42*, B084−B092.

(34) Driemeier, C.; Mendes, F. M.; Oliveira, M. M. Dynamic Vapor Sorption and Thermoporometry to Probe Water in Celluloses. *Cellulose* **2012**, *19*, 1051−1063.

(35) Hernandez, R.; Giacin, J.; Grulke, E. The Sorption of Water by an Amorphous Polyamide. *J. Membr. Sci.* **1992**, *65*, 187−199.

(36) Hernandez, R.; Gavara, R. Sorption and Transport in Nylon-6 Films. *J. Polym. Sci., Part B: Polym. Phys.* **1994**, *32*, 2367−2374.

(37) Ogieglo, W.; Wormeester, H.; Eichhorn, K.-J.; Wessling, M.; Benes, N. In Situ Ellipsometry Studies on Swelling of Thin Polymer Films: A Review. *Prog. Polym. Sci.* **2015**, *42*, 42−78.

(38) Rodahl, M.; Höök, F.; Krozer, A.; Brzezinski, P.; Kasemo, B. Quartz Crystal Microbalance Setup for Frequency and Q-Factor Measurements in Gaseous and Liquid Environments. *Rev. Sci. Instrum.* **1995**, *66*, 3924−3930.

(39) Höök, F.; Rodahl, M.; Brzezinski, P.; Kasemo, B. Energy Dissipation Kinetics for Protein and Antibody − Antigen Adsorption under Shear Oscillation on a Quartz Crystal Microbalance. *Langmuir* **1998**, *14*, 729−734.

(40) Reviakine, I.; Johannsmann, D.; Richter, R. P. Hearing What You Cannot See and Visualizing What You Hear: Interpreting Quartz Crystal Microbalance Data from Solvated Interfaces. *Anal. Chem.* **2011**, *83*, 8838−8848.

(41) Fujiwara, H. *Spectroscopic Ellipsometry*; John Wiley & Sons, Ltd.; Chichester, U.K., 2007.

(42) Rodenhausen, K. B.; Schmidt, D.; Rice, C.; Hofmann, T.; Schubert, E.; Schubert, M. Detection of Organic Attachment onto Highly Organized Three-Dimensional Nanostructure Thin Films by Generalized Ellipsometry and Quartz Crystal Microbalance with Dissipation Techniques. In *Ellipsometry of Functional Organic Surfaces and Films*, 1st ed.; Hinrichs, K., Eichhorn, K.-J., Eds.; Springer Series on Functional Organic Surfaces and Films; Springer-Verlag: Berlin, 2014; pp 135−154.

(43) Richter, R. P.; Rodenhausen, K. B.; Eisele, N. B.; Schubert, M. Coupling Spectroscopic Ellipsometry and Quartz Crystal Microbalance to Study Organic Films at the Solid-Liquid Interface. In *Ellipsometry of Functional Organic Surfaces and Films*, 1st ed.; Hinrichs, K., Eichhorn, K.-J., Eds.; Springer Series on Functional Organic Surfaces and Films; Springer-Verlag: Berlin, 2014; pp 223−248.

(44) May, A. R.; Flaherty, D. W.; Mullins, C. B.; Stevenson, K. J. Hybrid Generalized Ellipsometry and Quartz Crystal Nanogravimetry for the Determination of Adsorption Isotherms on Biaxial Metal Oxide Films. *J. Phys. Chem. Lett.* **2010**, *1*, 1264−1268.

(45) Niinivaara, E.; Faustini, M.; Tammelin, T.; Kontturi, E. Water Vapor Uptake of Ultrathin Films of Biologically Derived Nanocrystals: Quantitative Assesment with Quartz Crystal Microbalance and Spectroscopic Ellipsometry. *Langmuir* **2015**, *31*, 12170−12176.

(46) Niinivaara, E.; Faustini, M.; Tammelin, T.; Kontturi, E. Mimicking the Humidity Response of the Plant Cell Wall by Using

Two-Dimensional Systems: The Critical Role of Amorphous and Crystalline Polysaccharides. *Langmuir* **2016**, *32*, 2032−2040.

(47) Isogai, A.; Saito, T.; Fukuzumi, H. TEMPO-Oxidized Cellulose Nanofibres. *Nanoscale* **2011**, *3*, 71−85.

(48) Eronen, P.; Laine, J.; Ruokolainen, J.; Österberg, M. Comparison of Multilayer Formation between Different Cellulose Nanofibrils and Cationic Polymers. *J. Colloid Interface Sci.* **2012**, *373*, 84−93.

(49) IUPAC. *Compendium of Chemical Terminology*, 2nd ed. (The "Gold Book"); McNaught, A. D., Wilkinson, A., Eds.; Blackwell Scientific Publications: Oxford, 1997.

(50) Tammelin, T.; Abburi, R.; Gestranius, M.; Laine, C.; Setälä, H.; Österberg, M. Correlation between Cellulose Thin Film Supramolecular Structures and Interactions with Water. *Soft Matter* **2015**, *11*, 4273−4282.

(51) Sauerbrey, G. The Use of Quartz Oscillators for Weighing Thin Layers and for Microweighing. *Eur. Phys. J. A* **1959**, *155*, 206−222.

(52) Peresin, M. S.; Kammiovirta, K.; Setälä, H.; Tammelin, T. Structural Features and Water Interactions of Etherified Xylan Thin Films. *J. Polym. Environ.* **2012**, *20*, 895−904.

(53) Vieth, W.; Howell, J.; Hsieh, J. Dual Sorption Theory. *J. Membr. Sci.* **1976**, *1*, 177−220.

(54) Zimm, B.; Lundberg, J. Sorption of Vapors by High Polymers. *J. Phys. Chem.* **1956**, *60*, 425−428.

(55) Stannett, V.; Haider, M.; Koros, W. J.; Hopfenberg, H. B. Sorption and Transport of Water Vapor in Glassy Poly(Acrylnitrile). *Polym. Eng. Sci.* **1980**, *20*, 300−304.

(56) Orofino, T.; Hopfenberg, H.; Stannett, V. Characterization of Penetrant Clustering in Polymers. *J. Macromol. Sci., Part B: Phys.* **1969**, *3*, 777−788.

(57) Cranston, E. D.; Gray, D. G. Birefringence in Spin-Coated Films Containing Cellulose Nanocrystals. *Colloids Surf., A* **2008**, *325*, 44−51.

(58) Li, R.; Faustini, M.; Boissière, C.; Grosso, D. Water Capillary Condensation Effect on the Photocatalytic Activity of Porous TiO_2 in Air. *J. Phys. Chem. C* **2014**, *118*, 17710−17716.

Supporting Information

Interfacial Mechanisms of Water Vapor Sorption into Cellulose Nanofibril Films Revealed by Quantitative Models

Minna Hakalahti[1], Marco Faustini[2], Cédric Boissière[2], Eero Kontturi[3]*, Tekla Tammelin[1]*

[1] High Performance Fibre Products, VTT Technical Research Center of Finland Ltd, FI-02044, Espoo, Finland

[2] Sorbonne Universités, UPMC Univ Paris 06, CNRS, Collège de France, UMR 7574, Chimie de la Matière Condensée de Paris, F-75005, Paris, France

[3] Department of Bioproducts and Biosystems, School of Chemical Engineering, Aalto University, 02150 Espoo, Finland

*Corresponding author: tekla.tammelin@vtt.fi, eero.kontturi@vtt.fi

TABLE OF CONTENTS

NEUTRAL SUGAR COMPOSITION

The hemicellulose content of the TEMPO CNF was determined by high performance liquid chromatography (Dionex ICS-3000, Thermo Fischer Scientific Ltd, Waltham, MA, USA) after acid hydrolysis.[1] The results are summarized in Table S1.

Table S1. Neutral sugar composition of TEMPO CNF.

Glucose (%)	Galactose (%)	Mannose (%)	Arabinose (%)	Xylose (%)	Rhamnose (%)	Fructose (%)	Total (%)	Others[a] (%)
64.0	0	2.1	0	6.2	0	0	72.3	27.7

[a]Others predominantly consists of glucuronic acids originating from TEMPO oxidized cellulose nanofibrils.

RAW SPECTROSCOPIC ELLIPSOMETRY DATA AND CAUCHY MODELS

Figure S1a shows the raw data from spectroscopic ellipsometry (SE) measurements during the dynamic humidity cycle. Figure S1b shows the comparison between experimental results and generated (modelled) results as achieved through a fitting procedure. A regression algorithm is applied in order to calculate and adjust the variable parameters from (Cauchy) model and experimental data to a minimum value of mean-squared error (MSE), which is the quality estimator of the fitting procedure. The MSE is calculated as a sum of squares of differences between modelled and measured experimental data. Between data from the measurements of TEMPO CNF thin film and the fit by the classical Cauchy model, the MSE value was < 4, indicating that the effective thickness and refractive index values are physically meaningful and correct.[2]
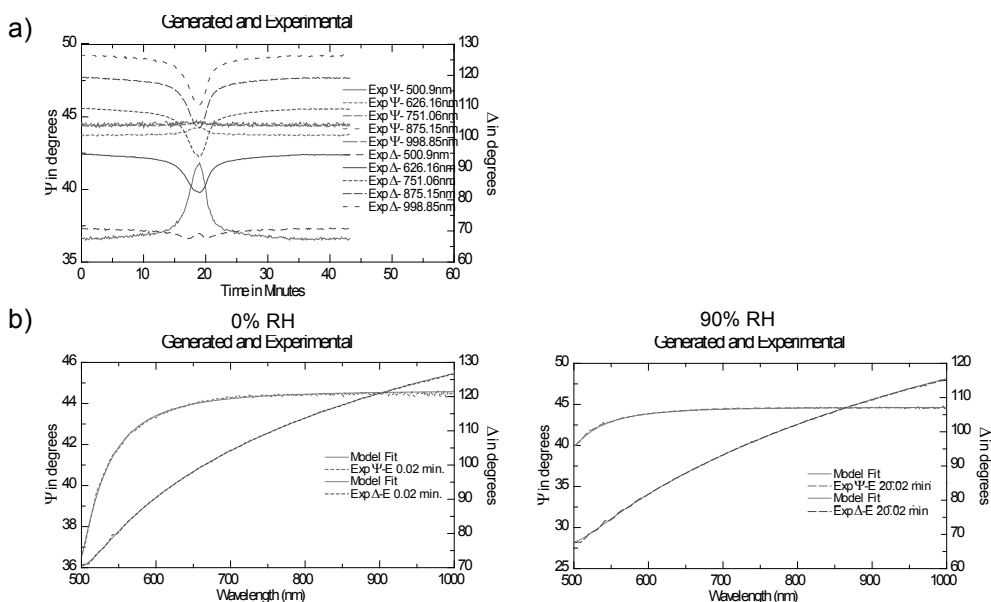
Figure S1. Raw ellipsometric data (Ψ and Δ values) as a function of time during the dynamic humidity cycle (sorption 0-19 min, desorption 20-40 min) for TEMPO CNF film. Five different wavelengths are shown. b) Fit between spectroscopic ellipsometry experimental data and Cauchy model data at low (left) and high (right) relative humidity.

CALCULATIONS FOR THICKNESS FRACTIONS OF WATER (SE)

Example calculation of optical thickness fraction of water in TEMPO CNF thin film at 50% RH:

Optical thickness of TEMPO CNF thin film (0% RH) = Refractive index (0% RH) × thickness (0% RH)

$$= 1.4909 \times 12.841 \text{ nm} = 19.145 \text{ nm}$$

Optical thickness of TEMPO CNF thin film (50% RH)

$$= \text{Refractive index (50\% RH)} \times \text{thickness (50\% RH)} = 1.4572 \times 14.934 \text{ nm}$$

$$= 21.762 \text{ nm}$$

Optical thickness fraction of water (50% RH)

$$= \frac{\text{Optical thickness of TCNF thin film (50\% RH)} - \text{Optical thickness of TCNF thin film (0\% RH)}}{\text{Optical thickness of TCNF thin film (50\% RH)}}$$

$$= \frac{21.762 \text{ nm} - 19.145 \text{ nm}}{21.762 \ nm} = 0.120$$

RELATIVE HUMIDITIES OF SATURATED SALT SOLUTIONS (QCM-D)

Table S2. Relative humidities of saturated salt solutions used in the QCM-D humidity experiments at 23 ˚C.[3]

Salt	Relative humidity %
$LiBr_{(aq)}$	6
$ZnBr_{2(aq)}$	8
$LiCl_{(aq)}$	11
$MgCl_{2(aq)}$	33
$Mg(NO_3)_{2(aq)}$	53
$NaCl_{(aq)}$	75
$K_2SO_{4(aq)}$	97

CALCULATIONS FOR AREAL MASS (QCM-D)

Example calculation for determining the initial mass of TEMPO CNF thin film at RH 6%. Masses shown here are calculated by the Sauerbrey equation (Equation S1) from the measured values of change in resonance frequency (Δf) using the third overtone. The Δf for TEMPO CNF film used in calculations were corrected by the respective responses for a pristine QCM-D sensor shown in Figure S2.

$$\Delta m = -C\frac{\Delta f}{n} \tag{S1}$$

Initial areal mass of TCNF thin film (6% RH)

$\qquad$ = Areal mass of the spincoated sensor (6% RH) − Areal mass of pristine sensor (6% RH)

$\qquad$ = 1995.2 ng cm^{-2} (data stitched using QTools software)

CALCULATIONS FOR MASS FRACTIONS OF WATER (QCM-D)

Example calculation of mass fraction of water in TEMPO CNF thin film at 53% RH:

$Mass\ fraction\ of\ water\ (53\%\ RH)$

$$= \frac{\text{Areal mass of TEMPO CNF thin film (53\% RH)} - \text{Areal mass of TCNF thin film (6\% RH)}}{\text{Areal mass of TCNF thin film (53\% RH)}}$$

$$= \frac{2195.5\ g\ cm^2 - 1995.2\ g\ cm^2}{2195.5\ g\ cm^2} = 0.091$$
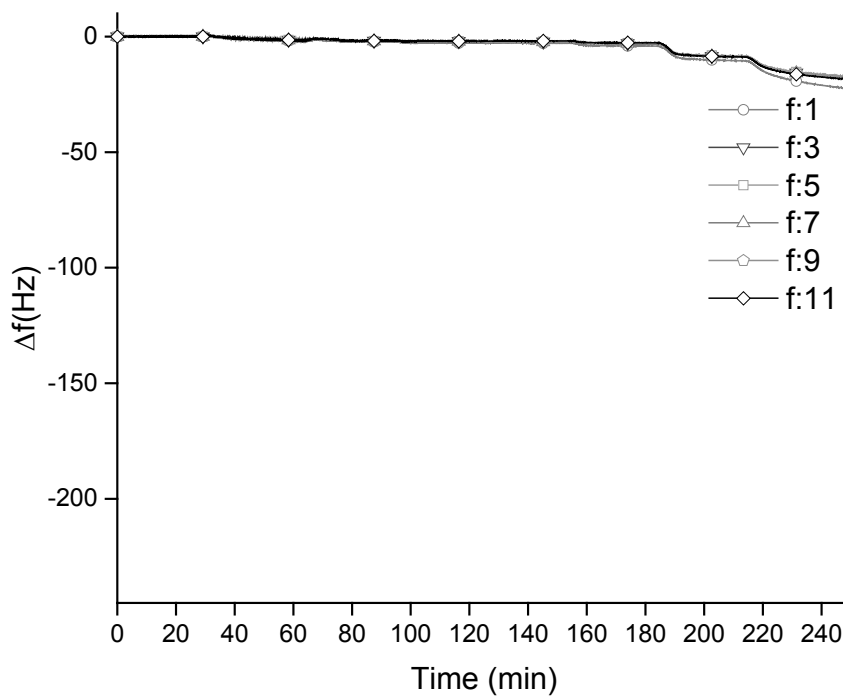
Figure S2. Change in frequency (Δf) as a function of time in stepwise increasing relative humidity (% RH) as detected by QCM-D water vapour adsorption measurements for pristine gold QCM-D sensors. Different overtones are indicated with colors.

FLORY-HUGGINS INTERACTION PARAMETER
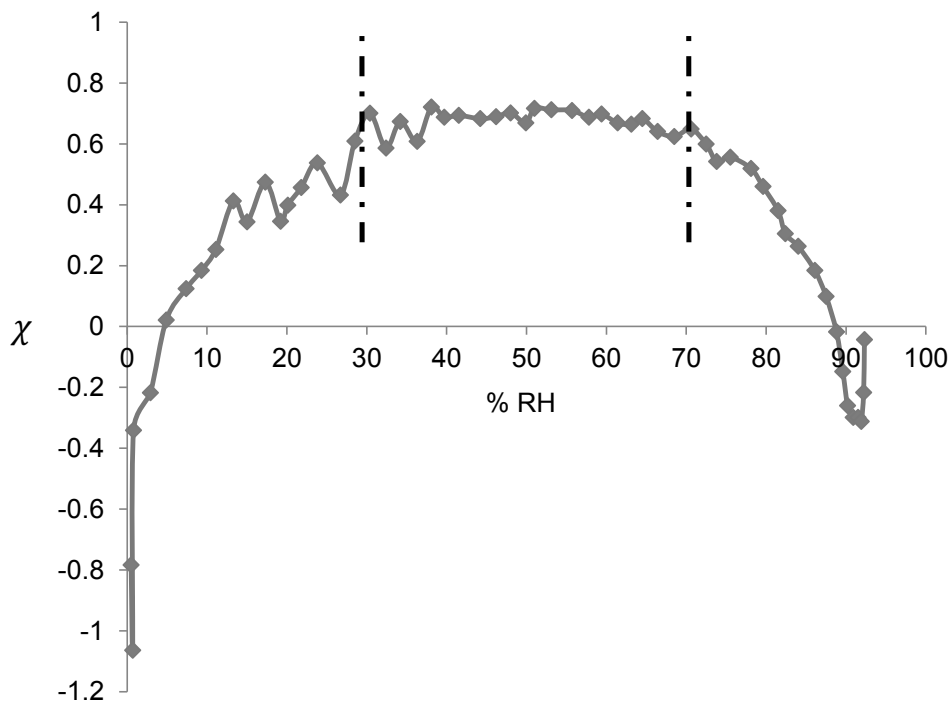
Figure S3. The Flory-Huggins interaction parameter (χ) of TEMPO CNF thin film as a function of relative humidity. The % RH range (30-70% RH) used for model calculations is marked with dashed lines.

BET CALCULATIONS

According to the linear equation, from Figure 4b it can be deduced that the values for y-intercept (b) and slope of the curve (m) are 1.1064 and 22.146 respectively. For the purpose of calculating the water molecule monolayer thickness (V_m) The c parameter for the BET equation can be calculated as shown in Equation S1:[2]

$$c = 1 + \frac{m}{b} = 1 + \frac{22.146}{1.1064} = 21.106 \tag{S1}$$

V_m can be calculated according to the BET model is calculated as shown in Equation S2:[4]

$$V_m = \frac{1}{m+c} \times 100\% = \frac{1}{22.146+1.1064} \times 100\% = 4.3\% \tag{S2}$$

REFERENCES

(1) Laukkanen, A.; Pere, J.; Mikkelsson, A. Analytical Method for Determining the Concentration of Oxidized Nanofibrillar Cellulose in a Sample. CA2908852, 2014.

(2) Woollam, J.A. Co., Inc.; Guide to using WVASE32 software for optical data analysis.

(3) Greenspan, L. Humidity Fixed Points of Binary Saturated Aqueous Solutions. *J. Res. Natl. Bureau*, Stand. **1977**, *81*, 89-96.

(4) Brunauer, S.; Emmett, P. H.; Teller, E. Adsorption of Gases in Multimolecular Layers. *J. Am. Chem. Soc.* **1938**, *60*, 309-319.

Paper II

Hakalahti, M.; Hjelt, T.; Faustini, M.; Boissière, C.; Kontturi, E.; Tammelin, T. Cellulose Nanofibril Film Structure Probed by Water Vapor Diffusion. *Submitted to J. Phys. Chem. Lett.*

Cellulose Nanofibril Film Structure Probed by Water Vapor Diffusion

Minna Hakalahti[1]*, Marco Faustini[2], Tuomo Hjelt[1], Cédric Boissière[2], Eero Kontturi[3], Tekla Tammelin[1]

[1] High Performance Fibre Products, VTT Technical Research Center of Finland Ltd, FI-02044, Espoo, Finland

[2] Sorbonne Universités, UPMC Univ Paris 06, CNRS, Collège de France, UMR 7574, Chimie de la Matière Condensée de Paris, F-75005, Paris, France

[3] Department of Bioproducts and Biosystems, School of Chemical Engineering, Aalto University, P.O. Box 16300 00076 Aalto, Finland

ABSTRACT: In this letter water vapor diffusion is depicted as not just a kinetic parameter, but also a means to probe the humidity-sensitive structure of cellulose nanofibril (CNF) thin films. Hydration of CNF thin films was precisely tracked by quartz crystal microbalance with dissipation monitoring and spectroscopic ellipsometry, and fitted by classical Fickian diffusion models. Below 33% RH water molecules were found to mainly diffuse into the pores of the film, whereas above 33% RH sorption was augmented by accumulation of water molecules on the surface of the CNF film. Thereby, through diffusion modeling distinct details about the flexible and humidity-responsive structure of CNF assemblies could be deduced. The work carries significance for understanding and controlling the structure of biomaterial assemblies to facilitate their use in advanced moisture-sensitive applications, such as sorption platforms and membranes.

Biological systems nearly always exist in aqueous media and many of their functions depend on interactions with water in liquid and vaporous forms[1,2]. Upon isolation of cellulose nanofibrils (CNFs) from their native surroundings, i.e. the woody plant cell wall, their inherently high hydroxyl group density and the consequential hydrophilic and hygroscopic nature is preserved. Importantly, assemblies made thereof exhibit intriguing water transport properties which facilitate the capturing of large volumes of water[3,4], and could challenge current state of the art moisture absorbent materials, e.g. metal organic frameworks and zeolites[5]. Unlike many inorganic assemblies, CNF films are prone to moisture-driven physical changes at the nanoscale, impeding reliable structural analysis by methods operating only in dry conditions. Here, we demonstrate that besides just entailing exceptional functional utility, diffusion of water vapor can be used as a means to probe the complex structure of CNF thin films as a function of relative humidity (RH).

In this structure-oriented study, we use rigorous physics to evaluate the diffusivity of water vapor in (2,2,6,6-tetramethylpiperidin-1-yl)oxyl oxidized (TEMPO) CNF[6] thin films (Figures 1a and 1b) from mass uptake data collected by the well-tried combination of quartz crystal microbalance with dissipation monitoring (QCM-D) and spectroscopic ellipsometry (SE)[4,7,8] (Figure 1c). Supported thin film assemblies of TEMPO oxidized CNF are especially well suited for linking diffusion properties to nanoscale structure due to their isotropic nature, restricted lateral expansion, well-known chemical composition

(Supporting Information) and carboxyl group enhanced affinity towards water[6,9,10].

The mass isotherm and the thickness isotherm (Figure 1c) of water vapor sorption into the TEMPO CNF thin film reveal that below 75% RH the uptake is gradual and increases significantly upon reaching high relative humidity levels (RH >75%). The maximum water vapor uptake capacity of TEMPO CNF thin film at 97% RH was 0.94 ± 0.11 g g^{-1}, which is significantly higher compared to other nanoscaled cellulosic materials, such as cellulose nanocrystals (0.28 g g^{-1})[7], native CNF (0.35 g g^{-1})[11] or even completely isotropic amorphous cellulose (0.45 g g^{-1})[8]. The higher sorption capacity in humid air can mainly be attributed to the numerous carboxyl groups introduced through TEMPO catalyzed oxidation. Due to osmotic pressure, their affinity toward water is stronger compared to hydroxyl groups[10] abundant in all cellulosic materials. In addition, the presence of ca. 10% of partially charged amorphous hemicellulose with the ability to swell significantly in water[11,12] further facilitates the vapor uptake. The maximum water vapor uptake capacity of the TEMPO CNF thin film at high humidities is 2-3 times higher compared to that of zeolites and similar compared to that of mesoporous metal organic frameworks[5] – materials that have been investigated for atmospheric water vapor collection due to their promising sorption properties.

When a porous solid film is placed in contact with a gaseous phase containing a sorbate, the sorbate proceeds to be taken up by the solid film[13,14]. Fick's
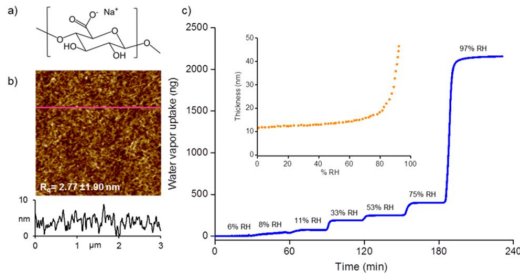
Figure 1. a) Chemical structure of TEMPO CNF. b) Topographic AFM image (3 × 3 µm) of a supported TEMPO CNF thin film with a height scan (pink line) and root-mean-square roughness (R_q). c) Water vapor uptake by TEMPO CNF thin film upon exposure to air with incrementally increasing relative humidity over time monitored by QCM-D and the thickness of the TEMPO CNF thin film monitored by SE (inset).

second law[13,14,15] correlates the concentration profile along the film thickness with diffusivity during the transient state:

$$\frac{\delta c}{\delta t} = \frac{\delta}{\delta x}\left(D\frac{\delta c}{\delta x}\right) \tag{1}$$

The mathematical model for transient uptake following Fickian diffusion in the case of plate geometry and the assumption of constant diffusion coefficient, D, can be expressed by equation 2[14]:

$$\frac{m_t}{m_\infty} = 1 - \sum_{n=0}^{\infty}\frac{8}{(2n+1)^2\pi^2}e^{\left(\frac{-D(2n+1)^2\pi^2 t}{l^2}\right)} \tag{2}$$

where t marks the time, m_∞, m_t, and m_o are the mass values of the TEMPO CNF thin film at equilibrium (at each %RH level) and at t=t and t=0, respectively, and l represents the thickness of the thin film. The diffusion model assumes that the rate of water vapor uptake is completely controlled by diffusion into the interior of the solid film[16], i.e. into the pores of the TEMPO CNF thin film. The equation can be simplified using the first term of the series of the right hand side in equation 2 and solved numerically for the diffusion coefficient (D)[17]:

$$-\frac{1}{\pi^2}\ln\left[\frac{(m_\infty-m_t)\pi^2}{8(m_\infty-m_0)}\right]\times l^2 = Dt \tag{3}$$

Following the fitting approach described by Lee et al.[17], transition zones from a lower RH to a higher RH in the range 11-97 % were selected for quantitative fitting by the diffusion model. Mass uptake data collected by QCM-D over the transition zones was coupled with thickness evolution of the film as determined from SE measurements and fitted to equation 3 (see Supporting Information for details). The curve slopes corresponding to diffusion coefficient values (Table 1) were obtained by linear regression method (Figure 2a) minimizing the least square errors[13]. As seen in Figure 2a, linear regression fitted the data with reasonable accuracy (R^2=0.93) only in the transition zone between 11% and 33% RH and increasingly more deviation from linearity occurred in higher RH. The poor accuracy of the diffusion model indicates

that mass uptake is not solely explicable by diffusion into the pores of the TEMPO CNF thin film beyond 33% RH.

Furthermore, under the assumption of Fickian diffusion, the effective diffusion coefficients (D_{eff}) were calculated by adapting Newman's original solution to Fick's second law describing the two-stage drying of porous solids with diffusion of liquid from the interior of the solid, and the continuously decreasing liquid film at the surface. Hence, when adapted for uptake of water vapor into the TEMPO CNF thin film, the effective diffusion model postulates not only diffusion into the pores of the solid film, but also the accumulation of a (liquid) water molecule layer on top of the film[13,16,18]:

$$\frac{m(t)}{m(\infty)} = 1 - \sum_{1}^{\infty}\frac{2\alpha^2}{\beta^2[\alpha(\alpha+1)+\beta^2]}e^{(-\beta\frac{Dt}{L^2})} \tag{4}$$

where β are the positive roots of the equation $\alpha = \beta\tan\beta$, L is half of the film thickness and α represents the ratio of diffusion into the interior of the film to accumulation of (liquid) water on top of the film.

The effective diffusion model (equation 4) correlates with the experimentally measured relative moisture uptake with sufficient accuracy (R^2 = 0.93) (Figure 2b) for allowing determination of the effective diffusion coefficients over the RH range from 11% to 97% RH. Whereas the diffusion model (equation 3) postulates only diffusion of water vapor into the pores of the film, the effective diffusion model also includes accumulation of a (liquid) water molecule layer on top of the film. The effective diffusion coefficients appear to increase as relative humidity increases (Table 1), possibly due to contribution of different underlying sorption mechanisms at different zones over the full RH range. Especially the onset of clustering of water vapor molecules at ~60% RH could facilitate larger overall diffusion coefficients at high RH: The packing of water molecules into areas of high density of hydrophilic groups, e.g. fibril intersections and interfibrillar cavities, could trigger local vapor-to-liquid transitions and increase the overall affinity of the hydrated TEMPO CNF thin film toward water.[4] Moreover, presence of water vapor and possible presence of liquid water induce rearrangement of the amorphous hemicellulose[11,19,20] and change the internal porous structure of the flexible and fibrillar film network. Overall, these features of the complex and heterogeneous biomaterial probably contribute to both effects accounted for in the effective diffusion model - diffusion of water vapor into the pores of the film and accumulation of (liquid) water on top of the TEMPO CNF thin film.

With respect to the effective diffusion model it should be noted that there is systematic deviation between the shapes of the experimental data curves and the model fit curves, as depicted in Figure 2b. The disparity probably derives from the complex and heterogeneous multicomponent nature of the TEMPO CNF thin film system: At low RH the film is in a non-swollen state with an abundance of functional groups with high affinities toward
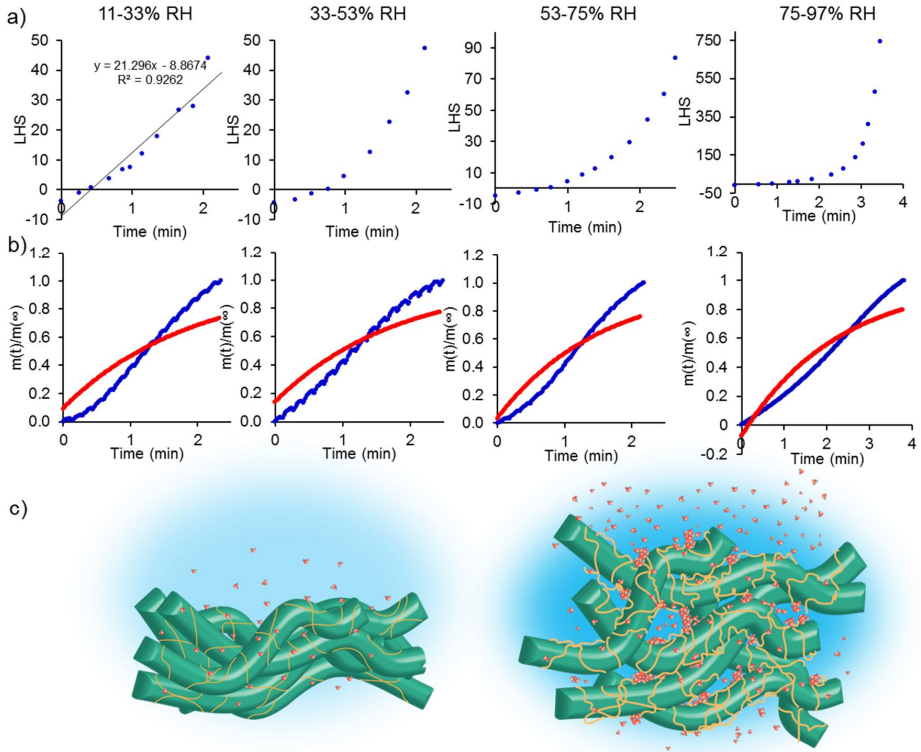
Figure 2. a) Left hand side ($-\frac{1}{\pi^2} ln\left[\frac{(m_\infty-m_t)\pi^2}{8(m_\infty-m_0)}\right] \times l^2 = Dt$) of equation 3 (diffusion model) with experimentally obtained data input to determine the diffusion coefficient (D) of water vapor in TEMPO CNF thin films during transitions to higher relative humidity levels fitted by linear regression (black line), with diffusion coefficients defined from the slope of the linear curve. LHS. b) Relative increase of mass due to water vapor uptake (blue) during transitions to higher RH levels fitted by the effective diffusion model (red) (equation 4). c) Proposed schematic representation of water vapor diffusing into the thin cellulose nanofibril film multicomponent system with ca. 10% hemicellulose (orange) in dry air (left) and in humid air (right) (not drawn to scale)

water on highly crystalline fibril surfaces and amorphous hemicellulose chains. As the RH level rises, water molecules penetrate between the TEMPO CNF fibrils, inducing expansion of the interfibrillar spacing. Simultaneously, the amorphous and flexible hemicellulose chains (ca. 10%) on fibril surfaces swell[12,19], gain more mobility and thereby expose new adsorption sites on TEMPO CNF fibril surfaces. The sequence of such phenomena generates a sigmoidally shaped sorption curve commonly detected for hydrophilic biomaterials[21,22] and exhibiting penetrant molecule sorption (or desorption) induced structural changes at finite rates. The diffusion behavior of materials exhibiting sigmoidally shaped sorption curves is generally non-Fickian and cannot be accurately predicted with simple Fickian diffusion models, which do not account for all the known aspects of anomalous diffusion, e.g. swelling and relaxation of polymer chains, increasing interfibrillar spacing and clustering of water molecules.[13,23] For deducing exact diffusion coefficient values, complex composite models synthesizing the anomalous effects would be needed to describe mass transfer into materials exhibiting time-dependent properties and finite structural

change response rates. The coefficients estimated by the diffusion and effective diffusion models are several decades smaller in comparison to diffusion coefficients reported under the assumption of Fickian behavior for nanoscaled cellulosic films in literature[18,22], probably deriving from numerous discrepancies in experimental set-ups and models.

While diffusivity is a kinetic parameter illustrating how fast water vapor moves through the thin film, solubility is a thermodynamic parameter illustrating the amount of water vapor that can be absorbed at a given %RH. The solubility coefficient was calculated by equation 5[13,14,17]:

$$S = \frac{m_\infty}{m_p \times p_v^0 \times a} \qquad (5)$$

where m_p represents the mass of the dry thin film, p_v^o is the saturation vapor pressure at 23 °C and a is water activity. Hence, the solubility of water vapor within the TEMPO CNF (Table 1) thin film was calculated from the mass change of the film between dry (RH 6%) and humid conditions at each measured humidity point in the range from 6 to 97%. The solubility coefficients of water vapor

demonstrated a significant increase upon reaching high relative humidity levels (RH > 75%), possibly due to the exposure of new adsorption sites and enlargement of pores within the film.

Table 1. Transport properties of water vapor in TEMPO CNF thin films based on Fickian diffusion models.

% RH	Diffusion $\frac{nm^2}{min}$		Solubility* $\frac{cm^3(STP)}{cm^3(kPa)}$	Effective Permeability $10^{-11} \times \frac{cm^3(STP) \times cm}{cm^2 \times s \times kPa}$
	D*	D_{eff}*		
11			67.97 ± 17.25	
33	24.92 ± 3.32	23.10 ± 3.39	84.57 ± 19.91	1.95
53	-	28.16 ± 7.93	79.55 ± 7.46	2.24
75	-	49.60 ± 7.20	187.47 ± 0.23	9.30
97	-	64.15 ± 20.53	408.18 ± 45.70	26.2

*The reported values for D, D_{eff} and S are average values of at least three measurements.

Effective permeability (P_{eff}) was calculated by taking into account the kinetic diffusion coefficient and the thermodynamic solubility coefficient, according to equation 6[13]:

$$P_{eff} = D_{eff} \times S \qquad (6)$$

The effective permeability coefficients of water vapor in TEMPO CNF thin films show strong dependency on RH (Table 1), which is probably a result of the structural changes induced by water molecule penetration. Considering the physical meaning of the terms in equation 6, it is apparent that two requirements must be met for permeation to occur: water must be absorbed into the film and it must diffuse across the film thickness. Due to the hygroscopicity and porosity of the fibrillar TEMPO CNF thin film network these pre-requisites are well met as also attested by the solubility and diffusion coefficients.

In conclusion, this study exploits moisture-driven responses, i.e., diffusion of water vapor, as a means to monitor physical changes of the TEMPO CNF thin film and to thereby elucidate the structure of the complex multicomponent system and its building blocks. In dry air (RH < 33%) a simple Fickian diffusion model describes the data well, indicating that the transfer of water molecules mainly occurs into the pores through the mechanism of specific binding of water molecules. Above 33% RH, a (liquid) layer of water forms on the surface of the film. Systematic deviations between the experimental sorption data coupled with detailed knowledge about the composition of the material suggest that water molecules penetrate between the fibrils of the flexible network, forming clusters and possibly undergoing vapor to liquid transitions. Simultaneously, amorphous hemicellulose chains on fibril surfaces swell and thereby expose new unsaturated hydrophilic regions, expediting further transfer of water molecules into the hygroscopic film. This work showcases the distinct moisture uptake and transport properties of CNF and opens a new window to structural analysis of nanoscaled biomaterials with complex moisture-sensitive structures. At present, much of the structural analysis is performed with microscopy that generally maps geometry of the surface or is performed *ex situ* with cryoscopic techniques by cross sectional analysis or tomography. Furthermore, the recent advances in high speed AFM[24] or in situ TEM[25] have been confined to fairly simple systems so far. The diffusion-based approach presented here may well prove to be an important tool for quantification of structural changes in future research on bio-based materials.

ASSOCIATED CONTENT

Supporting Information. Materials and methods, determination of transition ranges, diffusion model, effective diffusion model, solubility calculations, permeability calculations. This material is available free of charge via the Internet at http://pubs.acs.org.

AUTHOR INFORMATION

Corresponding Author

* minna.hakalahti@vtt.fi

ACKNOWLEDGMENT

REFERENCES

(1) Scott, P. In *Physiology and Behavior of Plants*. John Wiley & Sons: Chichester, 2008; Ch. 4.

(2) Kuntz, I. D.; Kauzmann, W. Hydration of Proteins and Polypeptides. *Adv Protein Chem.* **1974**, *28*, 239-345.

(3) Lavoine, N.; Desloges, I.; Dufresne, A.; Bras, J. Microfibrillated Cellulose – Its Barrier Properties and Applications in Cellulosic Materials: A Review. *Carbohydr. Polym.* **2012**, *90*, 735-764.

(4) Hakalahti, M.; Faustini, M.; Boissiere, C.; Kontturi, E.; Tammelin, T. Interfacial Mechanisms of Water Vapor Sorption as Revealed by Quantitative Models. *Biomacromolecules*, **2017**, *18*, 2951-2958.

(5) Rieth, A. J.; Yang, S.; Wang, E. N.; Dinca, M. Record Atmospheric Fresh Water Capture and Heat Transfer with a Material Operating at the Water Uptake Reversibility Limit. *ACS Cent. Sci.* **2017**, 3, 668-672.

(6) Isogai, A.; Saito, T.; Fukuzumi, H. TEMPO-Oxidized Cellulose Nanofibres, *Nanoscale*, **2011**, 3, 71–85.

(7) Niinivaara, E.; Faustini, M.; Tammelin, T.; Kontturi, E. Water Vapor Uptake of Ultrathin Films of Biologically Derived Nanocrystals: Quantitative Assessment with Quartz Crystal Microbalance and Spectroscopic Ellipsometry. *Langmuir*, **2015**, *31*, 12170-12176.

(8) Niinivaara, E.; Faustini, M.; Tammelin, T.; Kontturi, E. Mimicking the Humidity Response of the Plant Cell Wall by Using Two-Dimensional Systems: The Critical Role of Amorphous and Crystalline Polysaccharides. *Langmuir*, **2016**, *32*, 2032-2040.

(9) Kontturi, E.; Tammelin, T.; Österberg, M. Cellulose–Model Films and the Fundamental Approach. *Chem. Soc. Rev.* **2006**, *35*, 1287-1304.

(10) Piringer, O. Permeation of Gases, Water Vapour and Volatile Organic Compounds. In O. Piringer, & A. Baner (Eds.), Plastic Packaging Materials for Food (pp. 239-285). Weinheim: Wiley-VCH.

(11) Tenhunen, T.-M.; Peresin, M. S.; Penttila, P. A.; Pere, J.; Serimaa, R.; Tammelin, T. Signifigance of Xylan on the Stability and Water Interactions of Cellulosic Nanofibrils. *React. Funct. Polym.* **2014**, *85*, 157-166.

(12) Uetani, K.; Yano, H. Zeta Potential Time Dependence Reveals the Swelling Dynamics of Wood Cellulose Nanofibrils. *Langmuir*, **2011**, *28*, 818-827.

(13) Crank, J. Mathematics of Diffusion, Brunel University Uxbridge, 2nd Edition, 1975.

(14) Hernandez, R.; Gavara, R. Sorption and Transport in Nylon-6 Films. *J. Polym. Sci., Part B: Polym. Phys.* **1994**, *32*, 2367–2374.

(15) Fick, A. On Liquid Diffusion. *J. Membr. Sci* .**1995**, *100*, 33-38.

(16) Newman, A. The Drying of Porous Solids: Diffusion and Surface Emission Equations. *Trans. Am. Inst. Chem. Engr.* **1931**, *27*, 203-211.

(17) Lee, M. H.; Lim, B.; Kim, J. W.; An, E., J., Lee, D. Effect of composition on water permeability of model stratum corneum lipid membranes, *Soft Matter*, **2012**, *8*, 1539-1546.

(18) Bedane, A. H.; Eic, M.; Farmahini-Farahani, M.; Xiao, H. Water Vapor Transport Properties of Regenerated Cellulose and Nanofibrillated Cellulose Films. *J. Membr. Sci.* **2015**, *439*, 46-57.

(19) Tanaka, R.; Saito, T.; Hänninen, T.; Ono, Y.; Hakalahti, M.; Tammelin, T.; Isogai, A. Viscoelastic Properties of Core-Shell-Structured, Hemicellulose-Rich Nanofibrillated Cellulose in Dispersion and Wet-Film States. *Biomacromolecules*, **2016**, *17*, 2104-2111.

(20) Kontturi, E.; Suchy, M.; Penttilä, P.; Jean, B.; Pirkkalainen, K.; Torkkeli, M.; Serimaa, R. Amorphous Characteristics of an Ultrathin Cellulose Film. Biomacromolecules, **2011**, *12*, 770-777.

(21) Urquhardt, A.R.; Williams, A.M. The Effect of Temperature on the Adsorption of Water by Soda-Boiled Cotton. *J. Text. Inst., Trans.* **1924**, *75*, 559-572.

(22) Belbekhouche, S.; Bras, J.; Siquiera, G.; Chappey, C.; Lebrun, L.; Khelifi, B.; Marais, S.; Dufresne, A. Water Sorption Behavior and Gas Barrier Properties of Cellulose Whiskers and Microfibril Films. *Carbohydr. Polym.* **2011**, *83*, 1740-1748.

(23) Orofino, T.; Hopfenberg, H.; Stannett, V. Characterization of Penetrant Clustering in Polymers, J. Macromol. Sci., Part B: Phys. **1969**, *3*, 777-788.

(24) Ando, T.; Uchihashi, T.; Kodera, N. High-Speed AFM and Applications to Biomolecular Systems. *Annu. Rev. Biophys.* **2013**, *42*, 393-414.

(25) Luo, B.; Smith, J. W.; Ou, Z.; Chen, Q. Quantifying the Self-Assembly Behavior of Anisotropic Nanoparticles Using Liquid-Phase Transmission Electron Microscopy. *Acc. Chem. Res.* **2017**, *50*, 1125-1133.

SYNOPSIS TOC
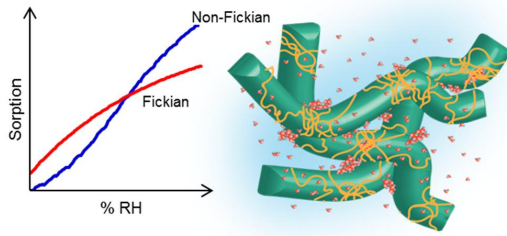
Supporting Information

Cellulose Nanofibril Film Structure Probed by Water Vapor Diffusion

Minna Hakalahti[1], Marco Faustini[2], Tuomo Hjelt[1], Cédric Boissière[2], Eero Kontturi[3], Tekla Tammelin[1]

[1] High Performance Fibre Products, VTT Technical Research Center of Finland Ltd, FI-02044, Espoo, Finland

[2] Sorbonne Universités, UPMC Univ Paris 06, CNRS, Collège de France, UMR 7574, Chimie de la Matière Condensée de Paris, F-75005, Paris, France

[3] Department of Bioproducts and Biosystems, School of Chemical Engineering, Aalto University, 02150 Espoo, Finland

TABLE OF CONTENTS

MATERIALS

Never dried bleached softwood pulp was obtained from a pulp mill in Finland. 2,2,6,6-tetramethylpiperidin-1-oxyl (TEMPO), sodium bromide (solid) and 10% sodium hypochlorite (aqueous) were purchased from Sigma-Aldrich. 0.1 M sodium hydroxide solution was obtained from Fluka Analytical and used without further treatment. Solution of poly(ethylene imine) (PEI, 30 wt.-%, Mw 70 000 g/mol) in water was obtained from PolySciences Inc., Warminster, PA, USA. LiBr (solid), $ZnBr_2$ (solid) and NaCl (solid) purchased from Sigma-Aldrich Oy, Helsinki, Finland and LiCl (solid), $MgCl_2 \cdot 6H_2O$ (solid), $Mg(NO_3)_2 \cdot 6H_2O$ (solid) and K_2SO_4 (solid) purchased from VWR International Oy, Helsinki, Finland were used for saturated salt solutions in water. The salt solutions were decanted used without any further treatment. Water was purified in a Milli-Q system (Millipore Corporation, Molsheim, France, resistivity 18.2 MΩ).

PRODUCTION OF TEMPO CNF

TEMPO oxidation of never dried softwood pulp was carried out by alkaline oxidation with hypochlorite catalyzed by TEMPO[1]. A standard conductometric titration procedure (SCAN-CM 65:02, 2002) was used to determine the charge of the oxidized pulp, 0.836 mmol g^{-1}. Microfluidics M-110EH-30 (Microfluidics Int., USA) high pressure fluidizer equipped with two Z-type chambers (diameters of 400 μm and 100 μm) was used to fibrillate the TEMPO oxidized pulp during two passes at 1850 bar pressure. Thereby TEMPO oxidized cellulose nanofibrils (CNF) with a final consistency of approximately 1 wt.-% was obtained. High performance liquid chromatography (Dionex ICS-3000, Thermo Fischer Scientific Ltd, Waltham, MA, USA) was applied to determine the hemicellulose content of the TEMPO CNF after acid hydrolysis was performed[2]. As shown in Table S1, the total neutral sugar content of hemicellulose in the TEMPO CNF was 8%.

Table S1. Neutral sugar composition of TEMPO CNF.

Glucose (%)	Galactose (%)	Mannose (%)	Arabinose (%)	Xylose (%)	Rhamnose (%)	Fructose (%)	Total (%)	Others[*] (%)
64.0	0	2.1	0	6.2	0	0	72.3	27.7

[*]Mainly glucuronic acids.

PREPARATION OF SUPPORTED THIN FILMS OF TEMPO CNF

TEMPO CNF thin films were prepared on AT-cut gold sensors purchased from Q-Sense AB, Gothenburg, Sweden. The sensors had a fundamental resonance frequency, f_0, of 5 MHz and sensitivity constant, C, of 0.177 mg m^{-2} Hz^{-1} as reported by the supplier. The preparation of supported thin films of TEMPO CNF was carried out according to the procedure reported by Eronen et al. In brief, gold coated QCM-D sensor surfaces were rinsed with water, dried with nitrogen gas and cleaned using UV/ozone (Bioforce Nanosciences, CA) for 10 minutes. Cleaned sensors were coated with 1 mg ml^{-1} PEI solution in water by 30 minutes of drop casting and rinsed with milli-Q water, dried with nitrogen gas and heated in an oven for 10 minutes at 80 ˚C. 0.15 wt.-% suspension of TEMPO CNF was sonicated using a Branson Digital Sonifier (400 W; 20 kHz) at 40% amplitude for 2 minutes. 200 µl of TEMPO CNF was dispensed onto the PEI coated sensors and spincoated (WS-400BZ-6NPP/Lite, Laurell, North Wales, PA, USA) at 3000 rpm for 3 minutes followed by annealing for 10 minutes in 80 ˚C oven to ensure fibril attachment.[3]

ATOMIC FORCE MICROSCOPY

TEMPO CNF thin film surface morphology was studied using afm+ from Anasys Instruments Inc. (Santa Barbara, CA, USA) in tapping mode. The probes HQ:NSC15/Al BS (µmasch, Tallinn, Estonia) had cantilever frequency 325 kHz, spring constant 40 N/m and curvature radius of ~8 nm according to the producer. The AFM images were analyzed using Analysis Studio software (version 3.11). Root mean squared roughness (R_q) value was obtained from three images and the average was reported. No image processing was performed.

SPECTROSCOPIC ELLIPSOMETRY

UV-Vis (λ = 500 - 998.85 nm) variable angle Spectroscopic Ellipsometer (Vase-2000U, Woollam Inc., Lincoln, NE, USA) equipped with a humidity chamber was used to perform the spectroscopic ellipsometry (SE) measurements. A beam of polarized light was focused on TEMPO CNF thin films supported by gold QCM-D sensor substrates inside a humidity chamber. The tilt of the sample plate was adjusted to align the sample with the light detector.

The initial theoretical thickness and refractive index were determined by conducting an SE scan and applying the classic Cauchy model. The measured refractive indices were fitted to model data (Figure S1) to validate the use of the Cauchy model. Dynamic scans consisting of incremental relative humidity (RH) steps of 2% RH each lasting 20 s were then performed by injecting a 3 l min^{-1} flux of air containing a fixed partial pressure of water to the humidity chamber. A humidity sensor placed inside the humidity chamber was used to monitor the % RH. Wvase32 software and the Cauchy model were used to perform data analyses and to determine the thickness of the TEMPO CNF thin film over the measured relative humidity range.

RAW SPECTROSCOPIC ELLIPSOMETRY DATA AND CAUCHY MODELS

The raw data from dynamic SE measurements (under changing % RH) is depicted in Figure S1a. The experimental results and the modelled results at 0 % RH and at 90% RH achieved through a fitting procedure are shown in Figure S1b. The modelling procedure involved using a regression algorithm achieved by minimizing the mean-squared error (MSE) between the experimental and modelled results. Between data from the measurements of TEMPO CNF thin film and the fit by the classical Cauchy model, the MSE value for the comparison of the experimental data for TEMPO CNF thin film and the Cauchy model was < 4, which indicates that analyzed layers can be considered as transparent and homogeneous throughout the thickness, whatever the relative humidity investigated in this manuscript.
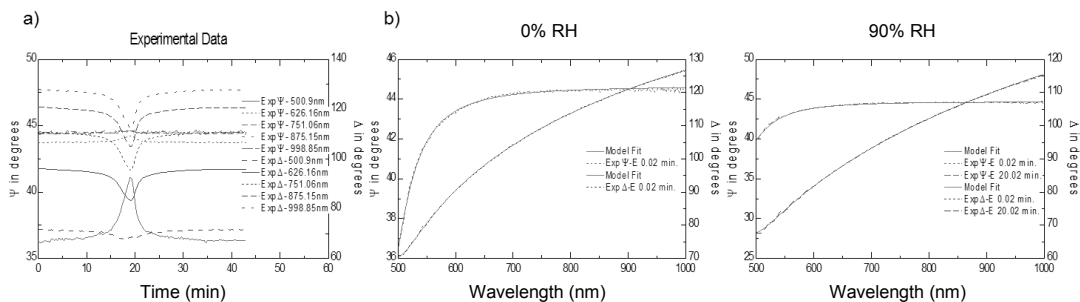
Figure S1. Ψ and Δ values measured for TEMPO CNF film by SE during the dynamic humidity cycle (sorption at 0-19 min, desorption at 20-40 min) with five wavelengths shown. b) Fit between experimental data (SE) and Cauchy model data at 0 % RH (left) and 90% RH (right).

QUARTZ CRYSTAL MICROBALANCE WITH DISSIPATION MONITORING

The E4 QCM-D instrument equipped with a QHM 401 humidity module (Q-Sense AB, Gothenburg, Sweden) was used for studying the water vapor uptake of TEMPO CNF thin films from 6% to 97% RH. Changes in areal mass and can be calculated according to the Sauerbrey equation (equation S1)[4,5,6]:

$$\Delta m = -C\frac{\Delta f}{n} \tag{S1}$$

where $\Delta f = f - f_0$ is the change in resonance frequency, C is the sensitivity constant of the sensor and n is the measurement overtone number ($n = 1, 3, 5, 7, 9, 11$).

INITIAL AREAL MASS DETERMINATION OF (DRY) TEMPO CNF THINS FILM BY QCM-D

Initial mass of pristine QCM-D sensors were measured in a QHM 401 humidity module (23 ˚C, air flow rate 0.1 ml min^{-1}) after 13 hour stabilization time under 6% RH. After TEMPO CNF thin film preparation and overnight stabilization under 6% RH for 13 hours, the initial areal mass of the TEMPO CNF thin films was determined. The QTools Software was used to stitch together the third overtone (15 MHz, $f_0 = 5$ MHz, $n = 3$) data and areal mass based on Δf according to the Sauerbrey equation (equation S1) was calculated.

HUMIDITY MEASUREMENTS BY QCM-D

Saturated salt solutions[7] (rate 0.1 ml min^{-1} for 30 min at 23 ˚C) were passed through the humidity module to achieve eight stepwise increasing relative humidity while monitoring the changes in resonance frequency (Δf) (Figure S2). Mass changes were calculated in QTools software using equation S1 and the third overtone (15 MHz, $f_0 = 5$ MHz, $n = 3$).
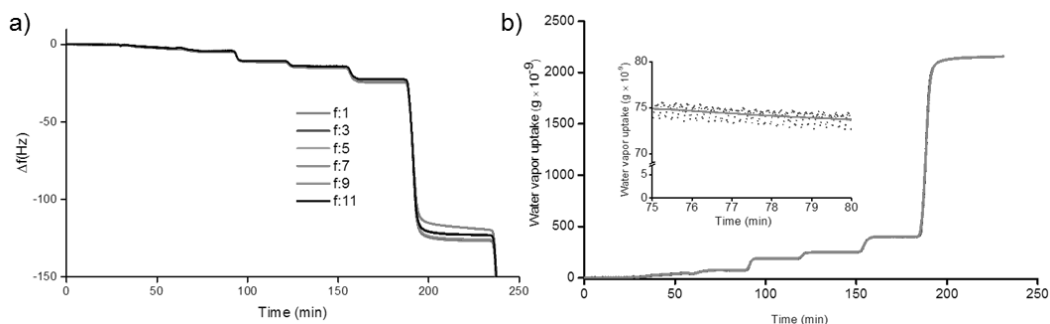

Figure S2. Change in a) frequency (Δf) and b) mass due to water vapor uptake as a function of time in stepwise increasing RH as detected by QCM-D for TEMPO CNF thin film. The inset shows a portion of the center moving average of the curve (50 data points in both directions).

DETERMINATION OF THE TRANSITION RANGES

The transition range between consecutive RH% levels was determined from the mass uptake data collected by QCM-D. Firstly, to reduce the noise related to the frequency response of the mass uptake curve, a central moving average was calculated (Figure S2b). A second derivative of the curve was calculated and the maximum and minimum inflexion points were selected as the onset and end points of the transition range (example shown in Figure S3).
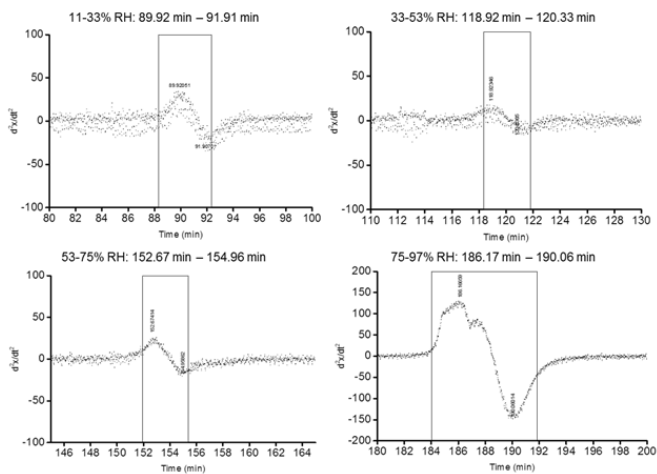
Figure S3. Second derivative of the mass uptake curve at different time intervals as measured by QCM-D with maximum and minimum inflexion points identified.

DIFFUSION MODEL

To determine the diffusion coefficient (D), the protocol described by Lee et al.[8] was adapted for TEMPO CNF thin films. Mass over the transition ranges (as measured by QCM-D) was coupled with thickness changes (as determined by SE) assuming a linear relationship. Equation S2 was used to calculate plot the graph of the left hand side (LHS) of the equation as a function of time:

$$-\frac{1}{\pi^2} ln\left[\frac{(m_\infty - m_t)\pi^2}{8(m_\infty - m_0)}\right] \times l^2 = Dt \tag{S2}$$

where m_∞, m_t, and m_0 are the mass values of the TEMPO CNF thin film at equilibrium (at each % RH % level) and at time $= t$ and time $= 0$, respectively, l represents the thickness of the thin film and t marks the time. Linear regression was applied to determine D. The reported value of D is an average calculated from three individual QCM-D measurements. Linear regression could only be applied in the transition range 11% - 33% RH with reasonable accuracy ($R^2 > 0.9$).

EFFECTIVE DIFFUSION MODEL

To determine the effective diffusion coefficient as previously shown by Bedane et al.[9] according to Newman's solution of Fick's second law[10], the evolution of the relative mass uptake, $m(t)/m(\infty)$, at each transition range was calculated. The relative mass uptake curve was fitted by Equation S3:

$$\frac{m(t)}{m(\infty)} = 1 - \sum_1^\infty \frac{2\alpha^2}{\beta^2(\alpha(\alpha+1)+\beta^2)} e^{-\beta\frac{Dt}{L^2}} \tag{S3}$$

where β are the positive roots of the equation $\alpha = \beta\sin\beta$, L is half of the film thickness and α represents the ratio of diffusion into the interior of the film to accumulation of (liquid) water on top of the film minimizing the least square errors and solving for D and α. The value of β was adjusted by applying the equation $\alpha = \beta\sin\beta$ to obtain the optimal solution.

CALCULATION OF SOLUBILITY

Solubility was calculated according to equation S4:

$$S = \frac{m_\infty/\rho_p}{(m_p/\rho_v) \times p_v^0 \times a} \tag{S4}$$

where m_p represents the mass of the dry thin film, p_v^0 is the saturation vapor pressure at 23 ˚C (=2.8104 kPa) and a is water activity. The values of ρ_p, the density of TEMPO CNF dry film, was 1.5 g/cm^3 and ρ_v, density of water vapor 0.00127 g/cm^3, as obtained from literature were used.

An example calculation of solubility at 33% RH for a TEMPO CNF thin film with a dry mass of 1995×10^{-9} g/cm^2 as determined by QCM-D.

$$S = \frac{m_\infty/\rho_p}{(m_p/\rho_v) \times p_v^0 \times a} = \frac{38 \times 10^{-9}g/1.5gcm^{-1}}{\left(1995 \times\frac{10^{-9}g}{0.00125gcm^{-1}}\right) \times 2.8104\ kPa \times 0.33} = 72.77\ \frac{cm^3}{cm^3 \times kPa}$$

CALCULATION OF EFFECTIVE PERMEABILITY

Effective permeability of water vapor was calculated according to equation S5:

$$P_{eff} = D_{eff} \times S \tag{S5}$$

At each consecutive transition step to a higher RH% level the solubility at the terminal end of the transition range was chosen for permeability calculations.

At 33% RH:

$$P_{eff} = D_{eff} \times S = 2.31 \times \frac{10^{-13} cm^2}{s} \times 84.57 \frac{cm^3}{s} = 1.95 \times 10^{-11} \frac{cm^3 (STP) \times cm}{cm^2 \times s \times kPa}$$

REFERENCES

(1) Isogai, A.; Saito, T.; Fukuzumi, H. TEMPO-Oxidized Cellulose Nanofibres, *Nanoscale*, **2011**, *3*, 71–85.

(2) Laukkanen, A.; Pere, J.; Mikkelsson, A. Analytical Method for Determining the Concentration of Oxidized Nanofibrillar Cellulose in a Sample. CA2908852, 2014.

(3) Eronen, P.; Laine, J.; Ruokolainen, J.; Österberg, M. Comparison of Multilayer Formation between Different Cellulose Nanofibrils and Cationic Polymers. *J. Colloid Interface Sci.* **2011**, *373*, 84-93.

(4) Sauerbrey, G. The Use of Quartz Oscillators for Weighing Thin Layers and for Microweighing. *Z. Phys.* **1959**, *155*, 206–222.

(5) Rodahl, M.; Höök, F.; Krozer, A.; Brzezinski, P.; Kasemo, B. Quartz Crystal Microbalance Setup for Frequency and Q-Factor Measurements in Gaseous and Liquid Environments. *Rev. Sci. Instrum.* **1995**, *66*, 3924-3930.

(6) Höök, F.; Rodahl, M., Brzezinski, P.; Kasemo, B. Energy Dissipation Kinetics for Protein and Antibody – Antigen Adsorption under Shear Oscillation on a Quartz Crystal Microbalance. *Langmuir*, **1998**, *14*, 729-734.

(7) Greenspan, L. Humidity Fixed Points of Binary Saturated Aqueous Solutions. *J. Res. Natl. Bureau*, Stand. **1977**, *81*, 89-96.

(8) Lee, M. H.; Lim, B.; Kim, J. W.; An, E., J., Lee, D. Effect of composition on water permeability of model stratum corneum lipid membranes, *Soft Matter*, **2012**, *8*, 1539-1546.

(9) Bedane, A. H.; Eic, M.; Farmahini-Farahani, M.; Xiao, H. Water Vapor Transport Properties of Regenerated Cellulose and Nanofibrillated Cellulose Films. *J. Membr. Sci.* **2015**, *439*, 46-57.

(10) Newman, A. The Drying of Porous Solids: Diffusion and Surface Emission Equations. *Trans. Am. Inst. Chem. Engr.* **1931**, *27*, 203-211.

Paper III

Hakalahti, M.; Salminen, A.; Seppälä, J.; Tammelin, T.; Hänninen, T. Effect of Interfibrillar PVA Bridging on Water Stability and Mechanical Properties of TEMPO/NaClO$_2$ Oxidized Cellulosic Nanofibril Films. *Carbohydr. Polym.* **2015**, *126*, 78-82.
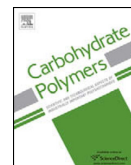
Effect of interfibrillar PVA bridging on water stability and mechanical properties of TEMPO/NaClO$_2$ oxidized cellulosic nanofibril films

Minna Hakalahti [a], Arto Salminen [b], Jukka Seppälä [b], Tekla Tammelin [a], Tuomas Hänninen [a,*]

[a] VTT Technical Research Centre of Finland, VTT, PO Box 1000, FIN-02044 Espoo, Finland
[b] Polymer Technology, Department of Biotechnology and Chemical Technology, Aalto University School of Chemical Technology, Aalto, PO Box 16100, FIN-00076 Espoo, Finland

ARTICLE INFO

ABSTRACT

TEMPO/NaClO$_2$ oxidized cellulosic nanofibrils (TCNF) were covalently bonded with poly(vinyl alcohol) (PVA) to render water stable films. Pure TCNF films and TCNF–PVA films in dry state showed similar humidity dependent behavior in the elastic region. However, in wet films PVA had a significant effect on stability and mechanical characteristics of the films. When soaked in water, pure TCNF films exhibited strong swelling behavior and poor wet strength, whereas covalently bridged TCNF–PVA composite films remained intact and could easily be handled even after 24 h of soaking. Wet tensile strength of the films was considerably enhanced with only 10 wt% PVA addition. At 25% PVA concentration wet tensile strengths were decreased and films were more yielding. This behavior is attributed to the ability of PVA to reinforce and plasticize TCNF-based films. The developed approach is a simple and straightforward method to produce TCNF films that are stable in wet conditions.

© 2015 Elsevier Ltd. All rights reserved.

1. Introduction

Cellulose nanofibrils (CNF) have attracted much interest due to their unique properties, such as mechanical strength, high surface-to-volume ratio and strong film-forming tendency (Syverud & Stenius, 2009; Yano & Nakahara, 2004). These characteristics enable exploitation of CNF films in applications such as gas-barriers (Fukuzumi, Saito, Iwata, Kumamoto, & Isogai, 2009), filters (Mautner et al., 2014) and templates for highly functional nanomaterials (Orelma et al., 2012). Due to high hygroscopicity of cellulose, most CNF films are not stable in water, which limits their use in aqueous or humid environments.

Recently, several strategies to improve water stability of CNF based films have been proposed. One approach is to prepare layered structures by, for example, atomic layer deposition (Hirvikorpi, Vähä-Nissi, Nikkola, Harlin, & Karppinen, 2011) or by coating with wax (Spence, Venditti, Rojas, Pawlak, & Hubbe, 2011; Österberg et al., 2013a). Some methods aim to improve water tolerance by reducing free volume by overpressure filtration and hot-pressing

(Österberg et al., 2013a). Other strategies lean on surface treatments (Chinga-Carrasco et al., 2012; Rodionova, Eriksen, & Gregersen, 2012), such as silylation (Peresin, Vartiainen, Kunnari, Kaljunen, & Tammelin, 2012; Österberg, Peresin, Johansson, & Tammelin, 2013b). Additionally, crosslinking chemically unmodified CNF with poly(acrylic acid) (PAA) (Lu & Hsieh, 2009) has been shown to render water insoluble CNF based membranes.

2,2,6,6-Tetramethylpiperidin-1-yl)oxy (TEMPO) mediated oxidation can be used to selectively oxidize primary alcohols on the surface of cellulose fibrils as pre-treatment for improving fibrillation (Saito, Nishiyama, Putaux, Vignon, & Isogai, 2006). In this pre-treatment most primary alcohols are oxidized to carboxyl groups, although some groups remain as aldehydes. These aldehyde groups can be further oxidized to carboxyls with NaClO$_2$ in neutral conditions (Saito et al., 2009), which further increases the hygroscopicity of cellulose.

Carboxyl groups can react with alcohols to form covalent ester bonds under acidic conditions. This chemistry has been used to overcome instability of water soluble polymers, such as PVA, by crosslinking with carboxyl containing PAA (Baştürk, Demir, Daniş, & Kahraman, 2013; Clemons, Sedlmair, Illman, Ibach, & Hirschmugl, 2013; Paralikar, Simonsen, & Lombardi, 2008). Recently, crosslinked CNF/PAA composites have been prepared (Lu & Hsieh, 2009; Spoljaric, Salminen, Luong, & Seppälä, 2013) in order to improve the material properties in humid environments.

* Corresponding author. Tel.: +358 40 6731621; fax: +358 20 722 7026.
E-mail addresses: minna.hakalahti@vtt.fi (M. Hakalahti), arto.salminen@aalto.fi (A. Salminen), jukka.seppala@aalto.fi (J. Seppälä), tekla.tammelin@vtt.fi (T. Tammelin), tuomas.hanninen@vtt.fi (T. Hänninen).

Whereas CNF has widely been blended with PVA to act as reinforcing fibres (Endo, Saito, & Isogai, 2013; Li, Zhao, Huang, & Liu, 2013; Virtanen, Vartiainen, Setälä, Tammelin, & Vuoti, 2014a; Virtanen, Vuoti, Heikkinen, & Lahtinen, 2014b; Zhou, Fu, Zheng, & Zhan, 2012), the potential of achieving water stability via covalently bonding TEMPO/NaClO$_2$ oxidized cellulose nanofibrils (TCNF) with PVA has not yet been fully explored. To the authors' knowledge, this is the first time a simple and easily up-scalable bridging method for preparation of water stable TCNF films is reported.

In this work, mechanical properties of TCNF films were enhanced by covalently bonding TCNF with PVA via acid-initiated esterification reaction. Water stable films containing only 10% PVA were produced by solvent casting and without any post-treatments, such as hot-pressing. Influence of amount and degree of hydrolysis (DH) of PVA on the mechanical properties of films was investigated using dynamic mechanical analysis (DMA) together with dynamic water sorption (DVS). Additionally, wet strengths of films were determined by wet tensile measurements.

2. Materials and methods

2.1. Materials

Never dried bleached softwood pulp obtained from a pulp mill in Finland was TEMPO oxidized according to procedure by Saito et al. (2006). Aldehydes formed due to TEMPO oxidation were further oxidized into carboxyls according to Shinoda, Saito, Okita, and Isogai (2012). Carboxylate content of the oxidized pulp was 1.12 mmol/g determined by conductometric titration (SCAN-CM 65:02, 2002). pH of the oxidized pulp was set to 4 using acetic acid and it was fibrillated with a high pressure fluidizer (Microfluidics M-110EH-30, Microfluidics Int., USA) equipped with two Z-type chambers. The chambers had diameters of 400 μm and 100 μm and the fibrillation was done in two passes at 1850 bar operating pressure. The final consistency of TCNF was approximately 1 wt%.

PVA with DH of 88% (88PVA) (Mowiol 40–88, M_w 205 000 g/mol, DP 4200), PVA with DH of 98% (98PVA) (Mowiol 56–98, M_w 195 000 g/mol, DP 4300) and all other chemicals were purchased from Sigma-Aldrich and used as received. Deionized water was used throughout the study.

2.2. Preparation of TCNF–PVA films

TCNF was diluted to 0.3 wt% with deionized water and sonicated using Branson Digital Sonifier (400 W; 20 kHz) at 40% amplitude for 5 min to form a homogeneous dispersion. Aqueous 0.3 wt% solutions of PVA were prepared by dissolving PVA in water at 95 °C for 5 h. Casting solutions were prepared by mixing PVA solution and TCNF suspension in 10:90 and 25:75 weight ratios. Casting solutions were poured into poly(styrene) Petri dishes and dried in controlled atmosphere (23 °C/50% RH) for at least five days.

2.3. Characterization

2.3.1. Microscopic analysis of TCNF–PVA films

Film surfaces were imaged by scanning electron microscope (SEM) LEO DSM 982 Gemini FEG-SEM (Noran Instruments Inc. Middleton, USA). Samples were attached on carbon adhesive discs and pressed on aluminum stubs. Typically, no conductive coating was applied on the specimen prior to SEM imaging, which was conducted using acceleration voltage of 0.50 keV.

Atomic force microscopy (AFM) imaging of film surfaces was performed using Nanoscope IIIa Multimode scanning probe microscope (Digital Instruments Inc, Santa Barbara, CA USA) equipped with E scanner. The images were taken in tapping mode in air

using aluminum coated silicon cantilevers (HQ:NSC15/Al BS, Micromasch, Tallinn, Estonia) with nominal resonance frequencies of 265–410 kHz. Images were not processed by any other means except flattening.

2.3.2. Tensile testing as a function of relative humidity

Dynamic mechanical analysis (DMA) was carried out on TCNF–PVA films using tensile mode and film geometry. The analysis was performed in controlled RH using a Q800 Dynamic Mechanical Analyzer (TA Instruments, USA) equipped with DMA-RH accessory. The film samples had average dimensions of $10.00 \times 5.30 \times 0.02$ mm^3. Preload force, amplitude and frequency of 0.05 N, 5.0 μm and 1 Hz, respectively, were used during the analysis. The storage modulus (E') was recorded as a function of time at 30 °C. A stepwise DMA scan was performed at RH 0%, 50%, 90% and once more at 0% to record the extent of material recovery. Each humidity level was maintained for 300 min. In order to take fluctuations into consideration, three specimens were measured from each sample. The E' values shown in the results section are average values of the measured E' of these three specimens at the end of each 300 min humidity step.

2.3.3. Determination of equilibrium water content

Water content of TCNF–PVA films was determined gravimetrically using DVS-1 instrument (Surface Measurement Systems, UK). Samples were weighed in a sample cup connected to a microbalance and the precise mass of the sample was registered with a resolution of 1 μg in controlled humidity. Temperature was kept at 30 °C throughout the experiment and a stepwise DVS scan was performed at RH 0%, 50% and 90% and again at 0%. Each humidity level was maintained for 300 min.

Residual moisture content of dry films was determined by Karl-Fischer titrations performed with Mettler Toledo DL31 apparatus. Hydranal Titrant 2 was used as the Karl-Fischer reagent. About 100 mg of shredded film samples were weighed into vials and water was extracted in anhydrous methanol for 16 h with continuous stirring before titration. The titrant was calibrated with water and sodium tartrate dihydrate was used as a calibration control. Amount of solvent injected into the titrator was determined gravimetrically. The water content values shown in Section 3 are measured at the end of each 300 min humidity step and corrected by the amount of residual moisture.

2.3.4. Wet strength testing

Tensile properties of wet TCNF–PVA films were determined with 33R4204 universal testing machine (Instron, UK) equipped with a 100 N static load cell. The specimens were immersed in deionized water for 24 h before wet strength measurements performed in controlled atmosphere (23 °C/50% RH). Five specimens were measured from each sample using crosshead speed of 0.5 mm/min. Dimensions (average dimensions: $20.00 \times 5.30 \times 0.012$ mm^3) of dry specimens were used to determine the tensile characteristics of wet films.

3. Results and discussion

Covalent bonding between TEMPO/NaClO$_2$ oxidized fibrils and PVA was expected to enhance mechanical properties of TCNF-based films in humid and wet environments. Films prepared from pure TCNF or a neutral mixture of TCNF and PVA were observed to quickly disintegrate in water. The TCNF–PVA films with 10 to 25% of fully or partly hydrolyzed PVA cast in presence of acid remained intact even after several months, suggesting that covalent ester bonds were formed upon drying (Fig. 1). As seen in Fig. 2a, free-standing TCNF films with 10% fully hydrolyzed PVA were
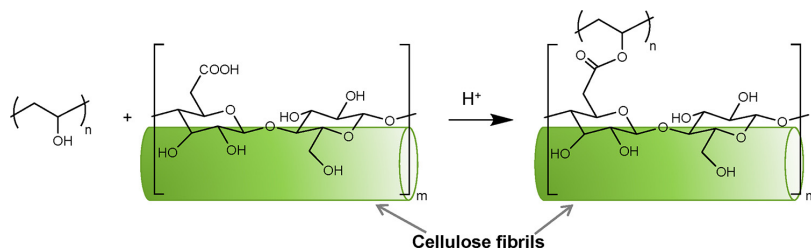
Fig. 1. Schematic illustration of the acid-initiated esterification reaction between TCNF and PVA on fibril surfaces.

transparent and did not show shrinking or defects. SEM micrograph shown in Fig. 2b revealed that fibrils appear to be uniformly distributed and randomly oriented in TCNF films with 10% fully hydrolyzed PVA. AFM height image presented in Fig. 2c showed that TCNF–98PVA10% film surface is relatively smooth. Differences between appearance or morphology of TCNF–PVA films with varying amounts of PVA could not be detected by visual inspection or AFM (see Supporting information).

Direct chemical analysis of the esterification by methods, such as FT-IR and Raman spectroscopies (see Supplementary data), proved to be very difficult due to small intensity and overlapping of relevant bands. Ester bonds can typically be seen as bands at around $1600\,cm^{-1}$ or in the fingerprint region (Fukuzumi, Saito, Okita, & Isogai, 2010). In case of TCNF–PVA films, bands corresponding to ester groups cannot be assigned and there are no visible differences between spectra of pure TCNF and TCNF–PVA films. Therefore, mechanical properties of the films measured by DMA and tensile testing in controlled humidity were used as indirect verification of esterification in TCNF–PVA films.

3.1. Storage modulus as a function of relative humidity

The storage moduli (E') of films determined by controlled humidity DMA are presented in Fig. 3a and in Supplementary data as a function of time. In dry conditions (0% RH), E' of films were in the range of 15.0–16.5 GPa and decreased slightly to 12.0–13.5 GPa at 50% RH. At higher RH level (90% RH), E' values exhibited a sharper decrease to 4.0–6.0 GPa. Humidity dependent behavior of pure TCNF and TCNF–PVA films was similar to each other and characteristic of polymer reinforced TCNF films (Bulota, Vesterinen, Hughes, & Seppälä, 2012). Pure PVA films showed significantly lower E' at all measured RH levels (see Supplementary data). Nonetheless, both PVA grades could be used at 10% and 25% concentration without significantly deteriorating the stiffness of films. In addition, no major structural deformations seemed to occur due to water adsorption, since E' values of films recovered almost to their original level at 0% RH upon drying. In dry conditions (0% RH) residual water remained in films due to the hygroscopic nature of TCNF and PVA, as indicated by DVS results in Fig. 3b.

According to the results, proportion of PVA in the film had an influence on E' values. At 50% and 90% RH, films containing 25% PVA had slightly lower E' values in comparison to films with 10% PVA. Although the equilibrium water content was smaller, plasticizing effect of PVA was more prominent when proportion of PVA was larger. While this matter is outside the scope of this study, differences in equilibrium water content could have been caused by different water binding abilities of available functional groups (Piringer, 2007) or by variances in structural porosity.

DH of PVA appeared to affect the elastic properties of films. Films containing partly hydrolyzed 88PVA showed smaller E' in comparison to the films containing fully hydrolyzed 98PVA at 50% and 90% RH. This effect could be associated with the larger amount of equilibrium water in 88PVA containing films.

3.2. Wet strength characteristics

Pure TCNF films exhibited strong swelling and very poor strength after immersion in water. This prevented determination of its wet strength properties by tensile testing and indicated that there was no covalent interfibrillar bonding. From a purely
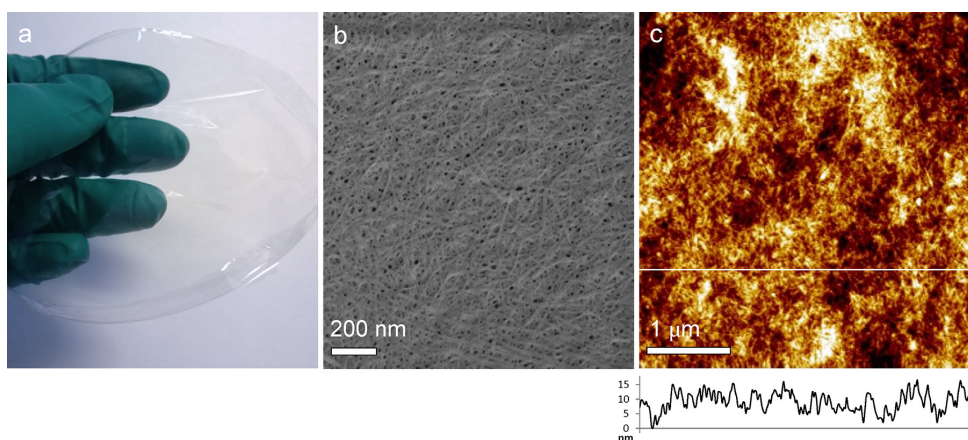

Fig. 2. (a) Photograph of transparent and free-standing TCNF–98PVA10% film, (b) SEM image (×50 000) of film surface showing the uniform distribution and random orientation of TCNF fibrils and (c) AFM height image displaying the surface topography of the film. The AFM image size is 4 μm².
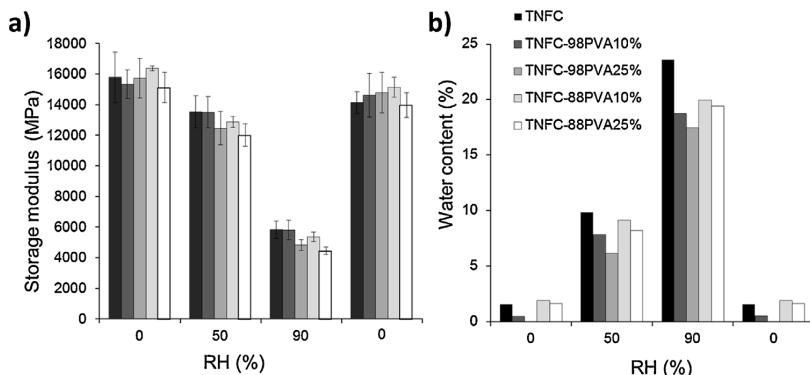
Fig. 3. (a) Storage moduli and (b) equilibrium water contents of pure TCNF films and TCNF–PVA films containing 10% or 25% of PVA at different RH levels. 98PVA and 88PVA refer to fully and partly hydrolyzed PVA, respectively.

Table 1
Mechanical properties of TCNF films and TCNF–PVA films containing 10% or 25% PVA, after soaking in water for 24 h.

Film sample	Young's modulus (MPa)	Work to fracture (MJ m^{-3})
TCNF	–	–
TCNF–88PVA10%	202 ± 18	2.2 ± 0.5
TCNF–88PVA25%	76 ± 6	2.1 ± 0.3
TCNF–98PVA10%	315 ± 108	1.7 ± 0.5
TCNF–98PVA25%	93 ± 18	1.6 ± 0.5

chemical point of view, carboxyl and hydroxyl groups of TCNF should react to form covalent ester bonds even without PVA. However, the amount of fibril–fibril contact points is likely to be low due to high fibril stiffness. Also, the majority of highly reactive primary hydroxyls have been converted into carboxyls in the TEMPO/NaClO$_2$ oxidation and only less reactive secondary hydroxyls are present (Klemm, Phillip, Heinze, & Wagenknecht, 1998). Without sufficient esterification, pure TCNF films are likely to swell freely and disintegrate in water.

The substantial difference between TCNF–PVA and pure TCNF films is the significantly improved wet strength. This behavior is indicative of the ability of TCNF to form covalent ester bonds with PVA. As seen in Table 1, TCNF films with 10% PVA exhibited the highest Young's moduli of 202 MPa and 315 MPa with 88PVA and 98PVA, respectively. Also, highest stresses at break were displayed by the films containing 10% PVA, as seen in Fig. 4 and Supplementary data.
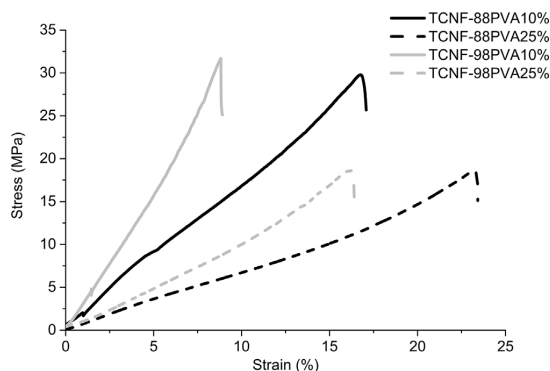

Fig. 4. Stress–strain curves of TCNF–PVA films containing 10% or 25% PVA following immersion in water for 24 h.

Films containing partly hydrolyzed 88PVA were less rigid than those containing fully hydrolyzed 98PVA, which was seen as lower Young's moduli values. Stress at break was also lower in films containing 88PVA. Partly hydrolyzed PVA contains a larger number of acetyl groups, which cannot participate in the formation of covalent ester bonds. This could result in reduced number of covalent ester linkages between TCNF and PVA and hence decrease rigidity of the films.

The toughness of wet TCNF–PVA films was expressed as work of fracture, obtained from the area under the stress–strain curves. As shown in Table 1, DH of PVA had some effect on the toughness of wet films, whereas the concentration of PVA did not clearly affect it in the 10–25 wt% concentration range. The combination of good strength and ductility yielded slightly better toughness for wet TCNF–PVA films containing partly hydrolyzed 88PVA. Wet TCNF–88PVA films displayed work of fracture of 2.1–2.2 MJ m^{-3}, whereas fully hydrolyzed 98PVA had slightly negative effect on toughness and values were 1.6–1.7 MJ m^{-3}. Higher toughness is attributed to better ductility of TCNF–88PVA films. When compared to some common biological materials, the wet TCNF–PVA films exhibit toughness inferior to collagen and bone (2.8–3.0 MJ m^{-3}) but comparable to keratin (1.8 MJ m^{-3}). (Vogel, 2003)

Mechanical testing results indicate that covalent ester bonding can effectively stabilize the film structure in aqueous environments. These results imply that PVA forms interconnecting bridges between TCNF fibrils, as illustrated in Fig. 5. It is assumed that hydroxyl groups of PVA react with carboxyls of several TCNF fibrils and form a network of TCNF fibrils covalently interconnected by PVA bridges.

Mechanical properties of wet films (Table 1 and Fig. 4) give evidence of higher interfibrillar bridging in films containing 10% PVA in comparison to 25% PVA containing films. This effect can be seen as higher Young's moduli and break at stress values. DMA
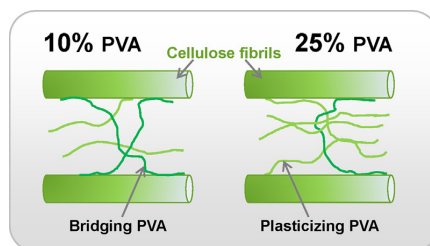

Fig. 5. Illustration of bridging and plasticizing effect of PVA in TCNF–PVA films.

results also support this hypothesis, as films containing 10% PVA seem to be stiffer at elevated RH in comparison to 25% PVA containing films. Higher proportion of PVA increases the likelihood of unbound polymer chains, giving the film structure more mobility. This effect can be seen as increased strain values and as reduced storage moduli. Based on the results, it appears that PVA can function as a reinforcing agent and with water also as a plasticizer in TCNF films.

The simple PVA bridging method demonstrated here significantly improved the wet strength of TCNF films. The production process of water stable films involved the use of inexpensive materials in an easily up-scalable process. The TCNF-based films developed in this study are relevant for a wide variety of applications requiring good mechanical performance in aqueous environments.

4. Conclusions

In this work, a simple solvent-casting method to produce water stable TCNF films without post-treatments was developed. Bridging TCNF with just 10% PVA resulted in films with considerably improved wet strength. These improved physical characteristics were maintained even after soaking in water for 24 h. Additionally, mechanical properties, such as stiffness and wet strength of TCNF–PVA films, could be tuned by adjusting the amount of PVA. PVA provided both reinforcement and plasticization, depending on its ratio to TCNF. The method described here has potential for scaled up production of water stable TCNF films.

Acknowledgements

Appendix A. Supplementary data

Supplementary data associated with this article can be found, in the online version, at http://dx.doi.org/10.1016/j.carbpol.2015.03.007.

References

Baştürk, E., Demir, S., Daniş, Ö., & Kahraman, M. (2013). Covalent immobilization of α-amylase onto thermally crosslinked electrospun PVA/PAA nanofibrous hybrid membranes. *Journal of Applied Polymer Science*, 127, 349–355.

Bulota, M., Vesterinen, A.-H., Hughes, M., & Seppälä, J. (2012). Mechanical behavior, structure and reinforcement processes of TEMPO-oxidized cellulose reinforced poly(lactic) acid. *Polymer Composites*, 34, 173–179.

Chinga-Carrasco, G., Kuznetsova, N., Garaeva, M., Leirset, I., Galilullina, G., Kostochko, A., & Syverud, K. (2012). Bleached and unbleached MFC nanobarriers: Properties and hydrophobisation with hexamethyldisilazane. *Journal of Nanoparticle Research*, 14, 1280–1289.

Clemons, C., Sedlmair, J., Illman, B., Ibach, R., & Hirschmugl, C. (2013). Chemically imaging the effects of the addition of nanofibrillated cellulose on the distribution of poly(acrylic acid) in poly(vinyl alcohol). *Polymer*, 54, 2058–2061.

Endo, R., Saito, T., & Isogai, A. (2013). TEMPO-oxidized cellulose nanofibril/poly(vinyl alcohol) composite drawn fibers. *Polymer*, 54, 935–941.

Fukuzumi, H., Saito, T., Iwata, T., Kumamoto, Y., & Isogai, A. (2009). Transparent and high gas barrier films of cellulose nanofibers prepared by TEMPO-mediated oxidation. *Biomacromolecules*, 10, 162–165.

Fukuzumi, H., Saito, T., Okita, Y., & Isogai, A. (2010). Thermal stabilization of TEMPO-oxidized cellulose. *Polymer Degradation and Stability*, 95, 1502–2108.

Hirvikorpi, T., Vähä-Nissi, M., Nikkola, J., Harlin, A., & Karppinen, M. (2011). Thin Al$_2$O$_3$ barrier coatings onto temperature-sensitive packaging materials by atomic layer deposition. *Surface Coating Technology*, 205, 5088–5092.

Klemm, D., Phillip, B., Heinze, U., & Wagenknecht, W. (1998). *Principles and characteristics of cellulose reactions under homogeneous conditions. Comprehensive cellulose chemistry* (1) Weinheim: Wiley-VCH.

Li, W., Zhao, X., Huang, Z., & Liu, S. (2013). Nanocellulose fibrils isolated from BHKP using ultrasonication and their reinforcing properties in transparent poly(vinyl alcohol) films. *Journal of Polymer Research*, 20, 210–216.

Lu, P., & Hsieh, Y.-L. (2009). Cellulose nanocrystal-filled poly(acrylic acid) nanocomposite fibrous membranes. *Nanotechnology*, 20, 1–9.

Mautner, A., Lee, K.-Y., Lahtinen, P., Hakalahti, M., Tammelin, T., Li, K., et al. (2014). Nanopapers for organic solvent nanofiltration. *Chemical Communications*, 50, 5778–5781.

Orelma, H., Filpponen, I., Johansson, L.-S., Österberg, M., Rojas, O., & Laine, J. (2012). Surface functionalized nanofibrillar cellulose (NFC) film as a platform for immunoassays and diagnostics. *Biointerphases*, 7, 1–12.

Paralikar, S., Simonsen, J., & Lombardi, J. (2008). Poly(vinyl alcohol)/cellulose nanocrystal barrier membranes. *Journal of Membrane Science*, 320, 248–258.

Peresin, S. M., Vartiainen, J., Kunnari, V., Kaljunen, T., & Tammelin, T. (2012). Large scale nanofibrillated cellulose film: An overview on its production, properties, and potential applications. In *4th International conference on pulping, papermaking and biotechnology (ICPPB'12)* Nanjing, China, (pp. 891–895).

Piringer, O. (2007). Permeation of gases water vapour and volatile organic compounds. In O. Piringer, & A. Baner (Eds.), *Plastic packaging materials for food* (pp. 239–285). Weinheim: Wiley-VCH.

Rodionova, G., Eriksen, Ø., & Gregersen, Ø. (2012). TEMPO-oxidized cellulose nanofiber films: Effect of surface morphology on water resistance. *Cellulose*, 19, 1115–1123.

Saito, T., Nishiyama, Y., Putaux, J., Vignon, M., & Isogai, A. (2006). Homogeneous suspensions of individualized microfibrils from TEMPO-catalyzed oxidation of native cellulose. *Biomacromolecules*, 7, 1687–1691.

Saito, T., Hirota, M., Tamura, N., Kimura, S., Fukuzumi, H., Heux, L., et al. (2009). Individualization of nano-sized plant cellulose fibrils by direct surface carboxylation using TEMPO catalyst under neutral conditions. *Biomacromolecules*, 10, 1992–1996.

Shinoda, R., Saito, T., Okita, Y., & Isogai, A. (2012). Relationship between length and degree of polymerization of TEMPO-oxidized cellulose nanofibrils. *Biomacromolecules*, 13, 842–849.

Spence, K., Venditti, R., Rojas, O., Pawlak, J., & Hubbe, M. (2011). Water vapour barrier properties of coated and filled microfibrillated cellulose composite films. *Bioresources*, 6, 4370–4388.

Spoljaric, S., Salminen, A., Luong, N., & Seppälä, J. (2013). Crosslinked nanofibrillated cellulose: Poly(acrylic acid) nanocomposite films; enhanced mechanical performance in aqueous environments. *Cellulose*, 20, 2991–3005.

Syverud, K., & Stenius, P. (2009). Strength and barrier properties of MFC films. *Cellulose*, 16, 75–85.

Virtanen, S., Vartiainen, J., Setälä, H., Tammelin, T., & Vuoti, S. (2014). Modified nanofibrillated cellulose–polyvinyl alcohol films with improved mechanical performance. *RSC Advances*, 4, 11343–11350.

Virtanen, S., Vuoti, S., Heikkinen, H., & Lahtinen, P. (2014). High strength modified nanofibrillated cellulose–polyvinyl-alcohol films. *Cellulose*, 21, 3561–3571.

Vogel, S. (2003). *Comparative biomechanics: Life's physical world*. Princeton, NJ, Oxford: Princeton University Press.

Yano, H., & Nakahara, S. (2004). Bio-composites produced from plant microfiber bundles with a nanometer unit web-like network. *Journal of Material Science*, 2, 1635–1638.

Zhou, Y., Fu, S., Zheng, L., & Zhan, H. (2012). Effect of nanocellulose isolation techniques on the formation of reinforced poly(vinyl alcohol) nanocomposite films. *eXPRESS Polymer Letters*, 6, 794–804.

Österberg, M., Vartiainen, J., Lucenius, J., Hippi, U., Seppälä, J., Serimaa, R., et al. (2013). A fast method to produce strong NFC films as a platform for barrier and functional materials. *ACS Applied Materials and Interphases*, 5, 4640–4647.

Österberg, M., Peresin, M. S., Johansson, L.-S., & Tammelin, T. (2013). Clean and reactive nanostructured cellulose surface. *Cellulose*, 20, 983–990.

Supplementary Data

Effect of interfibrillar PVA bridging on water stability and mechanical properties of TEMPO/NaClO$_2$ oxidized cellulosic nanofibril films

Minna Hakalahti, Arto Salminen, Jukka Seppälä, Tekla Tammelin, Tuomas Hänninen

Dry film samples were analysed using FT-IR in ambient conditions. The spectra were recorded with Nicolet iS50 FT-IR spectrometer equipped with iS50 ATR. All spectra were scanned within the range of 350 to 4000 cm^{-1} and spectra were obtained from 32 scans with resolution 4 cm^{-1}. Spectra were not normalized.
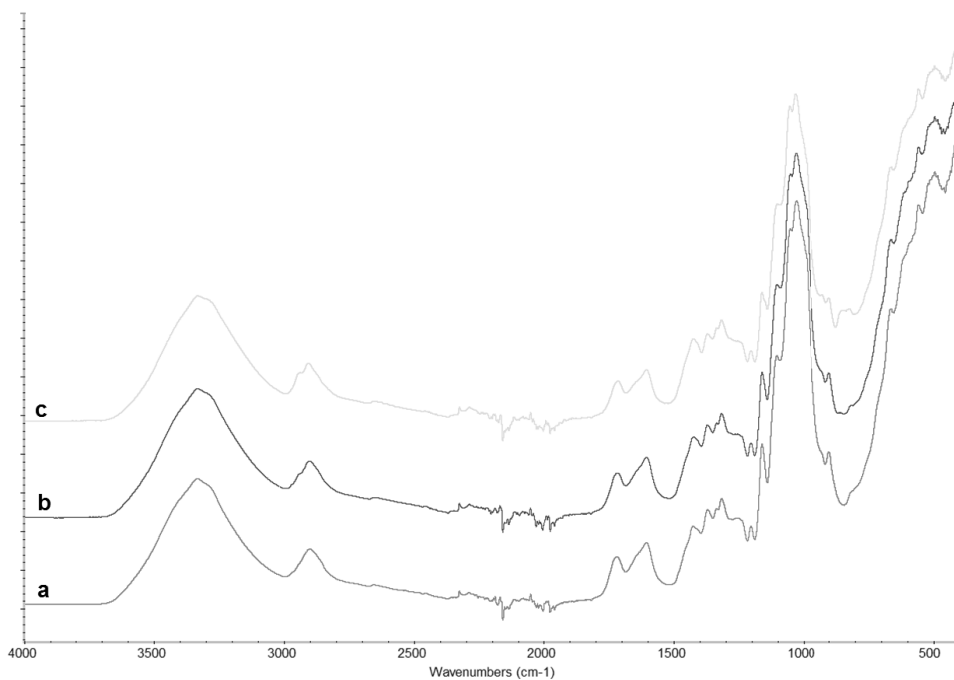
Figure S1. FT-IR spectra of a) TCNF, b) TCNF-98PVA10% and c) TCNF-98PVA25% films.

The film samples were analyzed using alpha300 R Confocal Raman microscope (Witec GmbH, Germany). The spectra were obtained using a frequency doubled Nd:YAG laser (532.35 nm, 10 mW) and a Nikon 100x (NA=0.95) air objective. The laser used for excitation was polarized horizontally. The microscope was equipped with DU970 N-BV EMCCD camera with 600 lines/mm grating. Measurements were made using integration time of 0.3 s and accumulation of 60. Raman spectra were not normalized.
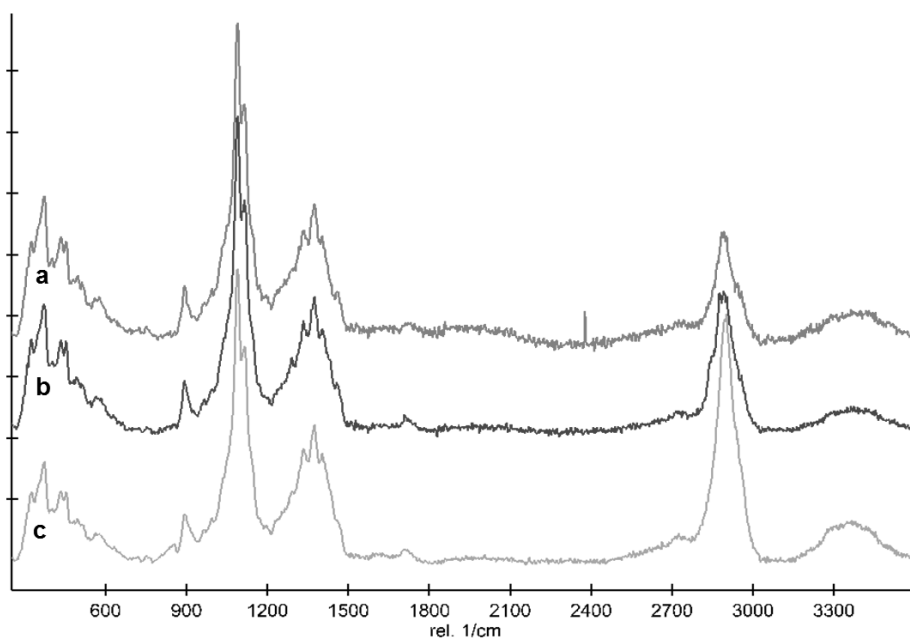

Figure S2. Raman spectra of a) TCNF film, b) TCNF film with 10% fully hydrolysed PVA (TCNF-98PVA10%) and c) TCNF film with 25% fully hydrolysed PVA (TCNF-98PVA25%)

Table S1. Storage moduli (E') of pure PVA films measured using DMA at different humidities.

	Storage moduli (MPa)	
RH%	88PVA	98PVA
0	5363 ± 145	6515 ± 932
50	977 ± 93	2486 ± 167
90	0 ± 0	24 ± 4
0	3992 ± 296	7593 ± 445

Table S2. Stress and strain of TCNF films and TCNF-PVA films containing 10 % or 25 % PVA, after soaking in water for 24 hours.

Film sample	Stress at break (MPa)	Strain at break (%)
TCNF	-	-
TCNF-88PVA10%	29.7 ± 4.7	15.2 ± 2.0
TCNF-88PVA25%	21.5 ± 2.5	22.7 ± 1.6
TCNF-98PVA10%	33.4 ± 6.0	11.4 ± 3.7
TCNF-98PVA25%	22.9 ± 5.5	17.7 ± 1.9
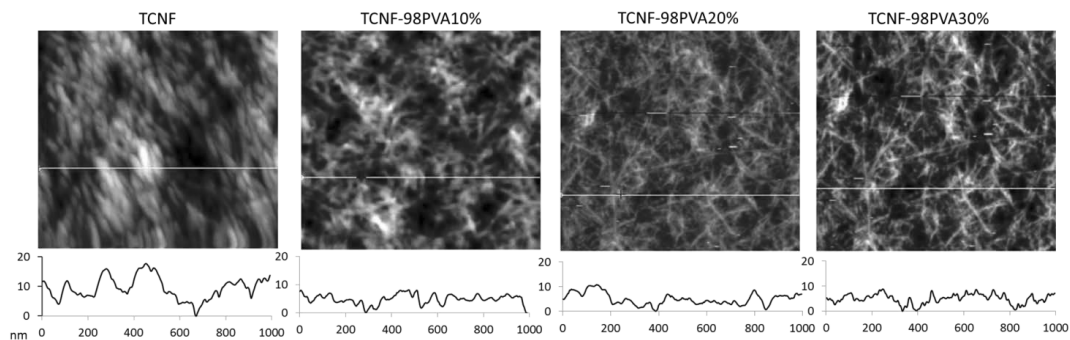
Figure S3. AFM height images of TCNF and TCNF-PVA films displaying the surface topography of the film. The AFM image size is 1 μm^2.
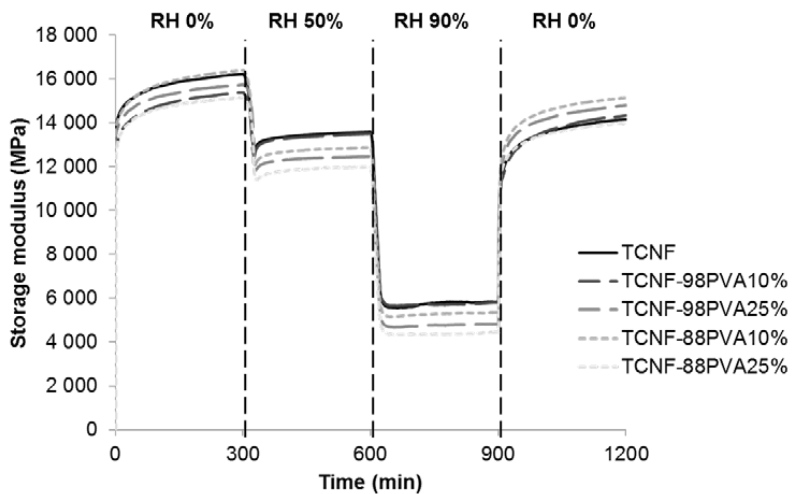
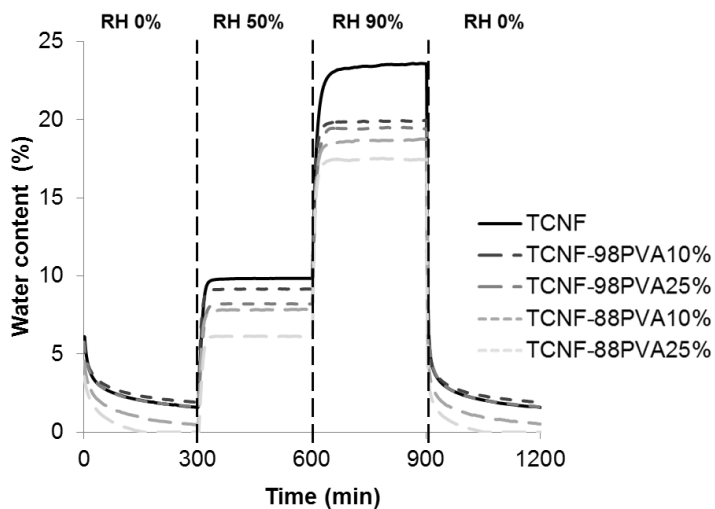Figure S4. Storage moduli (E') of TCNF and TCNF-PVA films measured by DMA as function of time.

Figure S5. Water content of TCNF and TCNF-PVA films measured by DVS as a function of time.

Paper IV

Hakalahti, M.; Mautner, A.; Johansson, L.-S.; Hänninen, T.; Setälä, H.; Kontturi, E.; Bismarck, A.; Tammelin, T. Direct Interfacial Modification of Nanocellulose Films for Thermoresponsive Membrane Templates. *ACS Appl. Mater. Interfaces* **2016**, *8*, 2923-2927.

Direct Interfacial Modification of Nanocellulose Films for Thermoresponsive Membrane Templates

Minna Hakalahti,[†] Andreas Mautner,[‡,§] Leena-Sisko Johansson,[∥] Tuomas Hänninen,[†] Harri Setälä,[†] Eero Kontturi,[∥] Alexander Bismarck,[‡,§] and Tekla Tammelin*,[†]

[†]High Performance Fibre Products, VTT Technical Research Center of Finland Ltd, FI-02044 VTT, Espoo, Finland

[‡]Polymer & Composite Engineering (PaCE) Group, Institute for Materials Chemistry & Research, University of Vienna, Währingerstrasse 42, A-1090 Vienna, Austria

[§]Polymer & Composite Engineering (PaCE) Group, Dept. of Chemical Engineering, Imperial College London, South Kensington Campus, London SW7 2AZ, United Kingdom

[∥]Department of Forest Products Technology, School of Chemical Technology, Aalto University, 02150 Espoo, Finland

Ⓢ *Supporting Information*

ABSTRACT: This letter proposes a strategy to construct tunable films combining the physical characteristics of cellulose nanofibrils and smart polymers for membrane applications. A functional membrane template was obtained by first fabricating a water stable film from cellulose nanofibrils and subsequently surface grafting it with a thermoresponsive polymer, poly(N-isopropylacrylamide). The behavior of the membrane template was dependent on temperature. The increment in slope of relative water permeance around the lower critical solution temperature of poly(N-isopropylacrylamide) increased from 18 to 100% upon polymer attachment. Although the membrane template essentially consisted of wood-based materials, the benefits of smart synthetic polymers were achieved.

KEYWORDS: cellulose nanofibrils, films, thermoresponsive polymers, surface modification, membranes, poly(N-isopropylacrylamide)
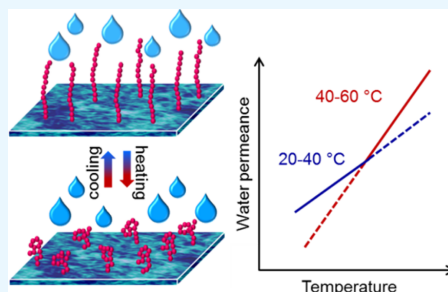
Membranes are selective barriers, which play an essential role in numerous biological systems and in key industrial processes, such as water purification.[1] In this realm, wood-based cellulose nanofibrils (CNF) are intriguing building blocks for membrane materials:[2] aside from their renewable status with forests as an inexhaustible natural source, the native origin of CNFs amounts to large surface to volume ratio and high hydrophilicity coupled with good film forming tendency.[3,4] However, many high-performance applications cannot rely solely on the inherent material properties and tunability with, e.g., smart polymers is often desired but unfortunately CNFs defy facile chemical adjustments. The seminal difficulty with chemical modification of CNFs lies in their hydrophilicity: water is their natural medium and tedious solvent exchange procedures to nonpolar solvents are required to enable the introduction of new organic functionalities, while simultaneously retaining the high surface area of CNFs in dispersion. In addition, the removal of reagents and side-products can be challenging requiring e.g. prolonged dialysis since nanoscaled materials prevent filtration and other conventional purification procedures. Here, we have omitted the dispersion-related challenges by first preparing a water stable film of CNFs using poly(vinyl alcohol) (PVA) as cross-linker[5] and subsequently performing interfacial polymer grafting directly onto the surface of the macroscopic film. By following this approach surface-only modification is achieved as

desired and purification of the product is easy as the macroscopic film can be cleansed with simple rinsing.

To demonstrate the viability of the approach, we have chosen to modify a CNF-PVA film (Figure 1b) with the popular poly(N-isopropylacrylamide) (poly(NIPAM)), which undergoes a temperature induced transition from hydrophilic to a more hydrophobic state at around 32 °C in water (Figure 1a)[6,7] and explore the film's tunability in permeance, a fundamental quality of membranes. The CNFs have been prepared by oxidation mediated with 2,2,6,6-tetramethylpiperidine (TEMPO), which introduces a high number of carboxylic acid groups on the CNF surface.[8] Consequently, TEMPO–CNFs not only possess vastly improved dispersion[9] and film forming properties,[10] but the carboxylate groups can also be used as precursors for further functionalization.[11,12] Amine groups are more prone to react with esters than directly with carboxylates to form amides.[13] Hence, as shown in Figure 1c, an intermediate esterification step was implemented to facilitate the attachment of amine terminated poly(NIPAM) on the membrane surface.
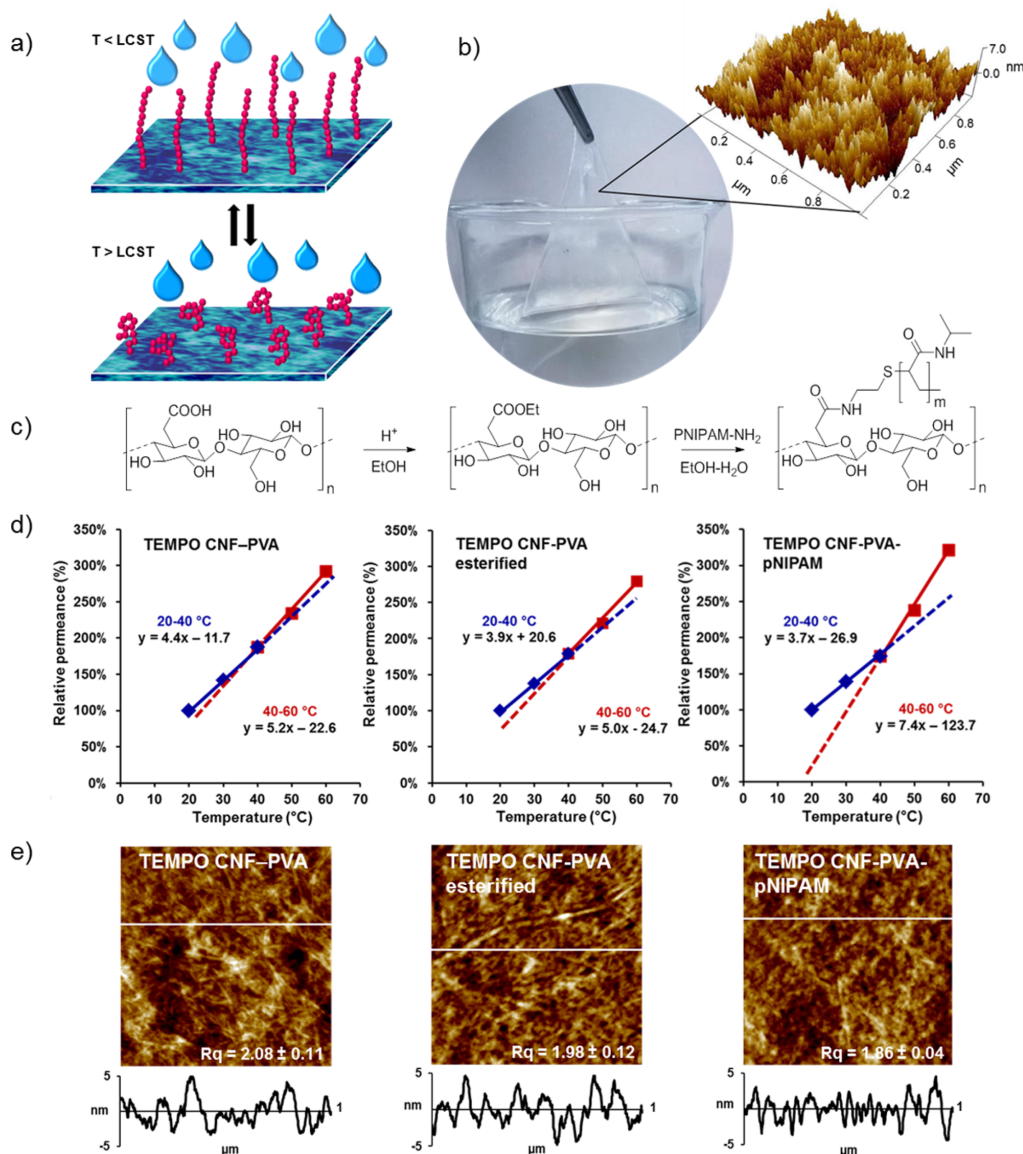
Figure 1. (a) Schematic illustration of thermoresponsive behavior of poly(NIPAM) chains grafted on CNF film surfaces in water around the LCST of poly(NIPAM) (32 °C). (b) TEMPO−CNF film enhanced with 10 wt % poly(vinyl alcohol) for improved wet strength and potential to function as a membrane template. In the inset an AFM 1 μm × 1 μm topography image of the dry film surface is displayed. (c) Proposed chemical pathway for poly(NIPAM) attachment onto the film surface. (d) Relative permeance of water through membranes plotted as a function of temperature for an unmodified TEMPO−CNF−PVA film, an esterified film and a poly(NIPAM) modified film. Linear regression based on real data points (r^2 values >0.992) was performed for temperature ranges 20−40 °C (blue) and for 40−60 °C (red). Dashed lines are linear extrapolations of the linear regression lines. The relative permeance was normalized to permeance values at 20 °C. (e) 1 μm × 1 μm topographic AFM images with height scans and corresponding root-mean-square roughness-values (R_q) of an unmodified TEMPO−CNF−PVA film, an esterified film and a poly(NIPAM) modified film. The representative height scans underneath the topographic images are indicated with a white line in each image.

The thermoresponsive behavior of poly(NIPAM) functionalized membrane templates was demonstrated by investigating the permeance of water through the films at various temperatures.

At 2 bar pressure, TEMPO−CNF−PVA films had absolute permeances in the range from 60 to 180 L m^{-2} h^{-1} MPa^{-1} (for 20−60 °C), whereas esterified and poly(NIPAM) modified films

showed significantly lower permeances ranging from 10 to 25 L m^{-2} h^{-1} MPa^{-1} and 10 to 45 L m^{-2} h^{-1} MPa^{-1}, respectively (see Figure S1). The differences in the permeance levels could be caused by differences in the densities of the films because of dehydration and lower affinity toward water. Sodium carboxylate groups of TEMPO oxidized CNFs have a pK_a value of 4.8[14] and hence have the tendency to be converted into their acidic form (−COOH) at low pH, for example, during esterification. This could lead to stronger interfibrillar bonding and decrease the water uptake capability,[15] causing lower permeance. Similarly, ethanol used as reaction medium in the esterification reaction step could cause further dehydration and lead to stronger interfibrillar bonding within the film structure.[16] Together with the structural changes, for example, different film densities, the changes in affinity toward water have influence on membrane permeance behavior. For example, Yu et al. showed that increased surface hydrophilicity increased the water flux through the polyacrylamide grafted hydrophobic polypropylene membranes especially at low grafting degrees.[17] In this work, all the membrane template materials showed highly hydrophilic character giving the equilibrium water contact angle values of ∼30° whether modified or not (see Figure S2). Therefore, it seems that structural changes, not the differences in hydrophilicity and water affinity, are attributed to the changes in permeance behavior of TEMPO CNF-PVA membrane templates.

For analysis of the temperature dependency, the absolute permeances were normalized to the permeance at 20 °C and plotted against temperature (Figure 1d). Expectedly, the permeances of all tested membranes grew as a function of increasing temperature. This phenomenon is well-known and reported in literature and typically explained by temperature causing the permeate flux to increase through a reduction in solvent viscosity and an increase in the solvent diffusion coefficient.[18,19] The relative permeance of unmodified and esterified films increased at an almost constant slope, whereas for poly(NIPAM) modified film the slope changed significantly above 40 °C. We observed two regions exhibiting a steady, linear increase of the relative permeance: between 20 and 40 °C as well as between 40 and 60 °C. These two different regions are present below and above the LCST of poly(NIPAM). The slopes of relative permeance increased by 18, 28, and 100% between these regions for unmodified TEMPO−CNF−PVA films, esterified films and poly(NIPAM)-modified films, respectively.

Attaching poly(NIPAM) on the membrane surface is known as an effective method to manipulate the thermoresponsive behavior of membranes through controllable gating mechanisms[20,21] and switchable wettability.[22] We observed a change in the slope of permeance increase above the LCST of poly(NIPAM). Whereas the slopes of unmodified and esterified films remained almost constant when going from low temperature (below 40 °C) to elevated temperature (above 40 °C), for the poly(NIPAM) modified film the slope of permeance increased by a factor of 2. At temperatures below the LCST, the slope has a similar, yet slightly lower value compared to unmodified and esterified films. This indicates that below the LCST poly(NIPAM) might slightly obstruct the movement of water through the film, perhaps due to being in a swollen state[4] and creating a physical barrier for water.[20] At elevated temperature, the permeance is augmented, which indicates that the physical barrier is removed through poly(NIPAM) taking its collapsed form.

As seen from the AFM images in Figure 1e, the topography of the TEMPO−CNF-PVA films in dry state is not significantly altered upon the chemical modifications. A similar fibrillar network with uniform fibril distribution and minor structural irregularities at nanoscale is clearly visible at all stages of the modification despite several washing and drying steps. In all cases, the root-mean-square roughness values remained below 2 nm, as determined from 1 μm^2 AFM topographic images, indicating that the film surface is very smooth. Attachment of poly(NIPAM) on the film surface does not appear to affect the roughness or morphology of the membrane templates.

The effect of different reaction conditions on poly(NIPAM) modification was surveyed with XPS analysis (Table 1), which

Table 1. Elemental Concentrations of Oxygen (O 1s), Carbon (C 1s), Sulfur (S 2p), and Nitrogen (N 1s) and Surface Coverage (%) Values in Film Samples As Analyzed by XPS^a

sample	elemental concentration (at %)				surface coverage (%)
	O 1s	C 1s	S 2p	N 1s	
TEMPO−CNF−PVA	37	62	0.0	0.0	
esterified TEMPO−CNF−PVA	38	63	0.0	0.2	
poly(NIPAM) modified film (RT, ethanol)	36	64	0.2	0.3	1.8
poly(NIPAM) modified film (RT, ethanol + water)	36	62	0.5	1.2	8.5
poly(NIPAM) modified film (50 °C, ethanol)	37	62	0.0	0.3	2.0
poly(NIPAM) modified film (50 °C, ethanol + water)	38	61	0.2	0.6	4.0

^{a}Surface coverage percentages are calculated from elemental concentrations. Low-resolution XPS survey spectra of the samples with high resolution spectra showing C 1s, N 1s, and S 2p regions are presented in Figure S3.

gives an idea of the elemental composition at the utmost sample surface. Significantly larger concentrations of nitrogen and sulfur are present in films that were prepared in the presence of water in addition to ethanol, possibly because of the better cleavage of ethyl esters and their replacement with poly(NIPAM) groups under water[23] (Figure 1c). Increasing the reaction temperature to 50 °C leads to lower N and S concentrations (Table 1). Here, poly(NIPAM) takes the coiled conformation above its LCST,[5] probably leaving fewer terminal amines available for the desired chemical reaction. In consequence, the highest N and S concentrations are achieved when the modification is performed in the presence of water at room temperature. This is also attested by the calculated surface coverage for poly(NIPAM) from XPS results (Table 1).

Bulk chemical characteristics of the film are shown in the FT-IR spectra in Figure 2a. Carbonyl (C=O) stretch at 1605 cm^{-1} due to sodium carboxylate groups[15] is clearly visible in the spectra for unmodified films (with PVA). After esterification, a new band appears at 1723 cm^{-1}, corresponding to esterified celluronic carbonyls. It is evident that this band originates mainly from the ethyl ester group, because counterion exchange to sodium at pH 10 does not shift the band from a possible overlapping protonated carboxyl (>1700 cm^{-1}) to sodium carboxylate (at 1605 cm^{-1}), whereas saponification at pH 13 cleaves the esters and shifts the band to sodium carboxylate at 1605 cm^{-1}.[24] Following the poly(NIPAM)
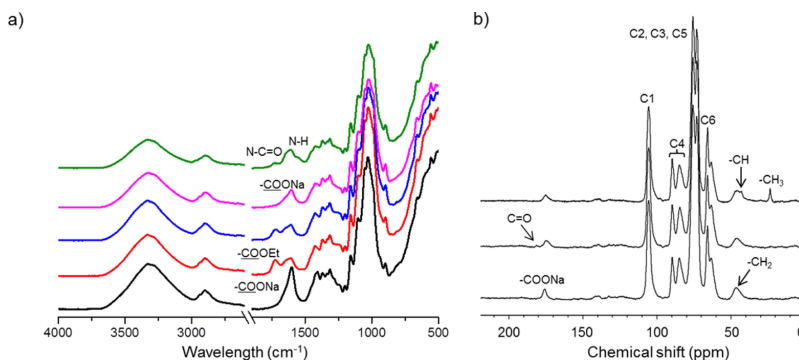
Figure 2. (a) FT-IR spectra of TEMPO−CNF−PVA film (black), esterified film (red), esterified film with counterion exchange (pH 10) (blue), esterified film with saponification (pH 13) (pink), and poly(NIPAM) modified film (green); and (b) ^{13}C NMR spectra of TEMPO−CNF−PVA film (bottom), esterified film (middle), and poly(NIPAM) modified film (top) with peak assignment.

grafting, an amide stretch and an amine bend appear at 1650 and 1550 cm^{-1}, respectively.[25]

Further information on the chemical composition was collected with solid state NMR (Figure 2b). For the unmodified TEMPO CNF-PVA film a typical ^{13}C NMR spectrum of TEMPO oxidized CNF is observed[26] with an additional peak at 45 ppm due to the − CH$_2$ groups of PVA.[27] The peak corresponding to the sodium carboxyl moiety arising from TEMPO oxidized CNF is observed at 175 ppm.[26] In the spectrum of the esterified film, the new peak at 179 ppm is attributed to C═O of ester group. The two new sharp peaks at 23 and 42 ppm appearing in the spectrum of the poly(NIPAM) modified film are attributed to the −CH and −CH$_3$ groups of poly(NIPAM).[25] The peak corresponding to the carboxyl moiety remains visible throughout the modification, whereas the signal corresponding to the ester group disappears after poly(NIPAM) attachment.

Overall, chemical characterization performed by XPS, FT-IR, and ^{13}C NMR provides evidence for successful attachment of poly(NIPAM) onto the film surface via the suggested chemical pathway involving esterification of TEMPO oxidized CNF followed by polymer grafting (Figure 1c). The modification was far easier to perform directly on the cross-linked TEMPO−CNF−PVA film where tedious solvent exchange steps, inevitable with a CNF suspension, could be omitted. AFM, in turn, revealed that the morphology and roughness of the films remained unaltered throughout the chemical modification. Although water permeance of films without poly(NIPAM) increased with an almost constant slope as a function of temperature, the slope for poly(NIPAM)-modified films exhibited a 2-fold increase above the LCST of poly(NIPAM). In conclusion, we were able to show the potential of the tunable biobased membrane templates as real alternatives in terms of performance and sustainability to various water purification systems. These findings are highly relevant with respect to the application areas such as membranes for nanofiltration of, for example, micropollutants or multivalent ions.

■ ASSOCIATED CONTENT

Ⓢ Supporting Information

The Supporting Information is available free of charge on the ACS Publications website at DOI: 10.1021/acsami.5b12300.

Description of materials and methods, figure showing permeance of water through films as a function of temperature, water contact angle results based on the sessile drop method, XPS wide and high-resolution spectra (C 1s, N 1s, S 2p) for films (PDF)

■ AUTHOR INFORMATION

Corresponding Author
*E-mail: tekla.tammelin@vtt.fi.

Notes
The authors declare no competing financial interest.

■ REFERENCES

(1) Cheryan, M. *Ultrafiltration and Microfiltration Handbook*; CRC Press: Boca Raton, FL, 1998; pp 1−28.
(2) Mautner, A.; Lee, K.-Y.; Lahtinen, P.; Hakalahti, M.; Tammelin, T.; Li, K.; Bismarck, A. Nanopapers for Organic Solvent Nanofiltration. *Chem. Commun.* **2014**, *50*, 5778−5781.
(3) Lavoine, N.; Desloges, I.; Dufresne, A.; Bras, J. Microfibrillated Cellulose − Its Barrier Properties and Applications in Cellulosic Materials: A Review. *Carbohydr. Polym.* **2012**, *90*, 735−764.
(4) Spence, K.; Venditti, R.; Habibi, Y.; Rojas, O.; Pawlak, J. The Effect of Chemical Composition on Microfibrillar Cellulose Films from Wood Pulps: Mechanical Processing and Physical Properties. *Bioresour. Technol.* **2010**, *101*, 5961−5968.
(5) Hakalahti, M.; Salminen, A.; Seppälä, J.; Tammelin, T.; Hänninen, T. Effect of Interfibrillar PVA Bridging on Water Stability and Mechanical Properties of TEMPO/NaClO$_2$ Oxidized Cellulosic Nanofibril Films. *Carbohydr. Polym.* **2015**, *126*, 78−82.
(6) Heskins, M.; Guillet, J. E. Solution Properties of Poly(N-isopropylacrylamide). *J. Macromol. Sci., Chem.* **1968**, *2*, 1441−1455.
(7) Azzam, F.; Heux, L.; Putaux, J.-L.; Jean, B. Preparation by Grafting Onto, Characterization, and Properties of Thermally Responsive Polymer-Decorated Cellulose Nanocrystals. *Biomacromolecules* **2010**, *11*, 3652−3659.
(8) Saito, T.; Kimura, S.; Nishiyama, Y.; Isogai, A. Cellulose Nanofibers Prepared by TEMPO-Mediated Oxidation of Native Cellulose. *Biomacromolecules* **2007**, *8*, 2485−2491.

(9) Fukuzumi, H.; Tanaka, R.; Saito, T.; Isogai, A. Dispersion Stability and Aggregation Behavior of TEMPO-Oxidized Cellulose Nanofibrils in Water as a Function of Salt Addition. *Cellulose* **2014**, *21*, 1553−1559.

(10) Fukuzumi, H.; Saito, T.; Iwata, T.; Kumamoto, Y.; Isogai, A. Transparent and High Gas Barrier Films of Cellulose Nanofibers Prepared by TEMPO-Mediated Oxidation. *Biomacromolecules* **2009**, *10*, 162−165.

(11) Lasseuguette, E. Grafting onto Microfibrils of Native Cellulose. *Cellulose* **2008**, *15*, 571−580.

(12) Fujisawa, S.; Saito, T.; Kimura, S.; Iwata, T.; Isogai, A. Surface Engineering of Ultrafine Cellulose Nanofibrils toward Polymer Nanocomposite Materials. *Biomacromolecules* **2013**, *14*, 1541−1546.

(13) Clayden, J.; Greeves, N.; Warren, S.; Wothers, P. *Organic Chemistry*; Oxford University Press: Oxford, U.K., 2005; pp 279−303.

(14) Wågberg, L.; Decher, G.; Norgren, M.; Lindström, T.; Ankerfors, M.; Axnas, K. The Build-Up of Polyelectrolyte Multilayers of Microfibrillated Cellulose and Cationic Polyelectrolytes. *Langmuir* **2008**, *24*, 784−795.

(15) Fujisawa, S.; Okita, Y.; Fukuzumi, H.; Saito, T.; Isogai, A. Preparation and Characterization of TEMPO-Oxidized Cellulose Nanofibril Films with Free Carboxyl Groups. *Carbohydr. Polym.* **2011**, *84*, 579−583.

(16) Peng, Y.; Gardner, D. J.; Han, Y. Drying Cellulose Nanofibrils: In Search of a Suitable Method. *Cellulose* **2012**, *19*, 91−102.

(17) Yu, H.-Y.; Xu, Z.-K.; Lei, H.; Hu, M.-X.; Yang, Q. Photoinduced Graft Polymerization of Acrylamide on Polypropylene Microporous Membranes for the Improvement of Antifouling Characteristics in a Submerged Membrane-Bioreactor. *Sep. Purif. Technol.* **2007**, *53*, 119−125.

(18) Bhattacharyya, D.; Williams, M. E. In *Membrane Handbook*; Winston, H., Sirkar, K., Eds.; Van Nostrand Reinhold: New York, 1992; Chapter 21, pp 265−268.

(19) Machado, D.; Hasson, D.; Semiat, R. Effect of Solvent Properties on Permeate Flow Through Nanofiltration Membranes. Part I: Investigation of Parameters Affecting Solvent Flux. *J. Membr. Sci.* **1999**, *163*, 93−102.

(20) Xie, R.; Li, Y.; Chu, L.-Y. Preparation of Thermo-Responsive Gating Membranes with Controllable Response Temperature. *J. Membr. Sci.* **2007**, *289*, 76−85.

(21) Schepelina, O.; Zharov, I. PNIPAAM-Modified Nanoporous Colloidal Films with Positive and Negative Temperature Gating. *Langmuir* **2007**, *23*, 12704−12709.

(22) Ganesh, A.; Ranganath, A.; Sridhar, R.; Raut, H.; Jayaraman, J.; Sahay, R.; Ramakrishna, S.; Baji, A. Cellulose Acetate−Poly(*N*-isopropylacrylamide)-Based Functional Surfaces with Temperature-Triggered Switchable Wettability. *Macromol. Rapid Commun.* **2015**, *36*, 1368−1373.

(23) Sykes, P. *A Guidebook to Mechanism in Organic Chemistry*; Longman: London, 1983; Chapter 8, pp 200−239.

(24) De Cuadro, P.; Belt, T.; Kontturi, K.; Reza, M.; Kontturi, E.; Vuorinen, T.; Hughes, M. Cross-Linking of Cellulose and Poly-(ethylene glycol) with Citric Acid. *React. Funct. Polym.* **2015**, *90*, 21−24.

(25) Zoppe, J.; Habibi, Y.; Rojas, O.; Venditti, R.; Johansson, L.-S.; Efimenko, K.; Österberg, M.; Laine, J. Poly(*N*-isopropylacrylamide) Brushes Grafted from Cellulose Nanocrystals via Surface-Initiated Single-Electron Transfer Living Radical Polymerization. *Biomacromolecules* **2010**, *11*, 2683−2691.

(26) Saito, T.; Hirota, M.; Tamura, N.; Kimura, S.; Fukuzumi, H.; Heux, L.; Isogai, A. Individualization of Nano-Sized Plant Cellulose Fibrils by Direct Surface Carboxylation Using TEMPO Catalyst under Neutral Conditions. *Biomacromolecules* **2009**, *10*, 1992−1996.

(27) Terao, T.; Maeda, S.; Saika, A. High-Resolution Solid-State ^{13}C NMR of Poly(vinyl alcohol): Enhancement of Tacticity Splitting by Intramolecular Hydrogen Bonds. *Macromolecules* **1983**, *16*, 1535−1538.

Supporting Information

Direct Interfacial Modification of Nanocellulose Films for Thermoresponsive Membrane Templates

Minna Hakalahti[1], Andreas Mautner[2,3], Leena-Sisko Johansson[4], Tuomas Hänninen[1], Harri Setälä[1], Eero Kontturi[4], Alexander Bismarck[2,3], Tekla Tammelin[1]*

[1]High Performance Fibre Products, VTT Technical Research Center of Finland Ltd, FI-02044 VTT, Espoo, Finland

[2]Polymer & Composite Engineering (PaCE) Group, Institute for Materials Chemistry & Research, University of Vienna, Währingerstrasse 42, A-1090 Vienna, Austria

[3]Polymer & Composite Engineering (PaCE) Group, Dept. of Chemical Engineering, Imperial College London, South Kensington Campus, London, SW7 2AZ, UK

[4]Department of Forest Products Technology, School of Chemical Technology, Aalto University, 02150 Espoo, Finland

*Corresponding author: tekla.tammelin@vtt.fi

Materials

Never dried bleached softwood pulp obtained from a pulp mill in Finland was 2,2,6,6-tetramethylpiperidine (TEMPO) oxidized according to a procedure by Saito et al.[1] The charge of the oxidized pulp, measured by a standard conductometric titration method (SCAN-CM 65:02, 2002), was found to be approximately 1.13 mmol g^{-1}. Oxidized pulp was fibrillated using a high pressure fluidizer Microfluidics M-110EH-30 (Microfluidics Int., USA) equipped with two Z-type chambers. The chambers had diameters of 400 μm and 100 μm and the pulp was passed through the fluidizer once at 1850 bar operating pressure. The final consistency of the TEMPO-CNF was approximately 2 wt.-%. Poly(vinyl alcohol) (PVA) with degree of hydrolysis of 98 % (Mowiol 56-98, M_w 195 000 g/mol, DP 4300), amine-terminated poly(NIPAM) (M_n 5500) and all other reagents were purchased from Sigma-Aldrich. Ethanol (Aa grade, 99.5 % (w/v)) was purchased from Altia Corporation (Rajamäki, Finland). Deionized water was further purified using a Milli-Q system (Millipore Corporation, Molsheim, France, resistivity 18.2 MΩ) and was used in all experiments unless otherwise stated.

Preparation of nanocellulose films

A 5 wt.-% solution of PVA in water was prepared by dissolving PVA in water at 95 °C during 4 hours under constant stirring. TEMPO- CNF suspension and PVA solution were diluted to 0.3 wt.-% and mixed together thoroughly in 9:1 weight ratio. This casting dope was degassed under vacuum and cast onto poly(styrene) petri dishes with areas of approximately 5000 mm^2. Petri dishes filled with casting dope were left to dry at 23 °C and 50 % relative humidity for at least 5 days to form TEMPO-CNF-PVA films.

Surface modification of nanocellulose films

Both sides of the TEMPO-CNF-PVA film were cleaned and activated using a UV/ozone cleaning procedure[2]. The treatment was performed using a UV/ozone ProCleaner (Bioforce Nanosciences) and the treatment time for each side was 10 min. The distance between the sample and the radiation source was 2 cm.

Dry TEMPO-CNF-PVA films were subjected to esterification reaction and following poly(NIPAM) attachment. Films were submerged in ethanol with a catalytic amount of concentrated H_2SO_4 (0.145 ml 98 % H_2SO_4/100 ml ethanol) and the reaction was continued at room temperature under mild stirring for 24 hours. Films were washed in three steps with ethanol and finally they were dried in air and activated again using the UV/ozone cleaning protocol.

1 g of amine-terminated poly(NIPAM) was dissolved in 100 ml of ethanol or ethanol-water mixture with 3:1 volume ratio at room temperature. Esterified films were submerged in the solution and the reactions were continued for 24 hours in room temperature or at 50 °C. Films were washed in three steps using ethanol to remove unreacted poly(NIPAM).

Water permeance of TEMPO-CNF-PVA films

The unmodified and modified TEMPO-CNF-PVA films' permeance was determined in a Sterlitech HP4750 dead-end stirred cell (Sterlitech, Kent, USA) with deionized water. Discs of nanopapers with a diameter of 49 mm were cut, soaked in deionized water for at least three days to ensure equilibration and placed on a sintered steel plate. Water was forced through the nanopapers using nitrogen at a head pressure of 0.2 MPa. The water permeance for the active filtration area (1460 mm^2) was obtained by measuring the volume permeated per unit area per unit time per unit pressure ($L\ m^{-2}\ h^{-1}\ MPa^{-1}$).

To determine the temperature dependence of the water permeance for each film type, the permeance was tested at various temperatures as shown in Figure S1. For this, the whole dead-end cell set-up was placed in a water bath. The temperature of the water bath was controlled with a magnetic stirrer connected to a temperature controller (RCT classic IKAMAG® safety control with VT-5 contact thermometer, VWR, UK). Five different temperatures were set (20, 30, 40, 50, 60 °C) and the permeance at each temperature was collected until it did not change more than one % per hour (Figure S1). The resulting permeances for the various temperatures were normalized to the permeance at 20 °C. For data points below and above 40 °C, respectively, a linear regression was performed and the slope was determined.
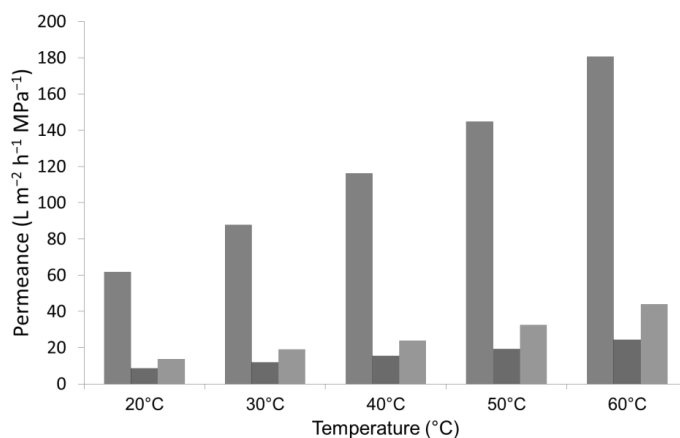
Figure S1. Permeance of water through membranes as a function of temperature for unmodified TEMPO-CNF-PVA film (red), esterified film (blue) and poly(NIPAM) modified film (green).

Fourier transform infrared spectroscopy (FT-IR)

A Nicolet iS50 FT-IR spectrometer (ThermoScientific, USA) equipped with a built-in diamond iS50 ATR was used to characterize the chemical structure of the modified films. The spectra were

scanned within the range of 350 to 4000 cm^{-1} with a total of 32 scans with resolution 4 cm^{-1}. Esterified films were subjected to counterion exchange at (pH 10) and to saponification (pH 13)[3].

Solid state nuclear magnetic resonance (^{13}C NMR)

The ^{13}C cross polarization (CP) magic angle spinning (MAS) NMR measurements were performed using an Agilent 600 NMR spectrometer with magnetic flux density of 14.1 T, equipped with a 3.2 mm triple-resonance MAS NMR probe operating at double resonance mode. Dry film samples were cut into small pieces before packing them into MAS rotors. In all experiments the MAS rate was set to 10 kHz. For all samples 30,000 transients were accumulated with a 3.0 s delay between successive scans. Cross polarization contact time was 1.0 ms, and a 70 kHz proton decoupling (spinal-64) was used. The chemical shifts were externally referenced via adamantane by setting the low field signal to 38.48 ppm. Rf-field strengths for cross polarization and decoupling were calibrated using α-glycine. All spectra were recorded at ambient temperature. Processing of the spectra was carried out with Bruker TopSpin 3.5 software.

Contact angle

The sessile drop method was employed for determination of water contact angles with a video camera based fully computer-controlled contact angle meter (CAM 200 from KSV Instruments Ltd., Finland). The measurements were performed at room temperature using deionized Milli-Q water. At least five separate measurements were performed for each sample at room temperature and the measurements were performed within 15 minutes of the UV/O$_3$ treatment[2].
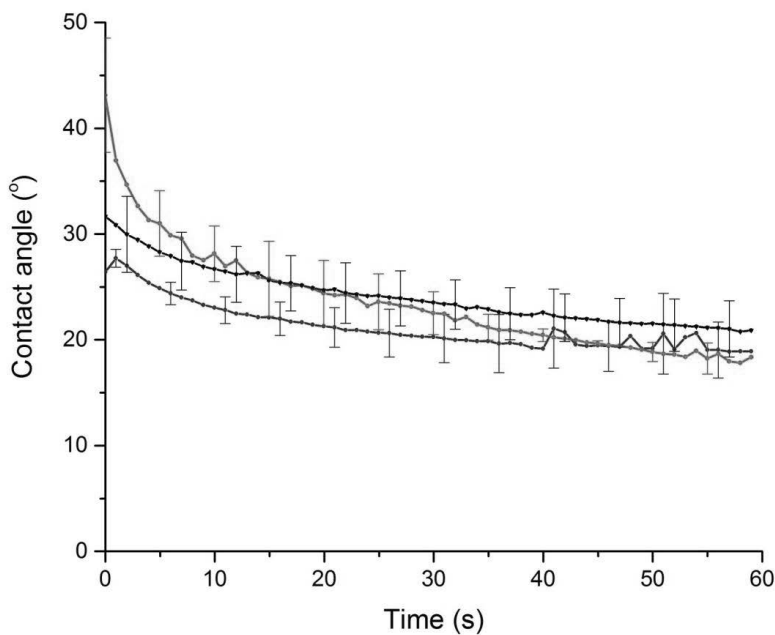
Figure S2. Water contact angle values as a function of time for the unmodified TEMPO CNF-PVA film (black curve), esterified film (blue curve) and poly(NIPAM) modified film (red curve).

Water contact angles presented in Figure S2 show that the surfaces of TEMPO CNF-PVA film, esterified film and poly(NIPAM) modified film are very similar and clearly hydrophilic at room temperature. Despite of the modification procedures, the equilibrium contact angles of the membrane templates are ~30˚. Fukuzumi et al.[4] reported water contact angle values of ~30 ᵒ for TEMPO oxidized CNF, which is in good accordance with the contact angle values of the TEMPO

CNF-PVA films. The addition of PVA (10 wt-%) did not appear to generate surfaces of higher hydrophobicity although contact angles as high as 79° have been reported for pure PVA.[5] The contact angle of pristine poly(NIPAM) ranges from approximately 30° to 90° depending on the temperature[6]. Here the poly(NIPAM) modified films display high hydrophilicity at room temperature giving the static water contact angle values $<30^o$ which is a value well supported by the literature.

X-ray photoelectron spectroscopy (XPS)

Analysis of the elemental composition on the surface of the film samples was studied using X-Ray photoelectron spectroscopy (XPS). Measurements were performed with a Kratos Analytical AXIS Ultra electron spectrometer with monochromatic A1 Kα irradiation at 100 W and effective charge neutralization with slow thermal electrons. The experimental set-up including acquisition parameters is reported in detail by Johansson et al.[7] Low resolution survey spectra and high resolution elemental spectra of carbon (C 1s) and oxygen (O 1s) were collected from the film samples at least from three different areas. The reported elemental concentrations are average values. The XPS analysis area was 0.2 mm × 0.8 mm in this study and the analysis depth is less than 10 nm. Ash-free 100 % cellulose filter paper was analyzed and used as a reference with each measurement batch. The surface coverage values were calculated using nitrogen as the elemental marker for poly(NIPAM). Based on the molecular formula of the repeating unit of poly(NIPAM), the ratio of nitrogen to the total number of atoms in NIPAM visible in XPS (carbon, nitrogen, oxygen) was assumed to be 1:8.

Figure S3 shows the survey spectra of the TEMPO-CNF-PVA film in unmodified, esterified and poly(NIPAM) modified stage with high resolution spectra for nitrogen, sulfur and carbon. The low resolution wide spectrum and high resolution spectrum for carbon revealed a typical spectrum of TEMPO-CNF (black line)[8]. Wide spectrum for esterified film (blue line) does not reveal any

differences compared to the reference TEMPO-CNF-PVA film spectrum (black line). In the high-resolution carbon signal the main feature is the "cellulose signature" with peaks for C-O, C-C and O-C-O bonded carbons. Successful esterification can be seen as an increase in the carbonyl (O-C=O) component in the high resolution spectrum after esterification[9] (blue line). As suggested by the presence of N 1 and S 2p peaks arising after poly(NIPAM) modification (red line), the attachment of poly(NIPAM) has successfully occurred on the surface of the film.
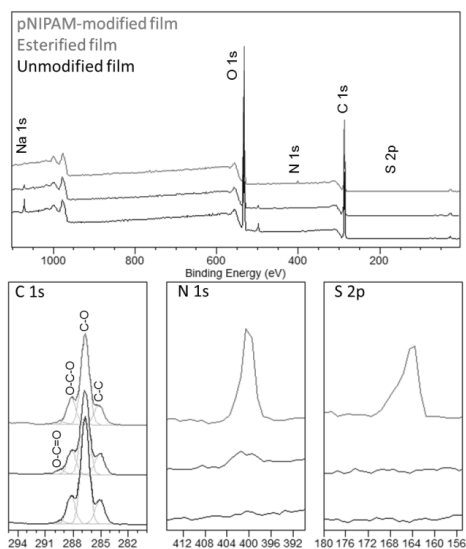
Figure S3. Low resolution XPS survey spectra (top) of unmodified film (black curve), esterified film (blue curve) and poly(NIPAM) modified film (red curve) showing peaks due to emission of Na 1s, O 1s, N 1s, C 1s and S 2p. Regional spectra (bottom) showing C 1s, N 1s and S 2p regions.

Atomic Force Microscopy (AFM)

Surface morphology and roughness of the films was studied by atomic force microscopy (AFM). Imaging was carried out using Nanoscope IIIa Multimode scanning probe (Digital Instruments Inc., Santa Barbara, CA, USA) in tapping mode. Dry films were imaged in air using aluminum coated

silicon cantilevers (Bruker Corporation, Billerica, MA, USA) with nominal resonance frequencies of 70 kHz. Image processing was performed using Nanoscope Analysis (Version 1.40, Bruker, Billerica, MA, USA). Root mean square roughness values (R_a) were extracted from topographic 1 μm × 1 μm AFM images. No other image processing other than flattening was performed. Three areas of each sample were scanned and the average roughness values are reported in Figure 1e.

REFERENCES

[1] Saito, T.; Nishiyama, Y.; Putaux, J.; Vignon, M.; Isogai, A. Homogeneous Suspensions of Individualized Microfibrils from TEMPO-catalyzed Oxidation of Native Cellulose. *Biomacromolecules,* **2006**, *7*, 1687-1691.

[2] Österberg, M.; Peresin, M. S.; Johansson, L.-S.; Tammelin, T. Clean and Reactive Nanostructured Cellulose Surface, *Cellulose,* **2013**, *3*, 983-990.

[3] De Cuadro, P.; Belt, T.; Kontturi, K.; Reza, M.; Kontturi, E.; Vuorinen, T.; Hughes, M. Cross-Linking of Cellulose and Poly(ethylene glycol) with Citric Acid, React. Funct. Polym., 2015, 90, 21-24.

[4] Fukuzumi, H.; Saito, T.; Iwata, T.; Kumamoto, T.; Isogai, A. Transparent and High Gas Barrier Films of Cellulose Nanofibers Prepared by TEMPO-Mediated Oxidation. *Biomacromolecules*, **2009**, *10*, 162-165.

[5] Weis, C.; Odermatt, E.; Kressler, J.; Funke, Z.; Wehner, T.; Freytag, D. Poly(Vinyl Alcohol) Membranes for Adhesion Prevention. *J. Biomed. Mater. Res., Part B*, **2003**, *70*, 191-202.

[6] Zhang, Z.; Pelton, R.; Deng, Y., Temperature-Dependent Contact Angles of Water on Poly(*N*-isopropylacrylamide) Gels. *Langmuir*, **1995**, *11*, 2301-2302.

[7] Johansson, L. S.; Campbell, J. Reproducible XPS on Biopolymers: Cellulose Studies, *Surf. Int. Analyt.*, **2004**, 36, 1018-1022.

[8] Orelma, H.; Filpponen, I.; Johansson, L.-S., Österberg, M.; Rojas, O.; Laine, J. Surface Functionalized Nanofibrillar Cellulose (NFC) Film as a Platform for Immunoassays and Diagnostics, *Biointerphases*, **2012**, *7*, 61-73.

[9] Vuoti, S.; Talja, R.; Johansson, L. S.; Heikkinen, H.; Tammelin, T. Solvent Impact on Esterification and Film Formation Ability of Nanofibrillated Cellulose, *Cellulose,* **2013**, *20*, 2359–2370.

Paper V

Mautner, A.; Lee, K.-Y.; Lahtinen, P.; Hakalahti, M.; Tammelin, T.; Li, K.; Bismarck, A. Nanopapers for Organic Solvent Nanofiltration. *Chem. Commun.* **2014**, *50*, 5778-5781.

COMMUNICATION

Nanopapers for organic solvent nanofiltration†

A. Mautner,[a] K.-Y. Lee,[bc] P. Lahtinen,[d] M. Hakalahti,[d] T. Tammelin,[d] K. Li[e] and A. Bismarck*[ac]

Would it not be nice to have an organic solvent nanofiltration membrane made from renewable resources that can be manufactured as simply as producing paper? Here the production of nanofiltration membranes made from nanocellulose by applying a papermaking process is demonstrated. Manufacture of the nanopapers was enabled by inducing flocculation of nanofibrils upon addition of trivalent ions.

Organic solvent nanofiltration (OSN) has found both widespread scientific and industrial interest since its emergence at the beginning of this century.[1] OSN describes the process of separating molecules or particles with a molecular weight (M_W) of some hundreds to thousands of Da – *i.e.* particles or molecules with nanometer dimensions – from an organic solvent.[1,2] Applications such as product purification and concentration, solvent exchange and recycling as well as recovery of homogeneous catalysts have been reported and compared favorably to classical methods, such as distillation, due to the lower energy consumption and milder conditions that chemical compounds experience during separation.[2] However, the utilization of organic solvents in NF operations still provides a significant challenge for the membranes from the materials point of view, in particular due to the required solvent-stability, which many traditional polymer membranes lack.[3] Several different engineering and high performance polymers have been tested for OSN membranes.[3–5] Typically,

polymer membranes do require a mechanical support, which is often made of polyamides, polysulfones or polyimides.[6] Besides polymer membranes, ceramics[7] or organic–inorganic hybrid materials[8] have been explored. Unfortunately, all these materials suffer from drawbacks; the production processes involve the use of large quantities of solvents and chemicals as well as extensive energy usage in the case of ceramics.[9] Thus, simple, clean and fast production processes would be desirable to manufacture solvent stable nanofiltration membranes.

In general, both everyday life and laboratory operations depend on filtration processes that are performed using membranes or cellulose filters. However, there are certain limitations when it comes to the removal of small M_W compounds using filter papers. In recent years, nanofibrillated cellulose (NFC) has gained significant attention due to its outstanding mechanical and chemical properties,[10] especially when used in composites.[11] NFC, when used in the paper form, also known as nanopaper, possesses outstanding mechanical properties, low thermal expansion coefficients, high optical transparency and good gas barrier properties.[12–15] These barrier properties have been exploited in food packaging films.[16] Nanopapers might offer potential for applications in separation processes due to their inherent pore dimensions in the nm range.[13] For example, the NFC paper was explored as a separator in Li-ion batteries.[17]

Here we introduce solvent stable nanofiltration (NF) membranes entirely made from nanocellulose. These membranes are produced by a papermaking process that utilizes an aqueous suspension of nanocellulose thus avoiding vast amounts of organic solvents that are usually necessary for the production of conventional OSN polymer membranes.[5] Manufacture of these nanopapers is enabled by inducing flocculation of nanofibrils upon addition of multivalent ions. This type of nanocellulose membrane represents a step forward within this important domain and demonstrates the utilization of a well-known material for an advanced application.

We discuss the use of nanopapers made entirely from (2,2,6,6-tetramethylpiperidin-1-yl)oxy (TEMPO) oxidized NFC (herein termed as NFC-O) with fibre diameters ranging from 5 to 30 nm (UPM-Kymmene Oyj, Helsinki, Finland) for NF

[a] *Department of Chemical Engineering, Polymer & Composite Engineering (PaCE) Group, Imperial College London, South Kensington Campus, SW7 2AZ London, UK. E-mail: a.bismarck@imperial.ac.uk; Fax: +44 (0)20759 45638; Tel: +44 (0)20759 45578*

[b] *Department of Chemical Engineering, University College London, Torrington Place, WC1E 7JE London, UK*

[c] *Polymer & Composite Engineering (PaCE) group, Institute for Materials Chemistry and Research, Faculty of Chemistry, University of Vienna, Währingerstraße 42, A-1090 Vienna, Austria. E-mail: alexander.bismarck@univie.ac.at*

[d] *VTT Technical Research Centre of Finland, Biologinkuja 7, FL-02044 Espoo, Finland*

[e] *Department of Chemical Engineering, Imperial College London, South Kensington Campus, SW7 2AZ London, UK*

† Electronic supplementary information (ESI) available: Further characterisation of the membranes and membrane compaction. See DOI: 10.1039/c4cc00467a

membranes. The production method of NFC-O is described in detail elsewhere.[18] It can be anticipated that these nanofibrils can be densely compacted to form a framework structure with pore-dimensions in the range of the diameter of the nanofibrils. This concept has been mathematically proven by Zhang.[19] To demonstrate the possibility of controlling the pore size, and thus the molecular weight cut-off (MWCO) and permeance of the nano-cellulose membranes, we also used another NFC grade produced by mechanical grinding (MKZA10-15J Supermasscolloider, Masuko Sangyo Co., Kawaguchi, Japan) of never-dried bleached kraft birch pulp as described by Lee et al.[14] Herein, we call these fibrils NFC-K, which possess fibre diameters of 50 to 100 nm (more details about the NFC grades can be found in the ESI†).

In general, for the production of paper, cellulose fibres are suspended in water. This suspension is then filtered, the resulting filter cake, i.e. the fibre mat, is pressed and water is removed until the desired quality is achieved. As for usual paper, the production of nanopapers started from an NFC in water suspension with a consistency of 0.3 wt%. This suspension was produced by blending (Breville VBL065-01, Oldham, UK) NFC feedstock for 2 min, which had an original consistency of 2.5 wt% and 1.8 wt%, respectively, for NFC-O and NFC-K. Nanopapers with the desired grammage were produced by vacuum-filtration of NFC suspensions containing a pre-determined amount of nano-cellulose onto cellulose filter papers (VWR 413, 5–13 μm pore size, Lutter-worth, UK). However, we observed that NFC-O passed through both the filter paper and the supporting glass frit (Schott, porosity No. 1, Mainz, Germany) due to its extremely small size. This effect was not observed for the filtration of the larger diameter NFC-K fibrils, which was consistent with our previous observations.[14] In order to facilitate the filtration of NFC-O, flocculation of the fibrils by changing the surface charge was required. Thus, we measured the ζ-potential of NFC as function of pH in a 1 mM KCl electrolyte using electrophoresis (Brookhaven ZetaPALS analyzer, Holtsville, USA). It can be inferred from the $\zeta = f(pH)$ curve that it is impossible to induce flocculation of NFC-O by changing the pH of the NFC-O suspension, since the isoelectric point (iep), where $\zeta = 0$, at which significant flocculation would occur, is very low (Fig. 1, left). To reach the iep, a pH of 1.5 (extrapolated) would be required, which could possibly result in acid hydrolysis of NFC.[20]

The ζ-potential as a measure of surface charge is dependent on the ionic strength, which is most effectively increased by addition of multivalent ions. Therefore, we measured ζ as a function of the salt ($MgCl_2$ and $AlCl_3$) concentration, from which the point of zero charge (pzc) was determined (Fig. 1, right).
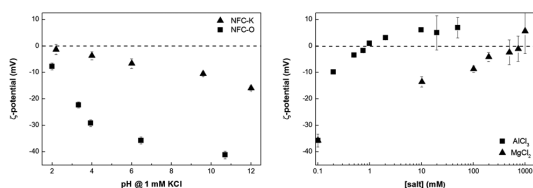
At the pzc, the NFC-O fibrils have zero net surface charge and, therefore, no electrostatic repulsion exists between NFC-O fibrils, which causes the whole NFC-O suspension to form a single gel. Multivalent cations specifically adsorb on negatively charged NFC-O surfaces causing the ζ-potential to decrease by effectively reducing the Debye length. Ultimately, the pzc was reached upon adjusting the electrolyte concentration to 800 mM for $MgCl_2$ and 1 mM for $AlCl_3$, respectively (Fig. 1, right), because the ionic strength of the electrolyte increases exponentially with increasing charge of the cations. To produce NFC-O filter cakes, $AlCl_3$ was added to achieve a concentration of 1 mM.

Wet NFC-O and -K filter cakes of 125 mm in diameter were pressed between blotting papers (Whatman 3MM Chr, Kent, UK) for 5 min under a weight of 10 kg to increase the NFC solid content to 15 wt%. These filter cakes were then sandwiched between blotting papers and metal plates for further hot pressing at 120 °C for 1 h under a weight of 1 t to dry and consolidate the filter cakes. The hot pressing also prevents the shrinkage of nanopapers and increases the density of the sheets, resulting in better mechanical properties of the papers.[15] Nano-papers with grammages between 10 and 70 g m^{-2} (gsm) were produced from both types of nanocelluloses. The thickness of these nanopapers was found to increase linearly with the grammage (Fig. S1, ESI†). The nanopapers produced were used as membranes directly.

Exemplarily, the permeance (P) of tetrahydrofuran (THF), n-hexane and water through the nanopapers was measured in a dead end cell (Sterlitech HP 4750, Kent, USA). The solvent was forced through the nanopapers at 20 °C by nitrogen at a head pressure of 0.2 MPa and 1 MPa for nanopapers with grammages <20 gsm and >20 gsm, respectively. The amount of solvent that passed through the nanopaper for a given time interval was measured gravimetrically and used to determine P [L m^{-2} h^{-1} MPa^{-1}]. For these measurements, discs of 49 mm in diameter were cut from the nanopapers and placed in the dead end cell on a ceramic support. In the beginning of the measurement, P decreased significantly (Fig. S2, ESI†) caused by membrane compaction due to the applied pressure.[21]

The permeance of different solvents is exemplarily shown for NFC-O nanopapers in Fig. 2(a). These measurements showed that P of the tested solvents passed through nanopapers increases in the following order: water < THF < n-hexane. Thus, irrespective of the hydrophilic nature of nanocellulose and the hydrophobicity of some of the solvents, P increases inversely with increasing hydrophobicity of the solvent. It should be noted
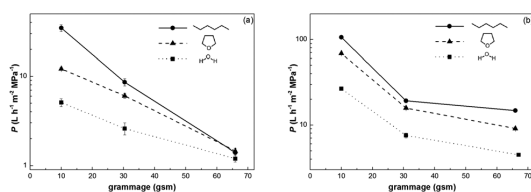

Fig. 1 ζ-potential of NFC-O and -K in 1 mM KCl aqueous solution as a function of pH (left) and of NFC-O as a function of $MgCl_2$ and $AlCl_3$ concentrations (right).

Fig. 2 Permeance P of different solvents for NFC-O (a) and NFC-K (b) nanopapers of different grammages.

that the calculation of P does not take into account the viscosity of the solvent.

In addition to this, we also observed that P is dependent on the grammage, and thus the thickness, of the nanopapers as well as the diameter of the fibrils (Fig. 2). Using nanofibrils with larger diameters (NFC-K) for membrane fabrication resulted in nanopapers with larger pore dimensions as compared to NFC-O, which, in conjunction with varying the grammage of the nanopapers, allows the permeance to be controlled over a wide range. Varying the aspect ratio of randomly packed high aspect ratio cylinders hardly affects the porosity of a mat.[22] Since the number of fibrils per unit mass within the same volume element is higher for smaller fibrils, this results in a larger number of pores, which are smaller in diameter due to the constant porosity (around 35%).

The nanofiltration membrane performance is generally quantified by the MWCO, which was determined by passing standard polymer solutions of known concentrations through the nanopapers. The amount of rejected polymer molecules was quantified using gel permeation chromatography (GPC, aqueous: Viscotek GPCmax VE2001, VE3580 RI detector, Malvern, UK; organic: Waters 515 HPLC pump, Waters 2410 RI detector, Milford, USA). The MWCO is defined as the molecular weight of a molecule which is rejected by 90%.[23] Poly(ethylene glycol) (PEG) dissolved in deionized water and polystyrene (PS) standards dissolved in THF with molecular weights ranging from 1 to 13 kDa were used to determine the MWCO for NFC-O nanopapers with a grammage of 65 gsm. The retention of PEG and PS standards as a function of the M_W is shown in Fig. 3(a).

For PS and PEG, the MWCO values were found to be 3.2 kDa and 6 kDa, corresponding to hydrodynamic radii of 1.6 nm[24] and 2.4 nm,[25] respectively, which represent the pore size. Thus, our nanopaper membranes have a MWCO at the upper end of the NF range. In the case of NFC-K papers (Fig. 3(b)), the MWCO of PEG was 25 kDa, which corresponds to a hydrodynamic radius of 5 nm (ref. 25) and for PS it was 40 kDa, which is equivalent to a hydrodynamic radius of 5.5 nm.[24] This demonstrated that by using differently sized cellulose nanofibrils, around 50 nm for NFC-K and down to 5 nm for NFC-O, it is possible to adjust the pore dimensions of the resulting nanopapers, which is due to a reduced pore size in the random packing of cylinders with smaller diameters.

To summarize, we produced nanocellulose based nano-filtration membranes by simply using a papermaking process. These nanopapers are suitable for NF of organic solvents and

water. It was observed that the permeance of nanopapers was dependent on the hydrophilicity of the solvents and that P was governed by the grammage of the nanopapers and the dimensions of the nanofibrils. We also observed that the MWCO was determined by the diameter of the nanofibrils, which affects the pore dimensions of the nanopapers. It is thus possible to tailor the membrane performance over a wide range of applications by selecting nanofibrils with different diameters. In conclusion, we can prepare, as simply as making paper, solvent-stable OSN membranes from renewable resources. If it eventually becomes possible to produce NFC with fibrils of evenly distributed lengths, potentially even thinner active membrane layers with smaller MWCO could be created, which would drastically improve the performance of these types of NF membranes.

Notes and references

1 P. Vandezande, L. E. M. Gevers and I. F. J. Vankelecom, *Chem. Soc. Rev.*, 2008, **37**, 365–405.
2 R. Othman, A. W. Mohammad, M. Ismail and J. Salimon, *J. Membr. Sci.*, 2010, **348**, 287–297; A. G. Livingston, L. Peeva, S. Han, D. Nair, S. S. Luthra, L. S. White and L. M. Freitas Dos Santos, *Ann. N. Y. Acad. Sci.*, 2003, **984**, 123–141; D. Peshev, L. G. Peeva, G. Peev, I. I. R. Baptista and A. T. Boam, *Chem. Eng. Res. Des.*, 2011, **89**, 318–327; M. Priske, K.-D. Wiese, A. Drews, M. Kraume and G. Baumgarten, *J. Membr. Sci.*, 2010, **360**, 77–83; A. Cano-Odena, P. Vandezande, D. Fournier, W. Van Camp, F. E. Du Prez and I. F. J. Vankelecom, *Chem. – Eur. J.*, 2010, **16**, 1061–1067; J. C.-T. Lin and A. G. Livingston, *Chem. Eng. Sci.*, 2007, **62**, 2728–2736; L. S. White and C. R. Wildemuth, *Ind. Eng. Chem. Res.*, 2006, **45**, 9136–9143.
3 M. Sairam, X. X. Loh, K. Li, A. Bismarck, J. H. G. Steinke and A. G. Livingston, *J. Membr. Sci.*, 2009, **330**, 166–174.
4 X. Li, P. Vandezande and I. F. J. Vankelecom, *J. Membr. Sci.*, 2008, **320**, 143–150; X. X. Loh, M. Sairam, J. H. G. Steinke, A. G. Livingston, A. Bismarck and L. Kang, *Chem. Commun.*, 2008, 6324–6326; M. Peyravi, A. Rahimpour and M. Jahanshahi, *J. Membr. Sci.*, 2012, **423–424**, 225–237; H. Siddique, L. G. Peeva, K. Stoikos, G. Pasparakis, M. Vamvakaki and A. G. Livingston, *Ind. Eng. Chem. Res.*, 2013, **52**, 1109–1121; S. Zeidler, U. Kätzel and P. Kreis, *J. Membr. Sci.*, 2013, **429**, 295–303.
5 I. Soroko, Y. Bhole and A. G. Livingston, *Green Chem.*, 2011, **13**, 162–168.
6 M. F. Jimenez-Solomon, P. Gorgojo, M. Munoz-Ibanez and A. G. Livingston, *J. Membr. Sci.*, 2013, **448**, 102–113; M. F. Jimenez Solomon, Y. Bhole and A. G. Livingston, *J. Membr. Sci.*, 2012, **423–424**, 371–382.
7 A. Buekenhoudt, F. Bisignano, G. De Luca, P. Vandezande, M. Wouters and K. Verhulst, *J. Membr. Sci.*, 2013, **439**, 36–47; P. Marchetti, A. Butté and A. G. Livingston, *J. Membr. Sci.*, 2012, **415–416**, 444–458.
8 F. Peng, L. Lu, H. Sun, Y. Wang, J. Liu and Z. Jiang, *Chem. Mater.*, 2005, **17**, 6790–6796; T. C. Merkel, B. D. Freeman, R. J. Spontak, Z. He, I. Pinnau, P. Meakin and A. J. Hill, *Science*, 2002, **296**, 519–522.
9 K. Li, *Ceramic Membranes for Separation and Reaction*, John Wiley & Sons, Ltd., Chichester, UK, 2007.
10 P. Chen, S. Y. Cho and H.-J. Jin, *Macromol. Res.*, 2010, **18**, 309–320; D. Klemm, F. Kramer, S. Moritz, T. Lindstroem, M. Ankerfors, D. Gray and A. Dorris, *Angew. Chem., Int. Ed.*, 2011, **50**, 5438–5466.
11 J. J. Blaker, K.-Y. Lee and A. Bismarck, *J. Biobased Mater. Bioenergy*, 2011, **5**, 1–16; S. J. Eichhorn, A. Dufresne, M. Aranguren, N. E. Marcovich, J. R. Capadona, S. J. Rowan, C. Weder, W. Thielemans, M. Toman, S. Rennecker, W. Gindl, S. Veigel,
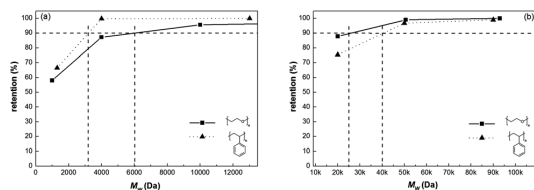
Fig. 3 Retention of PS & PEG = $f(M_W)$ for NFC-O (a) and NFC-K (b) nanopapers: MWCO is the molecular weight of which 90% is rejected.

J. Keckes, H. Yano, K. Abe, M. Nogi, A. N. Nakagaito, A. Mangalam, J. Simonsen, A. S. Benight, A. Bismarck, L. A. Berglund and T. Peijs, *J. Mater. Sci.*, 2010, **45**, 1–33.

12 S.-J. Chun, S.-Y. Lee, G.-H. Doh, S. Lee and J. H. Kim, *J. Ind. Eng. Chem.*, 2011, **17**, 521–526; A. Dufresne, *Nanocellulose: From Nature to High Performance Tailored Materials*, Walter de Gruyter & Co, Berlin/Boston, 2012; J. Gutierrez, S. C. M. Fernandes, I. Mondragon and A. Tercjak, *ChemSusChem*, 2012, **5**, 2323–2327; L. Hu, G. Zheng, J. Yao, N. Liu, B. Weil, M. Eskilsson, E. Karabulut, Z. Ruan, S. Fan, J. T. Bloking, M. D. McGehee, L. Wagberg and Y. Cui, *Energy Environ. Sci.*, 2013, **6**, 513–518; J. Huang, H. Zhu, Y. Chen, C. Preston, K. Rohrbach, J. Cumings and L. Hu, *ACS Nano*, 2013, 7, 2106–2113.

13 M. Henriksson, L. A. Berglund, P. Isaksson, T. Lindstroem and T. Nishino, *Biomacromolecules*, 2008, **9**, 1579–1585.

14 K.-Y. Lee, T. Tammelin, K. Schulfter, H. Kiiskinen, J. Samela and A. Bismarck, *ACS Appl. Mater. Interfaces*, 2012, **4**, 4078–4086.

15 M. Österberg, J. Vartiainen, J. Lucenius, U. Hippi, J. Seppälä, R. Serimaa and J. Laine, *ACS Appl. Mater. Interfaces*, 2013, **5**, 4640–4647.

16 A. Khan, T. Huq, R. A. Khan, B. Riedl and M. Lacroix, *Crit. Rev. Food Sci. Nutr.*, 2012, **54**, 163–174.

17 S.-J. Chun, E.-S. Choi, E.-H. Lee, J. H. Kim, S.-Y. Lee and S.-Y. Lee, *J. Mater. Chem.*, 2012, **22**, 16618–16626.

18 *WO Pat.*, WO 2012/168562 A1, 2012.

19 W. Zhang, PhD thesis, Louisiana State University, 2006.

20 J. F. Saeman, *Ind. Eng. Chem.*, 1945, **37**, 43–52.

21 E. Gibbins, M. D'Antonio, D. Nair, L. S. White, L. M. Freitas dos Santos, I. F. J. Vankelecom and A. G. Livingston, *Desalination*, 2002, **147**, 307–313.

22 M. Novellani, R. Santini and L. Tadrist, *Eur. Phys. J. B*, 2000, **13**, 571–578.

23 Y. H. See Toh, X. X. Loh, K. Li, A. Bismarck and A. G. Livingston, *J. Membr. Sci.*, 2007, **291**, 120–125.

24 E. Uliyanchenko, P. J. Schoenmakers and S. van der Wal, *J. Chromatogr. A*, 2011, **1218**, 1509–1518.

25 J. K. Armstrong, R. B. Wenby, H. J. Meiselman and T. C. Fisher, *Biophys. J.*, 2004, **87**, 4259–4270.

Supporting Information for:
Nanopapers for Organic Solvent Nanofiltration

A. Mautner, [a] K.-Y. Lee,[b,c] P. Lahtinen,[d] M. Hakalahti, [d] T. Tammelin,[d] K. Li[e] and A. Bismarck[a,c]

[a] Department of Chemical Engineering, Polymer & Composite Engineering (PaCE) Group, Imperial College London, South Kensington Campus, SW7 2AZ London, UK, E-mail: a.bismarck@imperial.ac.uk; Fax: +44 20759 45638; Tel: +44 20759 45578.
[b] Department of Chemical Engineering, University College London, Torrington Place, WC1E 7JE London, UK.
[c] Polymer & Composite Engineering (PaCE) group, Institute for Materials Chemistry and Research, Faculty of Chemistry, University of Vienna, Währingerstraβe 42, A-1090 Vienna, Austria.
[d] VTT Technical Research Centre of Finland, Biologinkuja 7, FL-02044 Espoo, Finland.
[e] Department of Chemical Engineering, Imperial College London, South Kensington Campus, SW7 2AZ London, UK.
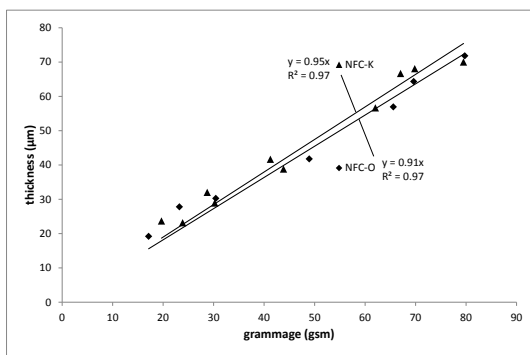
Supporting Figures:

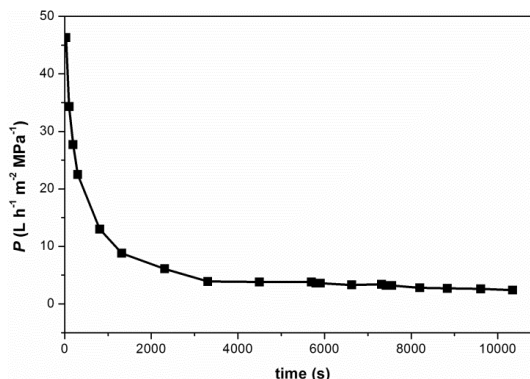**Fig. S1.** Correlation between grammage and thickness of NFC-O and -K papers.

Fig. S2. P (water) = f(time): NFC-O-paper with 30 gsm.

Materials:

Aluminium chloride hexahydrate (purity ≥ 97%) was purchased from BDH (Poole, UK), tetrahydrofuran (GPC grade) from Fisher Chemical (Loughborough, UK), n-hexane (HPLC grade) from VWR (Leuven, B), PS-standards from Alfa Aesar (Heysham, UK) and PEG-standards from Polymer Labs (Shropshire, UK).

Nanofibrillated cellulose (NFC-K) was produced by mechanical grinding of elemental chlorine free (ECF) never-dried bleached birch kraft pulp (UPM-Kymmene Corporation, Pietarsaari, Finland) as also described in Lee et al.[14]. The carbohydrate composition of the pulp and the NFC produced from were similar. The composition was 73% glucose, 26% xylose and 1% mannose.[1] The pulp furthermore contained 0.2% residual lignin and 0.09% residual extractives.[2] The charge of the pulp was approximately 0.04 mmol/g, which was determined using the standard titration method (SCAN CM 65:02). The grinding process of the kraft pulp was conducted using a Masuko Mass Colloider (MKZA10-15J Supermasscolloider, Masuko Sangyo Co., Kawaguchi, Japan). The pulp was passed through the grinder seven times and the final consistency of the aqueous gel-like NFC-K was approximately 1.8 wt-%. NFC-K fibrils possess a fibrous structure with diameters of approximately 50-100 nm and lengths of several micrometres.[14]

TEMPO-oxidized cellulose nanofibrils (NFC-O) with the trade name of UPM Biofibrils was supplied as 2.5 wt-% aqueous dispersion by UPM-Kymmene Corporation, Helsinki, Finland, for testing purposes. Prior to mechanical disintegration, the never-dried bleached birch kraft pulp with the similar chemical composition as above was TEMPO-oxidized as described elsewhere[3,4]. The charge of the oxidized pulp was 1.03 mmol/g determined by conductometric titration as reported by the supplier. The fibril diameter distribution varied within 5-25 nm (55% of fibrils possess the diameter of 10-15 nm) as also reported by the supplier. In addition to this, the size of the fibrils was analysed using Atomic Force Microscopy (AFM). AFM imaging was performed using a Nanoscope IIa Multimode scanning probe microscope (Digital Instruments Inc., Santa Barbara, CA, USA). The nanofibril samples were prepared by spin coating a dilute NFC dispersion on a silica surface as described in Ahola et al.[5] The images were scanned in tapping mode in air using silicon cantilevers (µMasch, Tallinn, Estonia) with nominal resonance frequencies of 320-360 kHz. No image processing except flattening was made and at least 5 areas on each sample were characterised. The diameter of the fibrils analysed using AFM gives a slightly higher average value of approximately 30 nm. This is due to the fact that the actual width of the fibrils is lower as that gained by AFM due to the finite AFM tip dimensions and curvature.

[1] P. Eronen, M. Osterberg, S. Heikkinen, M. Tenkanen and Laine J., *Carbohydr. Polym.* 2011, **86**, 1281–1290.

[2] S. Asikainen, A. Fuhrmann and L. Robertsen, *Nord. Pulp Pap. Res. J.* 2010, **25**, 269–276.

[3] WO Pat., WO 2012/168562 A1, 2012.

[4] R. Pönni, T. Pääkkönen, M. Nuopponen, J. Pere and T. Vuorinen, *Cellulose*, 2014, under revision.

[5] S. Ahola, J. Salmi, L.-S. Johansson, J. Laine and M. Österberg., *Biomacromolecules,* 2008, **9**, 1273-1282.
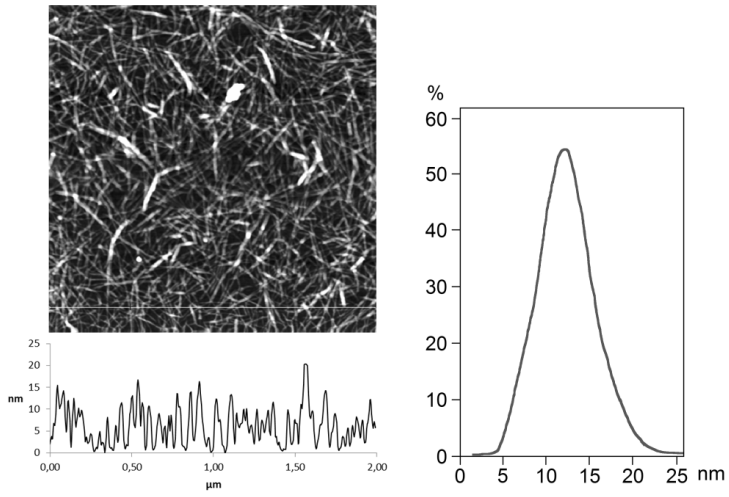
Fig. S3. AFM topography image with typical height profile (left) and fibril diameter-distribution provided by supplier (right) of NFC-O. The AFM image size is 2 µm × 2 µm

BUSINESS +
ECONOMY

ART +
DESIGN +
ARCHITECTURE

SCIENCE +
TECHNOLOGY

CROSSOVER

**DOCTORAL
DISSERTATIONS**